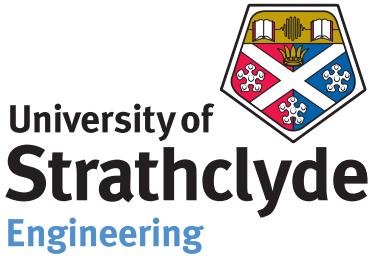

University of Strathclyde
Department of Electronic and Electrical Engineering

Non-Linear Precoding and Equalisation for Broadband MIMO Channels

by
Waleed Eid Al-Hanafy

A thesis presented in fulfilment of the requirements for the degree of
Doctor of Philosophy

2010

Dedicated to

my wife, my children Roaa, Reem and Abdelrahman,
and in loving memory of my parents

Declaration

This thesis is the result of the author's original research. It has been composed by the author and has not been previously submitted for examination which has led to the award of a degree.

Signed: Date:

Abstract

Multiple-input multiple-output (MIMO) technology promises significant capacity improvements in order to more efficiently utilise the radio frequency spectrum. To achieve its anticipated multiplexing gain as well as meet the requirements for high data rate services, proposed broadband systems are based on OFDM or similar block based techniques, which are afflicted by poor design freedom at low redundancy, and are known to suffer badly from co-channel interference (CCI) in the presence of synchronisation errors. Non-block based approaches are scarce and use mostly decision feedback equalisation (DFE) or V-BLAST approaches adopted for the broadband case, as well as Tomlinson-Harashima precoding (THP). These methods do not require a guard interval and can therefore potentially achieve a higher spectral efficiency. The drawback of these schemes is the large effort in determining the optimum detection order in both space and time, often motivating the adoption of suboptimal approaches.

In this thesis, we focus on non-block based precoding and equalisation schemes aiming to achieve higher data throughputs with improved bit error ratio (BER) compared to existing approaches. In order to achieve this, a recently developed broadband singular value decomposition (BSVD) technique is applied to decouple a broadband MIMO channel into independent frequency selective single-input single-output (SISO) subchannels of ordered qualities, thereby cancelling CCI. Secondly, these dispersive broadband SISO subchannels are individually equalised using non-linear DFE or THP schemes with a variable transmission rate that best matches the individual qualities of the respective subchannels, whereby the decision delay can be independently optimised for every subchannel. This method is benchmarked through simulations against a state-of-the-art broadband MIMO THP technique with optimised spatio-temporal ordering showing that improved BER performance can be achieved under the constraints of identical data throughput and transmit power.

In order to maximise the data throughput of our proposed method or similar multichannel systems, adaptive bit and power loading schemes have been applied.

A rate-optimal approach known as a greedy algorithm is considered, whereby optimality is guaranteed by considering an appropriate bit allocation cost function and then iteratively assigning one bit at a time to the least cost-expensive subchannel. Constraining the transmit power budget and target BER of the overall transmission system, we propose a greedy power allocation (GPA) algorithm to optimise the achieved data throughput. While maximising data rate, the GPA algorithm can also save some unused power from the total transmit budget. This power is further utilised to enhance the mean BER w.r.t. the constrained target through two proposed power redistribution algorithms.

It is well known that the GPA algorithm is computationally very expensive due to the iterative nature of the algorithm. In order to efficiently reduce the computational complexity of the GPA algorithm, suboptimal GPA schemes are proposed by considering a subchannel grouping concept. We show by numerical results that these schemes, while hardly sacrificing any performance compared to the original GPA algorithm, can significantly reduce the computational complexity by an order of magnitude.

Acknowledgements

First of all, I would like to express my deep and most sincere gratitude to my supervisor Dr. Stephan Weiss. Despite his extremely busy schedule, Dr. Weiss made himself available to me at every stage in my PhD journey to assist, encourage and inspire me in order to enhance my research. I will be eternally grateful to Dr. Weiss for his support and insightful guidance, particularly in the early stages of this work. Without his encouragement and his enthusiastic attitude towards my work, none of this would have been possible.

I would also like to express my gratitude towards Prof. John G. McWhirter and Prof. Malcolm D. Macleod for kindly agreeing to examine this thesis.

I would like to thank the academic and support staff in the Centre for excellence in Signal & Image Processing (CeSIP) for making my time at Strathclyde such a pleasant experience and for providing a stimulating research environment. I have no doubt that the skills I have learned and developed during my time as a student in CeSIP will serve me well for many years to come.

I would also like to thank my colleagues and fellow PhD students in CeSIP for the many friendly discussions we had, and for their constant encouragement during my studies. My colleagues not only provided a technically excellent environment, but also a rich source of friendship, which led to a socially fulfilling time at Strathclyde.

Finally, I would like to express my sincere gratitude to the Egyptian Government for granting me a scholarship from Menoufia University and the Ministry of Higher Education and State for Scientific Research, which allowed me to pursue a PhD.

List of Publications

Publications Directly Related to the Thesis

1. **Waleed Al-Hanafy** and **Stephan Weiss,** "Suboptimal Greedy Power Allocation Schemes for Discrete Bit Loading," invited paper for *IET Communications Journal*, submitted July 2010.

2. **Waleed Al-Hanafy** and **Stephan Weiss,** "Discrete Rate Maximisation Power Allocation with Enhanced BER," invited paper for *IET Communications Journal*, submitted July 2010.

3. **Waleed Al-Hanafy, Mohamed Nuri Hussin,** and **Stephan Weiss,** "Incremental Rate Maximisation Power Loading with BER Improvements," *18th European Signal Processing Conference, EUSIPCO 2010,* Aalborg, Denmark, August 2010.

4. **Waleed Al-Hanafy** and **Stephan Weiss,** "Reduced Complexity Schemes to Greedy Power Allocation for Multicarrier Systems," *18th International Conference on Microwave, Radar and Wireless Communications, MIKON 2010*, Vilnius, Lithuania, June 2010.

5. **Waleed Al-Hanafy** and **Stephan Weiss,** "Trade-Off Between Complexity and BER Performance of a Polynomial SVD-Based Broadband MIMO Transceiver," *27th National Radio Science Conference, NRSC 2010*, Menouf, Egypt, March 2010.

6. **Waleed Al-Hanafy** and **Stephan Weiss,** "Greedy Power Allocation for Multicarrier Systems with Reduced Complexity," *27th National Radio Science Conference, NRSC 2010*, Menouf, Egypt, March 2010.

7. **Waleed Al-Hanafy** and **Stephan Weiss,** "Comparison of Precoding Methods for Broadband MIMO Systems," *3rd IEEE International Workshop*

on Computational Advances in Multi-Sensor Adaptive Processing, CAMPSAP 2009, Aruba, Dutch Antilles, December 2009.

8. **Waleed Al-Hanafy** and **Stephan Weiss,** "A New Low-Cost Discrete Bit Loading using Greedy Power Allocation,"[1] *3rd Mosharaka International Conference on Communications, Computers and Applications, MIC-CCA 2009*, Amman, Jordan, October 2009.

9. **Waleed Al-Hanafy** and **Stephan Weiss,** "Sum-Rate Maximisation Comparison using Incremental Approaches with Different Constraints," *3rd Mosharaka International Conference on Communications, Computers and Applications, MIC-CCA 2009*, Amman, Jordan, October 2009.

10. **Waleed Al-Hanafy** and **Stephan Weiss,** "Efficient Tomlinson-Harashima Precoding Ordering using QR Decomposition," *17th European Signal Processing Conference, EUSIPCO 2009*, Glasgow, Scotland, UK, August 2009.

11. **Waleed Al-Hanafy, Andrew P. Millar, Chi Hieu Ta** and **Stephan Weiss,** "Broadband SVD and Non-Linear Precoding and Equalisation Applied to Broadband MIMO Channels," *42nd Asilomar Conference on Signals, Systems and Computers, ACSSC 2008*, Pacific Grove, CA, USA, October 2008.

Other Publications

1. **Stephan Weiss, Paul Yarr, Waleed Al-Hanafy, Andrew P. Millar and Chi-Hieu Ta,** "An Oversampled Modulated Filter Bank Transmultiplexer With Precoding and Equalisation," *3rd Workshop on Power Line Communications*, Udine, Italy, October 2009.

2. **Samir Bendoukha, Waleed Al-Hanafy and Stephan Weiss,** "A Concurrent Blind Receiver for STBC over Doubly Dispersive Channels," *17th European Signal Processing Conference, EUSIPCO 2009*, Glasgow, Scotland, UK, August 2009.

[1] This paper won the "Best Paper Award" at the MIC-CCA 2009 Conference.

Abbreviations

AGC	automatic gain control
AWGN	additive white Gaussian noise
BER	bit error ratio
BPSK	binary phase-shift keying
BSVD	broadband singular value decomposition
CCI	co-channel interference
CDF	cumulative distribution function
CFO	carrier-frequency offset
CP	cyclic prefix
CSI	channel state information
DFE	decision feedback equalisation
DFT	discrete Fourier transform
DoF	degrees of freedom
DPC	dirty paper coding
DSP	digital signal processing
FIR	finite impulse response
FPR	fairness-BER power redistribution
GBA	greedy bit allocation
GPA	greedy power allocation
g-GPA	grouped greedy power allocation
IBI	inter-block interference
IDFT	inverse discrete Fourier transform
ISI	inter-symbol-interference
LA	linear algebra
LO	left-over
LZ	leading zeros
Md-GPA	power moving-down greedy power allocation
Mu-GPA	power moving-up greedy power allocation

MIMO	multiple-input multiple-output
ML	maximum-likelihood
MSE	mean square error
MMSE	minimum mean square error
M-QAM	M-ary quadrature amplitude modulation
NoI	number of iterations
OFDM	orthogonal frequency division multiplexing
PAPR	peak-to-average power ratio
P/S	parallel-to-serial
QPSK	quadrature phase-shift keying
S/P	serial-to-parallel
SER	symbol error ratio
SIC	successive interference cancellation
SISO	single-input single-output
SNR	signal-to-noise ratio
SVD	singular value decomposition
THP	Tomlinson-Harashima precoding
TZ	trailing zeros
UPA	uniform power allocation
UPR	uniform power redistribution
V-BLAST	vertical Bell laboratories layered space-time
WSS	wide-sense stationary
ZF	zero forcing

Mathematical Notations

General Notations

a	scalar quantities are denoted by lowercase plain fonts
$\boldsymbol{a}$ or $\underline{A}$	vectors are denoted by lowercase boldface or uppercase underlined plain fonts
$\mathbf{A}$	matrices are denoted by uppercase boldface
a_{ij}	the entry of the ith row and jth column of matrix $\mathbf{A}$
$\mathbf{A}_i$	the ith diagonal entry of matrix $\mathbf{A}$
$(\mathbf{A})_i$	the ith row of matrix $\mathbf{A}$
$[\mathbf{A}]_j$	the jth column of matrix $\mathbf{A}$
$\mathrm{diag}\,(\mathbf{A})$	the diagonal entries of matrix $\mathbf{A}$
$\mathrm{diag}\,(\boldsymbol{a})$	a diagonal matrix with diagonal entries of a vector $\boldsymbol{a} = [a_1, a_2, \cdots]$

Operators

$\lvert\mathbf{A}\rvert$	determinant of matrix $\mathbf{A}$
$\lvert x\rvert$	absolute value of symbol x
$\lVert\mathbf{x}\rVert_2$	euclidian norm of vector $\mathbf{x}$
$\lVert\mathbf{X}\rVert_F$	Frobenius norm of matrix $\mathbf{X}$
$\delta\,[n]$	discrete delta function
$\otimes$	Kronecker product
$\star$	convolution in time
$(\cdot)^{\mathrm{T}}$	transposition
$(\cdot)^*$	complex conjugate
$(\cdot)^{\mathrm{H}}$	Hermitian transpose or complex conjugate transpose
$\tilde{(\cdot)}$	Parahermitian, $\tilde{\mathbf{A}}\,(z) = \mathbf{A}^{\mathrm{H}}\,(z^{-1})$
$\lceil\cdot\rceil$	ceil operator, rounding to the nearest integer towards $+\infty$

$\lfloor \cdot \rfloor$	floor operator, rounding to the nearest integer towards $-\infty$
$\mathbb{E}[\cdot]$	expectation operator
$\mathrm{tr}(\cdot)$	trace operator
$\mathcal{M}(\cdot)$	modulo operator
$q(\cdot)$	decision device (quantisation) operator
$\Re(\cdot)$	real part
$\Im(\cdot)$	imaginary part

Sets

$\mathbb{Z}$	set of integer numbers
$\mathbb{R}$	set of real numbers
$\mathbb{C}$	set of complex numbers
$\mathbb{C}^{M\times N}$	set of $M \times N$ matrices with complex entries
$\mathcal{S}$	set of symbol alphabets that is assigned for transmission

Symbols and Variables

N_t	number of transmit antennas
N_r	number of receive antennas
N	number of subchannels or subcarriers
N_b	data block size
M	constellation size (or order) of an M-QAM modulation scheme
Q	channel order
L	filter order
$\mathbf{0}_{M\times N}$	$M \times N$ zero matrix
$\mathbf{I}_N$	identity matrix of size N
$\boldsymbol{e}_i$	the ith column of the correct size identity matrix
σ_x^2	variance or average power of the scalar random process $x[n]$
$\mathbf{R}_{xx}$	covariance matrix of the vector random process $\mathbf{x}[n]$
$\mathbf{R}_{xy}$	covariance matrix between vector random processes $\mathbf{x}[n]$ and $\mathbf{y}[n]$
$\mathcal{CN}(0,1)$	complex Gaussian random variable of zero-mean and unit-variance

Contents

Chapter 1

Introduction

1.1 Motivation

A significant leap in the world of wireless communication systems has emerged due to the substantial advances in digital signal processing (DSP) along with the tremendous progress in semiconductor technologies. The most obvious example for such evolution is the mobile communication sector, where highly standardised forms of ubiquitous communications can be provided nowadays at low cost. Noticeably, higher data rate services with high link reliability, such as high quality multimedia, have started to come into dramatic demand. These services are known to require high bandwidth segments of the radio frequency spectrum. However, the allocated electromagnetic spectrum for wireless communication systems is limited and therefore a limit to such services is inevitably exists. Moreover, the propagation of the broadband wireless channel is characterised by effects such as time-varying behaviour, fading and multipath interference [1, 2]. Accordingly, wireless communication designers are now focusing on the development of systems that can provide high spectral efficiency to address the scarcity of the radio frequency spectrum, and aim for a quality comparable to digital subscriber lines (DSL).

Frequency reuse and cell sectorisation can be regarded as conventional design methods to achieve higher spectral efficiency for cellular wireless communications, such as, for example, applied in GSM systems. The capacity of these systems is limited and is unlikely to be able to support the continuously growing demand for higher data rate services. In contrast, over the last decade the spatial dimension has been identified as a means to efficiently boost spectral efficiency and enhance wireless system capacity without the need for extra bandwidth expansion. Thus, in current second and third generation wireless systems smart antennas play an

important role to release such capacity improvement by the adoption of e.g. adaptive antenna array processing techniques at least at one end of a communications link [3]. By incorporating multiple antennas at both transmit and receive side of a link, referred to as multiple-input multiple-output (MIMO) channel, spectral efficiency of the overall configuration can be significantly increased. In particular, it has been shown that the MIMO capacity increases linearly with the minimum number of antennas of both sides at high signal-to-noise ratio (SNR), provided that a rich scattering environment between antenna pairs exists and therefore the different transmit paths in a MIMO channel are uncorrelated [4, 5]. This makes MIMO technology a leading candidate for future communication systems in order to keep in step with the demand for high speed wireless broadband services.

MIMO technology becomes a prominent and state-of-the-art component of modern wireless communication systems and continues to motivate significant research in space-time processing techniques to efficiently realise the anticipated MIMO capacity gain (see for example [6, 7]). Nevertheless, the performance of MIMO transceiver systems is highly dependent on the characteristics of propagation scenarios, traffic patterns, and most importantly interference profiles. Since for high data rate services the coherence bandwidth of the MIMO channel is smaller than the transmission bandwidth required to communicate these services, the MIMO channel cannot be assumed flat-fading, and a more challenging frequency-selective — sometimes called broadband — scenario emerges for communication. Assuming stationarity, this frequency-selective channel can be modelled as a finite impulse response (FIR) linear time-invariant filter. The order of this FIR filter modelling the channel can be obtained as [8]

$$L = \left\lceil \frac{\tau^d_{\max}}{T_s} \right\rceil, \tag{1.1}$$

where $\tau^d_{\max}$ denotes the maximum delay spread of the multipath channel, T_s is the sampling period, and $\lceil \cdot \rceil$ is the ceiling operator, which rounds up the argument to the nearest greater integer. Obviously, this frequency selective MIMO channels incurs inter-symbol-interference (ISI) in the time domain known as temporal interference and co-channel-interference (CCI) or spatial interference in the spatial dimension. In order to mitigate both interference terms — often terminologically combined as spatio-temporal interference — and consequently achieve higher spectral efficiency of the overall MIMO system, it is crucial to develop sophisticated signal processing algorithms for transceiver designs of a precoder and/or an equaliser, in order to achieve processing for adequate retrieval of ba-

seband signals [2].

MIMO gains are mainly due to the fact that a rich scattering environment provides independent transmission paths forming a multichannel system that permits diversity. This gain promises significant improvements in terms of spectral efficiency achieved through maximising the multiplexing gain, known as spatial multiplexing, or maximising the diversity gain by enhancing the link reliability, as for example in the case of space-time coding. In the following, both multiplexing and diversity gains are briefly highlighted.

- **Multiplexing gain** is achieved by exploiting the spatial dimension for transmitting several independent substreams of data across a MIMO channel. As discussed earlier, the improvement in capacity increases linearly with the minimum number of antennas at both transmit and receive sides. In order to optimally translate this capacity gain into a multiplexing gain, a good transceiver design has to incorporate an efficient precoder and/or equaliser to create independent subchannels — by decoupling the MIMO system or providing suitable spatial interference cancellation — over which signals can be spatially multiplexed.

- **Diversity gain** describes the enhancement in link reliability resulting from multiple transmission of the same information over independently fading paths. Diversity gain is achieved as the increase in probability that at least one path of the MIMO channel will not be in a deep fade at any given time instance. This form of spatial diversity decreases the fluctuations that may be experienced in the received signal power and helps to provide an instantaneous link-reliable path.

Sometimes array gain is noted as another form of exploiting diversity, whereby the coherent combination of signals leads to an enhanced SNR and therefore improved link reliability to what is aimed for by maximising the diversity gain [9].

In this thesis, the aim is to consider methods for maximising the multiplexing gain for a frequency-selective MIMO channel.

The design of block-based precoding and equalisation schemes for enhancing the multiplexing gain over broadband MIMO channels has been widely addressed in the literature and resulted in a number of useful filter-bank based solutions obtained for different optimisation criteria [10, 11], of which orthogonal frequency-division multiplexing (OFDM) [12] is a subset. The drawback of a block-based design is that the first number of degrees of freedom have to be spent invariably

on the cancellation of inter-block-interference. It is only once inter-block interference (IBI) is removed in a zero-forcing fashion, that the optimality criterion, such as in the MMSE sense, can be applied.

Typical non-block based precoding and equalisation approaches for the broadband case are scarce and use mostly decision feedback equalisation (DFE) [13], V-BLAST approaches [14] adapted to the broadband case, or a mixture thereof [15], as well as Tomlinson-Harashima precoding (THP) [16, 17]. These methods do not require a guard interval, can be globally optimised w.r.t. to e.g. mean squared error (MSE), and can therefore potentially achieve a higher spectral efficiency than block-based approaches. The drawback of these schemes is the large effort in determining the optimum detection order in both space and time, often motivating the adoption of suboptimal approaches [14, 17].

Besides spectral efficiency, which is the primary concern in the design of future wireless communication systems, transmission power is another important issue. Transmission power is controlled in order to limit interference in multiuser scenarios or minimise the radiation due to perceived health influences, and extend the battery life-time of portable wireless devices. For multichannel systems, where parallel subchannels available for communications are characterised by different gains and SNRs, the role of transmit power allocation among these subchannels becomes a key issue in realising higher data rates or enhanced quality of service (QoS). This can be achieved through adaptive bit loading schemes which however requires the availability of channel state information (CSI) at the transmitter. Without the knowledge of CSI at the transmitter, non-adaptive power allocation — such as uniform power allocation (UPA) — is generally a suboptimal bit allocation scheme resulting in reduced performance. Knowledge of CSI at the transmitter is not a realistic assumption for time-varying channels unless the channel can be regarded as time invariant for a sufficiently long period. Otherwise it can be modelled by resorting to ensemble approximation of some invariant parameters such as mean and variance that can be estimated and employed to predict the channel evolution with sufficient accuracy [11]. This form of statistical CSI can be either obtained at the transmitter through sounding experiments prior to the information transmission phase, or it can be passed from the receiver to the transmitter if a feedback channel is available [8].

Therefore, in this thesis, we will focus on exploiting the multiplexing gain of MIMO systems by proposing a non-block based approach to precoding and/or equalisation. This approach is based on a generalisation of the singular value decomposition (SVD) — optimal in many senses such as mutual information, ca-

pacity, maximum likelihood, etc., to enable communication over a narrowband MIMO channel [18] — to the broadband case. A recently proposed broadband SVD (BSVD) [19] is applied to decouple the broadband MIMO system into frequency-selective single-input single-output (SISO) subchannels of ordered quality. Instead of linear processing as proposed in [20, 21], here each broadband SISO subchannel is equalised using a DFE or non-linear THP [22, 23], whereby the decision delay can be independently optimised for every subchannel. Moreover, power and bit allocation schemes are also proposed to efficiently and adaptively maximise the overall data throughput of the outcome subchannels.

1.2 Thesis Contributions

The following contributions are considered novel to the best of our knowledge.

- **Efficient THP precoding ordering [24]**
  A THP system for a MIMO flat-fading channel with a simple precoding ordering scheme is proposed. Inspired by a modified Gram-Schmidt algorithm to compute the QR decomposition, the maximisation of diagonal entries of the R-factor is performed in every orthogonalisation step. This was tested for the equalisation case [25] and we extend this for the precoding case by examining the influence on a THP system. Compared to the optimal ordering of V-BLAST detection, this precoding order demonstrates comparable results, which are however reached via a much simplified ordering algorithm.

- **A non-linear BSVD-based precoder and equaliser design with a heuristic bit loading and simplified processing [26, 27, 28]**
  A new non-block based precoding method for MIMO frequency-selective channels based on a BSVD algorithm is proposed. This method is a two-step approach. Firstly the broadband MIMO channel is decoupled into a number of independent dispersive spectrally majorised SISO subchannels using the BSVD algorithm. We thereafter apply the non-linear THP precoding to mitigate the dispersiveness (ISI) of these SISO subchannels. Bit loading is proposed to optimally utilise the spectral majorisation of the resulting SISO subchannels in a heuristic fashion. This method is benchmarked against recent results of both MMSE linear and THP designs for frequency-selective MIMO channels. Simulation results show that an improved BER can be achieved especially for higher throughput targets compared to state-of-the-art benchmarks. The overall system is bandwidth efficient

as it does not rely on guard periods, such as found in linear block-based transceiver approaches. The advantage over existing MIMO-DFE, THP, or V-BLAST systems is that the determination of the detection order is much simplified, as optimisation only has to be performed in the temporal dimension of each individual SISO subchannel rather than in the spatio-temporal domain. Finally, we investigate the influence of insufficient diagonalisation by the BSVD algorithm on system performance, which can arise due to insufficient CSI or the desire to reduce the computational steps and order of the BSVD algorithm.

- **Greedy (incremental) power allocation algorithm with BER improvements [29, 30]**
  The rate maximisation problem of a multichannel/multicarrier system is considered. An optimal greedy power allocation (GPA) algorithm is proposed with the design constrained by the target BER, the total power budget, and fixed discrete modulation orders. The key aspect of this algorithm lies in adjusting the power to fulfil the BER constraint as best as possible across all subchannels resulting in a uniform power allocation (UPA) scheme. Generally, some excess power remains unused which is iteratively allocated according to the greedy approach. This method is compared to other existing constrained mean-BER greedy bit allocation (GBA) schemes showing advantages of the GPA algorithm in terms of data throughput and power conservation. Finally, once the design constraints are satisfied, the remaining power is utilised to improve the mean BER in two possible ways, leading to improved performance of both GPA and UPA algorithms. This redistribution is analysed for fairness in BER performance across all active subchannels using the bisection method.

- **Reduced-complexity schemes for greedy power allocation for MIMO and multicarrier systems [31, 32, 33]**
  The implementation of the above GPA algorithm requires, at each iteration step of the bit allocation, a global search for the subchannel that requires the least power to achieve an improvement. For multicarrier systems with a considerably large number of subcarriers such as OFDM for digital video broadcast [34, 35, 36] this algorithm becomes computationally inefficient. Therefore we propose reduced-complexity schemes for the optimal GPA algorithm. Three suboptimal schemes are suggested, which independently perform GPA on subsets of subchannels only. These subsets are formed

in an initialisation step of a UPA algorithm by considering the QAM level boundaries of a given target BER. We demonstrate by analysis and simulation how these schemes can significantly reduce the computational complexity. Two of the proposed algorithms can achieve near optimal performance by including a transfer of residual power between subsets at the expense of a very small extra cost. Numerical results show that the two near optimal schemes perform best in two separate and distinct SNR regions. A complexity reduction figure of an order of magnitude can be reached with a very small degradation in data throughput provided that the proper algorithmic version is chosen.

1.3 Thesis Organisation

The remainder of this thesis is organised as follows.

Chapter 2 addresses a number of linear precoding and equalisation methods for narrowband and broadband MIMO channels. Analysis for equalisation of narrowband (i.e., frequency-flat) channels is provided for both ZF and MMSE criteria and supported by simulation results. For broadband or frequency-selective channels, both block-based methods such as OFDM and non-block based transmission schemes, including a recently developed BSVD algorithm, are reviewed.

Chapter 3 proposes non-linear precoding and equalisation approaches for broadband MIMO channels. The first part of this Chapter is concerned with flat-fading MIMO channels with emphasis on the impact of precoding ordering on BER performance. Secondly, based on the BSVD algorithm, a broadband MIMO channel is decoupled into a number of independent dispersive spectrally majorised SISO subchannels over which either THP or DFE is used as a non-linear precoder or equaliser to mitigate ISI incurred by these subchannels. We focus on THP schemes since better performance can be achieved by overcoming the common problem of DFE's error propagation. Heuristic bit loading is applied for the resulting ISI-free SISO subchannels to efficiently utilise the inherent spectral majorisation property of the BSVD algorithm. Simulation results show that better performance can be achieved when compared with a state-of-the-art broadband MIMO techniques. Finally, the impact of a premature truncation in the BSVD's computation, resulting in a poorer decoupling, is investigated in terms of BER performance and computational cost. The same effect would also be incurred if the BSVD is applied in the presence of channel estimation errors.

Chapter 4 considers discrete bit and power loading schemes to maximise the data throughput of a multichannel system. This problem arises in our BSVD-based approach, but also in general for transmultiplexed systems such as OFDM. Different from the standard water-filling algorithm, which assumes real-valued data rates and thus reveals unsatisfactory results due to the indispensable final rounding step, greedy approaches offer optimal discrete data throughputs through an incremental allocation of data bits. Two greedy algorithms — both aiming to maximise the data rate under a specified target BER constraint — are studied and compared with the non-adaptive uniform power allocation, of which one controls the power allocation (GPA) and the other concerns the bit allocation (GBA). Results show that GPA performs better than GBA in terms of achieved data througput, while both achieve higher data throughput than UPA. Since the bit allocation strategy of both GPA and UPA algorithms is to implement the BER constraint with its maximum target, some excess power is generally saved as a result. This power is reconsidered by a second optimisation step to improve the achieved mean BER.

Chapter 5 explores reduced complexity schemes of the optimal discrete GPA algorithm presented in Chapter 4. Compared to the standard GPA three suboptimal schemes are proposed, which perform GPA on subsets of subchannels only. These subsets are created by considering the minimum SNR boundaries of QAM levels for a given target BER. The common theme amongst the proposed algorithms is to restrict the greedy algorithm to these subsets which are grouped according to the QAM level assigned to them in the UPA stage. In order to exploit excess (i.e. unused) power in each subset, two algorithms are proposed which carry left-over power forward into the next subset that is optimised by a local greedy algorithm. In the first proposed, the algorithm moves the left-over power upwards from the lowest to the highest subset, whereas the second scheme moves the power from the highest towards the lower subsets. Computational complexity of the proposed schemes is analysed and evaluated revealing that a significant reduction in complexity can be achieved especially for a large numbers of subchannels and at high SNRs. Highlighted by simulation results, the two proposed algorithms can achieve near optimal performance in two separate and distinctive SNR regions, however, at a much reduced complexity.

Chapter 6 summarises the work presented in this dissertation, draws final conclusions, and provides suggestions for future research leading on from this thesis.

Chapter 2

Linear Precoding and Equalisation Techniques

MIMO systems promise significant capacity improvements which can facilitate parallel transmission of different data streams [4, 5]. In order to realise the anticipated multiplexing gain, separation of these data streams is required either in the transmitter or at the receiver leading to different precoding or equalisation schemes, respectively (see e.g. [13]). Based on the strategy of how to equalise the communication channel and separate the multiple data streams, these schemes can be broadly divided into linear and non-linear approaches. It is well known that linear precoding and equalisation methods have lower complexity than non-linear methods, however, they often cannot achieve the same performance of data detection that is produced by non-linear approaches [37].

In this Chapter, mitigation of interference and noise of the communication channel is achieved using linear precoding and equalisation strategies. Both narrowband and broadband MIMO channel models are considered. Moreover, block-based and non-block based approaches are addressed and highlighted with some simulation results.

2.1 Channel Model

A MIMO frequency selective channel created by N_t transmit and N_r receive antennas as shown in Fig. 2.1 can be described by a finite impulse response (FIR) filter $\mathbf{H}[n]$ of order Q or its corresponding transfer function $\mathbf{H}(z)$ given by

$$\mathbf{H}(z) = \sum_{n=0}^{Q} z^{-n} \mathbf{H}[n] \ . \tag{2.1}$$

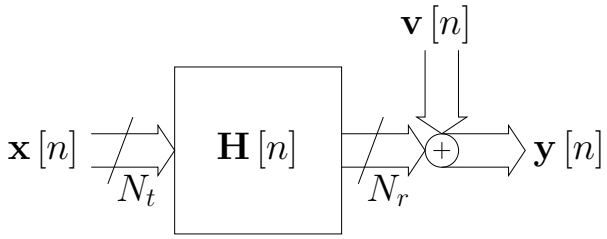

Figure 2.1: Generalised MIMO ISI channel model with N_t transmit and N_r receive antennas.

The matrix-valued character of (2.1) results in a transmission system suffering from both spatial interference in terms of co-channel interference (CCI) as well as temporal interference in terms of inter-symbol interference (ISI) such that the received data vector $\mathbf{y}[n] \in \mathbb{C}^{N_r}$ is given by

$$\mathbf{y}[n] = \sum_{\nu=0}^{Q} \mathbf{H}[\nu] \cdot \mathbf{x}[n-\nu] + \mathbf{v}[n]\,. \tag{2.2}$$

Where $\mathbf{x}[n] \in \mathbb{C}^{N_t}$ is the transmitted data vector at symbol period n and $\mathbf{v}[n] \in \mathbb{C}^{N_r}$ is additive white Gaussian noise (AWGN) at the receiver, which we assume to be spatially and temporally uncorrelated, i.e. $\mathbb{E}\left[\mathbf{v}[n] \cdot \mathbf{v}^{\mathrm{H}}[n-\tau]\right] = \sigma_v^2 \delta[\tau]\, \mathbf{I}_{N_r}$. In (2.1), $\mathbf{H}[n]$ is an $N_r \times N_t$ matrix containing the channel impulse response coefficients at time period n such that $h_{ij}[n]$ is the nth complex baseband channel coefficient of the FIR filter describing the path from the jth transmit antenna to the ith receive antenna.

2.2 Precoding and Equalisation for Narrowband Channels

Linear algorithms are based on a linear computation of the channel matrix using linear algebra (LA) manipulation, hence easy to implement [38]. Fig. 2.2 constitutes the general model of a linear equalisation system, whereby the interference

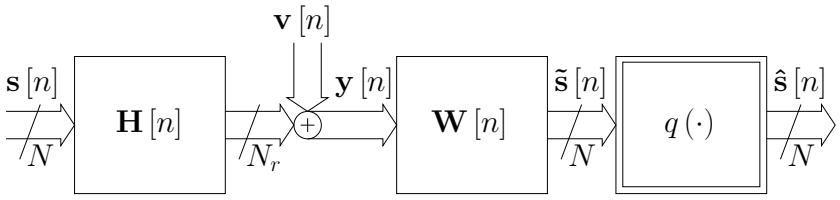

Figure 2.2: General linear equalisation transceiver system model, where $\mathbf{s}[n] = \mathbf{x}[n]$ in Fig. 2.1.

caused by the MIMO channel $\mathbf{H}[n] \in \mathbb{C}^{N_r \times N}$ is mitigated at the receiver using a linear equaliser $\mathbf{W}[n] \in \mathbb{C}^{N \times N_r}$. The operator $q(\cdot)$ represents the decision device (or quantiser) which maps the entries of $\tilde{\mathbf{s}}[n]$ to the nearest alphabet defined by the constellation set $\mathcal{S}$ corresponding to the used M-QAM modulation scheme, which results in a receiver's replica $\hat{\mathbf{s}}[n]$ of the transmitted data vector $\mathbf{s}[n]$. In the following, the narrowband MIMO channel equalisation case is considered, whereby the time index n is dropped from the notation leading to the simple communication system depicted in Fig. 2.3 and defined by a reduced version of (2.2) given as

$$\mathbf{y} = \mathbf{H}\mathbf{s} + \mathbf{v}\,. \tag{2.3}$$

Where $\mathbf{y}$ is the noisy N_r-dimensional received vector of the N_t-dimensional transmit vector $\mathbf{s}$ over the $N_r \times N_t$ flat-fading channel $\mathbf{H}$ after adding the noise term $\mathbf{v}$ with dimension $N_r \times 1$. The channel entries h_{ij} are assumed i.i.d. complex Gaussian random variables with zero-mean and unit-variance $\mathbb{E}\left[|h_{ij}|^2\right] = 1$, i.e., $h_{ij} \in \mathcal{CN}(0,1)$, this is a common assumption in the literature (see for example [14, 39]). The transmitted data vector $\mathbf{s} \in \mathcal{S}^N$ is assumed to be a spatially-uncorrelated and uniformly distributed complex random vector process with zero-mean and variance σ_s^2 (i.e. $\mathbf{R}_{ss} = \mathbb{E}\left[\mathbf{s}\mathbf{s}^{\mathrm{H}}\right] = \sigma_s^2\mathbf{I}_{N_t}$), while the noise vector $\mathbf{v}$ is drawn from $\mathcal{CN}(0,\sigma_v^2)$, or equivalently $\mathbf{R}_{vv} = \mathbb{E}\left[\mathbf{v}\mathbf{v}^{\mathrm{H}}\right] = \sigma_v^2\mathbf{I}_{N_r}$.

The equaliser $\mathbf{W}^{\mathrm{H}}$ is used to decouple the channel $\mathbf{H}$ and produce an estimate $\tilde{\mathbf{s}}$ of the transmitted data vector $\mathbf{s}$ under the design criterion of either zero forcing (ZF) or minimum mean square error (MMSE). In the following both schemes will be analysed and compared.

2.2.1 Zero Forcing Equaliser

The ZF approach is a very simple linear filter scheme that projects the channel vectors of each receiver onto the subspace orthogonal to that spanned by the channel vectors of all other receivers [40]. This is accomplished mathematically

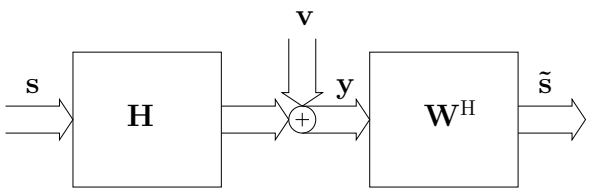

Figure 2.3: Narrowband equivalent linear equalisation system model of Fig. 2.2 with equaliser $\mathbf{W}^{\mathrm{H}}$.

by computing the Moore-Penrose pseudo-inverse of the channel matrix, $\mathbf{H}^{+}$. Accordingly, nulling in the ZF criterion is equivalent to completely cancelling the interference contributed by streams of other users (transmitting antennas) [41]. This has the advantage of creating independent virtual parallel subchannels. However, ZF receivers generally suffer from noise enhancement [42, 43]. The ZF filter is therefore given by

$$\mathbf{W}_{\mathrm{ZF}}^{\mathrm{H}} = \mathbf{H}^{+} = \left(\mathbf{H}^{\mathrm{H}}\mathbf{H}\right)^{-1}\mathbf{H}^{\mathrm{H}}, \tag{2.4}$$

and its output as

$$\tilde{\mathbf{s}}_{\mathrm{ZF}} = \mathbf{W}_{\mathrm{ZF}}^{\mathrm{H}}\mathbf{y} = \mathbf{s} + \left(\mathbf{H}^{\mathrm{H}}\mathbf{H}\right)^{-1}\mathbf{H}^{\mathrm{H}}\mathbf{v}\,. \tag{2.5}$$

The error covariance matrix is therefore given by

$$\mathbf{\Phi}_{\mathrm{ZF}} = \mathbb{E}\left[\left(\tilde{\mathbf{s}}_{\mathrm{ZF}} - \mathbf{s}\right)\left(\tilde{\mathbf{s}}_{\mathrm{ZF}} - \mathbf{s}\right)^{\mathrm{H}}\right] = \sigma_v^2\left(\mathbf{H}^{\mathrm{H}}\mathbf{H}\right)^{-1}\,. \tag{2.6}$$

Note that since the ZF criterion nulls completely the spatial interference, it is expected that the resulting error covariance matrix in (2.6) equals exactly the covariance matrix of the noise $\mathbf{v}$ at the output of $\mathbf{W}_{\mathrm{ZF}}^{\mathrm{H}}$.

Noticeably, by referring to (2.6), it is evident that small eigenvalues of $\mathbf{H}^{\mathrm{H}}\mathbf{H}$ will lead to significant errors due to noise amplification. This, in fact, represents the main drawback of the ZF filter design as it disregards the noise term from the overall design and focuses only on perfectly removing the interference term from signal $\mathbf{s}$.

2.2.2 Minimum Mean Square Error Equaliser

The problem of noise enhancement of the ZF filter has already been addressed. An improved performance can be achieved by considering the noise term in the design of the linear filter $\mathbf{W}^{\mathrm{H}}$ of Fig. 2.3. This is achieved by the MMSE equaliser, whereby the filter design accounts for a trade-off between noise amplification and interference suppression [41]. The MMSE filter is obtained by solving for error minimisation of the error criterion defined by

$$\varphi = \mathbb{E}\left[\mathbf{e}^{\mathrm{H}}\mathbf{e}\right] = \mathrm{tr}\left(\mathbb{E}\left[\mathbf{e}\mathbf{e}^{\mathrm{H}}\right]\right), \tag{2.7}$$

where the error vector $\mathbf{e} \overset{d}{=} \mathbf{s} - \tilde{\mathbf{s}} = \mathbf{s} - \mathbf{W}^{\mathrm{H}}\mathbf{y}$. Minimisation of φ leads to the Wiener-Hopf equation [44]

$$\mathbf{W}_{\mathrm{MMSE}}^{\mathrm{H}}\mathbf{R}_{yy} = \mathbf{R}_{sy}\,. \tag{2.8}$$

This equation can also be obtained directly by invoking the orthogonality principle [45, 46] which states that the estimate $\tilde{\mathbf{s}}$ achieves minimum mean square error if the error sequence $\mathbf{e}$ is orthogonal to the observation $\mathbf{y}$, i.e., their cross-correlation matrix has to be the zero matrix $\mathbb{E}\left[\mathbf{e}\mathbf{y}^{\mathrm{H}}\right] = \mathbf{0}$. After some algebraic manipulation, the linear MMSE-sense filter is given by

$$\mathbf{W}_{\mathrm{MMSE}}^{\mathrm{H}} = \left(\mathbf{H}^{\mathrm{H}}\mathbf{H} + \frac{\sigma_v^2}{\sigma_s^2}\mathbf{I}_{N_t}\right)^{-1}\mathbf{H}^{\mathrm{H}}, \tag{2.9}$$

the derivation of which is continued in Appendix A.1. Similar to (2.6) it is not difficult to obtain the error covariance matrix using the MMSE filter in (2.9) as [41]

$$\mathbf{\Phi}_{\mathrm{MMSE}} = \sigma_v^2\left(\mathbf{H}^{\mathrm{H}}\mathbf{H} + \frac{\sigma_v^2}{\sigma_s^2}\mathbf{I}_{N_t}\right)^{-1}. \tag{2.10}$$

Obviously by comparing (2.10) and (2.6), the error rate of the MMSE solution $\mathbf{\Phi}_{\mathrm{MMSE}}$ is less than its ZF counterpart $\mathbf{\Phi}_{\mathrm{ZF}}$ specifically at low signal-to-noise ratio (SNR) defined as

$$\mathrm{SNR} = \frac{\mathbb{E}\left[\|\mathbf{s}\|_2^2\right]}{\mathbb{E}\left[\|\mathbf{v}\|_2^2\right]} = \frac{\mathrm{tr}\left(\mathbf{R}_{ss}\right)}{\mathrm{tr}\left(\mathbf{R}_{vv}\right)} = \frac{\sigma_s^2 N_t}{\sigma_v^2 N_r} = {}^{P_{\mathrm{budget}}}\!/_{\mathcal{N}_0}, \tag{2.11}$$

where P_{budget} is the total transmit power budget and $\mathcal{N}_0$ is the total noise power at the receiver. At high SNR, the second term in (2.10) will vanish, which leads to asymptotic error performance similar to the ZF filter. Compared to the ZF filter in (2.4), the MMSE filter in (2.9) can be viewed as a "regularised" expression by a diagonal matrix of entries $\frac{\sigma_v^2}{\sigma_s^2}$, which is equal to the reciprocal of the SNR in (2.11) for equal numbers of transmit and receive antennas. This regularisation introduces a bias that gives a much more reliable result than (2.4) when the matrix is ill-conditioned[1] and/or the estimation of the channel is noisy.

2.2.3 Precoding

So far the equalisation problem of the communication channel is performed at the receiver. Before proceeding further, it is worth noting that the detailed analysis presented above for both ZF and MMSE equalisation can also be derived in case of transmit processing [47, 48, 13], i.e. pre-equalisation (precoding). The transmitter in this case pre-distorts the transmit data in such a way that it cuts

[1] A matrix is said to be ill-conditioned if its condition number (the absolute ratio between the maximum and minimum eigenvalues) is too large.

the interference seen at the receiver to a tolerable level. However, this necessitates the knowledge of channel state information (CSI) to be available at the transmit side as well. In addition, a careful design of the precoder has to consider a scaling factor to control the transmit power not to exceed P_{budget}. Furthermore, for better performance of precoding systems, a sort of power allocation scheme should be incorporated otherwise most of the transmit power will be exerted on weak eigenmodes thus wasting energy. In Sec. 2.3.3, transmit processing for the broadband case will be discussed in detail.

2.2.4 Joint Transmit/Receive Processing

Unlike channel equalisation at the receiver or precoding at the transmitter, the task of interference cancellation can be jointly shared between transmitter and receiver if CSI is assumed to be available at both sides. In fact, CSI can be obtained at the transmitter by assuming channel reciprocity in case of time division duplex systems or through feedback in frequency division duplex systems. To this end a popular strategy based on the singular value decomposition (SVD) technique of the channel matrix $\mathbf{H}$ can be used to decompose the MIMO channel into a set of SISO subchannels, for which power loading schemes (e.g. water-filling) can be used to maximise the channel capacity. As each subchannel has a different SNR value, variable-rate coding is usually used among the data streams, which increases the transceiver complexity [49]. The SVD scheme can be formulated by factorising $\mathbf{H}$ as

$$\mathbf{H} = \mathbf{U}\mathbf{\Sigma}\mathbf{V}^{\mathrm{H}}, \tag{2.12}$$

where $\mathbf{U} \in \mathbb{C}^{N_r \times N_r}$ and $\mathbf{V} \in \mathbb{C}^{N_t \times N_t}$ are unitary[2] matrices while $\mathbf{\Sigma} \in \mathbb{C}^{N_r \times N_t}$ is a diagonal matrix that contains the singular values of $\mathbf{H}$, $\sigma_i, i = 1, \cdots, N$ with

$$N = \min\left(N_t, N_r\right), \tag{2.13}$$

sorted in a descending order such that $\sigma_1 \geq \sigma_2 \geq \cdots$.

Now in order to decompose $\mathbf{H}$ into its singular values $\mathbf{\Sigma}$, a precoder $\mathbf{V}$ and an equaliser $\mathbf{U}^{\mathrm{H}}$ can be jointly applied at the transmitter and at the receiver, respectively, such that the overall effective channel is given as

$$\mathbf{H}_{\text{eff}} = \mathbf{U}^{\mathrm{H}}\mathbf{H}\mathbf{V} = \mathbf{U}^{\mathrm{H}}\mathbf{U}\mathbf{\Sigma}\mathbf{V}^{\mathrm{H}}\mathbf{V} = \mathbf{\Sigma}, \tag{2.14}$$

[2] A matrix $\mathbf{A}$ is said to be unitary if $\mathbf{A}\mathbf{A}^{\mathrm{H}} = \mathbf{A}^{\mathrm{H}}\mathbf{A} = \mathbf{I}$.

thus decoupling the MIMO system. This, in fact, is equivalent to transmitting over N independent parallel subchannels with different gains $\sigma_i, i = 1, \cdots, N$. Here, in contrast to linear precoding and equalisation neither transmit power is increased, nor channel noise is amplified due to the unitarity of precoder and equaliser [16, 50]. It is also worth mentioning that applying SVD is optimal in many senses (e.g. mutual information, capacity, Maximum Likelihood, etc.) to enable communication over a narrowband MIMO channel [18] for scenarios where cooperative transmit-receive processing is possible [51, 52].

Noticeably, transmit processing as well as receive processing can be regarded as a constrained category of the joint optimisation of transmit and receive filters, hence they act as suboptimum solutions of the joint optimisation case [48]. This is true of course if a sort of power and/or bit loading scheme is considered to either optimise (maximise) data rate under a constrained bit error ratio (BER) or minimise BER for a given target data rate. However, if all subchannels are loaded with the same data bits and the transmit power is uniformly allocated across all subchannels this may result in inferior performance of the SVD scheme as will be shown next.

A comparison of ZF and MMSE linear receivers along with the SVD scheme for a 4×4 MIMO system, where $N_t = N_r = 4$, using QPSK transmission is shown in Fig. 2.4. Results are obtained by averaging over 1,000 different channel realisations of a flat-fading channel where channel entries are drawn from a complex Gaussian random process with zero-mean and unit-variance, i.e. $h_{ij} \in \mathcal{CN}(0, 1)$. It is clearly noted that the MMSE filter outperforms its ZF counterpart and their BER performance converges at higher SNR where the regularisation factor $\sigma_v^2/\sigma_s^2 \ll 1$. The BER of the SVD scheme is dominated by the error performance at the lowest subchannel gain, σ_4 in this case as discussed above. Different performances of different subchannels are also motivated by Fig. 2.5 where individual layers of the undecided substreams $\tilde{s}_i, i = 1, \ldots, 4$ are separately plotted showing difficult correct decisions arising for layer four.

2.3 Precoding and Equalisation for Broadband Channels

In Section 2.2 precoding and equalisation schemes are discussed for the case of narrowband MIMO systems where the channel is assumed flat-fading. However in recent wireless communications and with the increased demand for higher data rate applications the channel coherence bandwidth can no longer be assumed

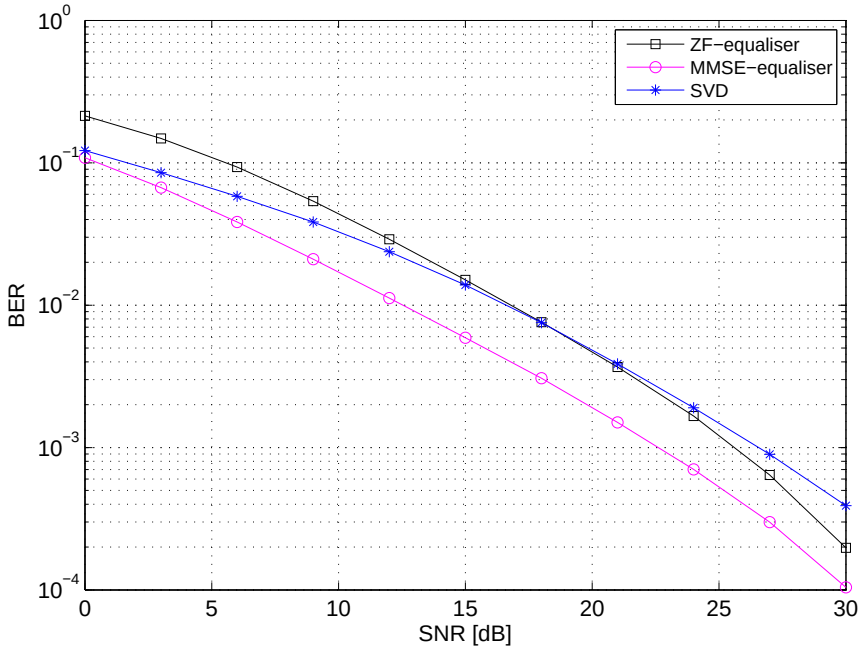

Figure 2.4: Linear ZF and MMSE equalisation performance compared with the SVD scheme of a 4×4 MIMO system.

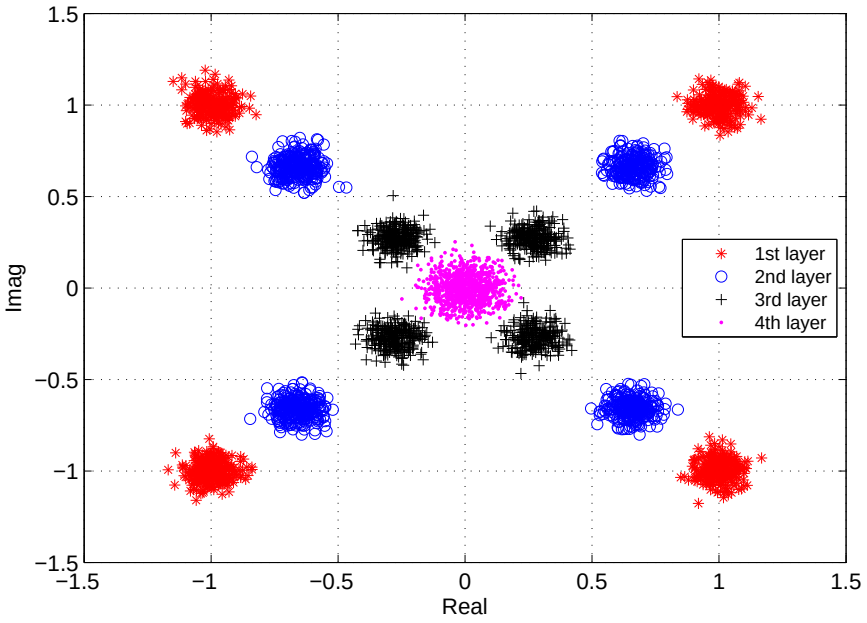

(a)

Figure 2.5: Undecided symbols $\tilde{\mathbf{s}}$ of the SVD scheme for the different data layers of a 4×4 MIMO system at SNR $= 25\,\mathrm{dB}$. Constellation moduli equal the squared singular values σ_i^2 of the four subchannels.

flat. Therefore, in addition to spatial interference between data substreams of adjacent transmit/receive antenna pairs, inter-symbol-interference (ISI) due to channel frequency selectivity dispersion is incurred. MIMO systems with such interference scenarios are usually referred to as broadband MIMO or MIMO ISI systems whereas the resulting interference is known in the literature as spatio-temporal interference [53, 54]. Hence, next-generation wireless communication systems featuring high-rate transmission schemes have to consider such MIMO ISI channels and aim to minimise the impact of both CCI and ISI plus the channel noise for reliable data detection.

2.3.1 Linear Block Transmission

Given is the broadband MIMO channel in (2.1) of order Q. By assuming stationarity, this channel can additionally be multiplexed into P polyphase components, resulting in a block pseudo-circulant matrix $\mathbf{H}^{(P)}(z) \in \mathbb{C}^{PN_r \times PN_t}(z)$ of order $\lceil \frac{Q}{P} \rceil$ expressed as

$$\mathbf{H}^{(P)}(z) = \begin{bmatrix} \mathbf{H}_0^{(P)}(z) & z^{-1}\mathbf{H}_{P-1}^{(P)}(z) & \cdots & z^{-1}\mathbf{H}_1^{(P)}(z) \\ \mathbf{H}_1^{(P)}(z) & \mathbf{H}_0^{(P)}(z) & \cdots & \vdots \\ \vdots & \ddots & \ddots & z^{-1}\mathbf{H}_{P-1}^{(P)}(z) \\ \mathbf{H}_{P-1}^{(P)}(z) & \cdots & \mathbf{H}_1^{(P)}(z) & \mathbf{H}_0^{(P)}(z) \end{bmatrix}, \tag{2.15}$$

with matrix-valued polyphase components $\mathbf{H}_p^{(P)}(z)$ such that

$$\mathbf{H}(z) = \sum_{p=0}^{P-1} z^{-p}\mathbf{H}_p^{(P)}(z^P)\,. \tag{2.16}$$

The selection of P allows a trade-off between the dimension and order of the MIMO system matrix $\mathbf{H}^{(P)}(z)$. Note however that for a polynomial matrix $\mathbf{H}(z)$ with $Q > 0$, $\mathbf{H}^{(P)}(z)$ will also be polynomial even for large P. With $\mathbf{H}^{(P)}[n] \rightleftharpoons \mathbf{H}^{(P)}(z)$, the received data vector $\mathbf{y}^{(P)}[m] \in \mathbb{C}^{PN_r}$ in (2.2) can be rewritten as

$$\mathbf{y}^{(P)}[m] = \sum_{\nu=0}^{\lceil Q/P \rceil} \mathbf{H}^{(P)}[\nu] \cdot \mathbf{s}^{(P)}[m-\nu] + \mathbf{v}^{(P)}[m], \tag{2.17}$$

where

$$\mathbf{s}^{(P)}[m] \in \mathcal{S}^{PN_t} = \begin{bmatrix} \mathbf{s}\,[mP-P+1] \\ \mathbf{s}\,[mP-P+2] \\ \vdots \\ \mathbf{s}\,[mP] \end{bmatrix},\ \mathbf{v}^{(P)}[m] \in \mathbb{C}^{PN_r} = \begin{bmatrix} \mathbf{v}\,[mP-P+1] \\ \mathbf{v}\,[mP-P+2] \\ \vdots \\ \mathbf{v}\,[mP] \end{bmatrix}$$

are, respectively, the transmitted data vector and the noise vector at time period $m = P \cdot n$.

Block transmission utilises the sparseness of $\mathbf{H}^{(P)}(z)$ for $P > Q$ in combination with the insertion of guard intervals to remove interference between successively transmitted data vectors $\mathbf{s}^{(P)}[m]$, known as inter-block interference (IBI). For $P > Q$, (2.17) reduces to

$$\mathbf{y}^{(P)}[m] = \mathbf{H}^{(P)}[0] \cdot \mathbf{s}^{(P)}[m] + \mathbf{H}^{(P)}[1] \cdot \mathbf{s}^{(P)}[m-1] + \mathbf{v}^{(P)}[m], \tag{2.18}$$

whereby the term $\mathbf{H}^{(P)}[1] \cdot \mathbf{s}^{(P)}[m-1]$ represents IBI by the data vector $\mathbf{s}^{(P)}[m-1]$, which has been transmitted during the previous time slot $m-1$. The matrix $\mathbf{H}^{(P)}[1]$ is block-banded and upper right triangular with

$$\mathbf{H}_1 = \begin{bmatrix} \mathbf{0} & \cdots & \mathbf{0} & \mathbf{H}_L^{(P)}[0] & \cdots & \mathbf{H}_1^{(P)}[0] \\ \vdots & \ddots & & \ddots & \ddots & \vdots \\ \vdots & & \ddots & & \ddots & \mathbf{H}_L^{(P)}[0] \\ \mathbf{0} & & & \ddots & & \mathbf{0} \\ \vdots & \ddots & & & \ddots & \vdots \\ \mathbf{0} & \cdots & \mathbf{0} & \cdots & \cdots & \mathbf{0} \end{bmatrix} \tag{2.19}$$

such that IBI can be suppressed by either inserting $(Q-1)N_t$ trailing zeros (TZ) into the transmit vector $\mathbf{s}^{(P)}[m]$, or by discarding the first $(Q-1)N_r$ elements of the receive vector $\mathbf{y}^{(P)}[m]$, which is referred to the leading zeros (LZ) approach [55, 11].

In case of the availability of CSI at both transmitter and receiver, the remaining system can be decoupled by performing an SVD of the now IBI-free relation between $\mathbf{y}^{(P)}[m]$ and $\mathbf{s}^{(P)}[m]$. If no CSI is available, specific channel-independent schemes can be utilised for decoupling the overall system, such as OFDM, which is a subset of TZ block transmission.

The drawback of block-transmission schemes lies in the required inclusion of redundancy, which in first place has to be spent for IBI cancellation, whereby

any remaining degrees of freedom can be applied to noise suppression and to the exploitation of strong eigenmodes of the MIMO system.

2.3.2 OFDM in Brief

Orthogonal frequency division multiplexing (OFDM) [56, 57, 8] is a block-based multicarrier modulation scheme. It converts the broadband channel into a number of narrowband (flat-fading) subchannels over which blocks of data symbols are transmitted in parallel. With the aid of discrete Fourier transform (DFT) and inverse DFT (IDFT) operators, the OFDM transmission system can be implemented as shown in Fig 2.6 for a SISO channel $h\,[n]$. Theoretically, in order to obtain an IBI-free transmission, a redundancy cyclic prefix (CP) of length not less than the channel order has to be added to each transmitted block. By inserting CP at the transmitter and removing it at the receiver, circular convolution is converted to linear convolution. This CP redundancy, however, reduces the overall spectrum efficiency of a block-based transceiver system. Recently, it has been shown that the rate gain offered by CP of shorter lengths may exceed the losses due to both ISI and IBI [58, 59].

OFDM systems are coupled with two main problems, namely: i) peak-to-average power ratio (PAPR) and ii) sensitivity to synchronisation errors such as carrier-frequency offset (CFO). The PAPR problem arises due to the application of the IDFT at the OFDM modulator which results in a high dynamic range of the transmitted power at each antenna. Consequently transmitted signals are subjected to non-linear distortion of the transmit power amplifier. To avoid this, either the transmit power has to be scaled down or PAPR-reduction schemes have to be incorporated in OFDM systems [8].

Synchronisation is very important in OFDM-based systems since subcarriers need to remain orthogonal with a defined frequency spacing between them. Due to Doppler shifts and mismatch between transmit-receive local oscillators, a CFO may arise which will lead to non-orthogonality of subcarriers and subsequently inter-subcarrier interference. Often sophisticated CFO estimators to adjust the synchronisation of transmission are required [56].

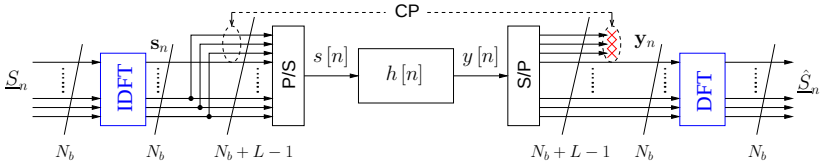

Figure 2.6: A SISO-OFDM system model.

2.3.3 MMSE Linear Precoder

The drawbacks of the above block-based transmission schemes lie in the required inclusion of redundancy to cancel IBI in the form of CP or either TZ or LZ for, respectively, OFDM or block transmission systems. In order to improve the spectrum efficiency, non-block based schemes that do not require any redundancy are of particular interest. In this Section a non-block based linear precoding scheme for the MIMO broadband channel in Section 2.1 is depicted in Fig. 2.7, where the transmitted signal $\mathbf{s}[n] \in \mathcal{S}^N$ is pre-processed by the FIR precoder

$$\mathbf{P}[n] = \sum_{l=0}^{L} \mathbf{P}_l \delta[n-l] \; . \tag{2.20}$$

Where L is the filter order and $\mathbf{P}_l \in \mathbb{C}^{N_t \times N}, l = 0, \cdots, L$ is the time slices of $\mathbf{P}[n]$. The filter output

$$\mathbf{x}[n] = \sum_{l=0}^{L} \mathbf{P}_l \mathbf{s}[n-l] \in \mathbb{C}^{N_t}$$

is then transmitted over an $N \times N_t$ MIMO ISI channel

$$\mathbf{H}[n] = \sum_{q=0}^{Q} \mathbf{H}_q \delta[n-q] \tag{2.21}$$

of order Q and channel responses $\mathbf{H}_q \in \mathbb{C}^{N_r \times N_t}$, where $N_r = N$ in this case (cf. Fig. 2.7), such that the received signal $\mathbf{y}[n] \in \mathbb{C}^N$ is given as

$$\begin{aligned} \mathbf{y}[n] &= \mathbf{H}[n] \star \mathbf{P}[n] \star \mathbf{s}[n] + \mathbf{v}[n] \, , \\ &= \sum_{q=0}^{Q} \sum_{l=0}^{L} \mathbf{H}_q \mathbf{P}_l \mathbf{s}[n-q-l] + \mathbf{v}[n] \, , \end{aligned} \tag{2.22}$$

where $\mathbf{v}[n]$ is, as above, representing the channel noise. A scalar receiver filter acting as an automatic gain control (AGC) $g \in \mathbb{C}$ is applied to $\mathbf{y}[n]$ resulting in estimates $\tilde{\mathbf{s}}[n] = g\mathbf{y}[n]$ of data symbols. These estimates are finally mapped to

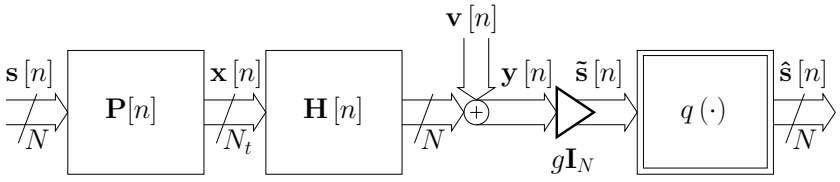

Figure 2.7: A typical linear broadband precoding system with $N_t \geq N_r = N$.

the nearest respective appropriate alphabets $\hat{\mathbf{s}}[n]$ using the decision (quantiser) device $q(\cdot)$.

As in Sec. 2.2.2, the MMSE solution can be obtained by formulating the mean square error (MSE) between the data symbol $\mathbf{s}[n]$ and its estimate $\tilde{\mathbf{s}}[n]$ under a total transmit power constraint such that

$$\begin{aligned} \{\mathbf{P}_{\text{opt}}[n], g_{\text{opt}}, \nu_{\text{opt}}\} &= \underset{\{\mathbf{P}[n],g,\nu\}}{\text{argmin}} \quad \mathbb{E}\left[\|\mathbf{s}[n-\nu]-\tilde{\mathbf{s}}[n]\|_2^2\right] \\ &\qquad \text{subject to} \quad \mathbb{E}\left[\|\mathbf{x}[n]\|_2^2\right] = P_{\text{budget}}, \end{aligned} \tag{2.23}$$

where a latency time ν is introduced in the above optimisation problem to account for the optimum decision delay [17]. Intuitively, the feasible range for the discrete ν is $[0, Q+L]$, i.e. $\nu \in \{0, 1, \cdots, Q+L\}$. In order to simplify the convolution operator in (2.22) in a matrix formalisation, the solution presented in [17] defines matrices

$$\begin{aligned} \mathbf{H} &= \sum_{q=0}^{Q} \left[\mathbf{0}_{L+1\times q}, \mathbf{I}_{L+1}, \mathbf{0}_{L+1\times Q-q}\right]^T \otimes \mathbf{H}_q \in \mathbb{C}^{N(Q+L+1)\times N_t(L+1)}, \\ \text{and} \quad \mathbf{P} &= \left[\mathbf{P}_0^T, \cdots, \mathbf{P}_L^T\right]^T \in \mathbb{C}^{N_t(L+1)\times N}, \end{aligned} \tag{2.24}$$

where $\otimes$ denotes the Kronecker product, such that the convolution coefficients of $\mathbf{H}[n] \star \mathbf{P}[n]$ in (2.22) are simply computed by the product $\mathbf{HP}$, that is, the ith $N \times N$ block element of $\mathbf{HP}$ is the ith coefficient $\sum_{q+l+1=i} \mathbf{H}_q\mathbf{P}_l$ of $\mathbf{H}[n] \star \mathbf{P}[n]$. Invoking (2.24) into (2.22) simplifies the computation of $\tilde{\mathbf{s}}[n]$ as

$$\tilde{\mathbf{s}}[n] = g\mathbf{y}[n] = g\sum_{i=0}^{Q+L} \boldsymbol{S}^{(i)}\mathbf{HPs}[n-i] + g\mathbf{v}[n], \tag{2.25}$$

where a selection matrix

$$\boldsymbol{S}^{(i)} = \boldsymbol{e}_{i+1}^T \otimes \mathbf{I}_N \in \{0,1\}^{N\times N(Q+L+1)} \tag{2.26}$$

is introduced to return the ith block rows of size N starting from the $(Ni+1)$th row to row $N(i+1)$ of a matrix when applied from left, with $\boldsymbol{e}_i \in \{0,1\}^{Q+L+1}$ being the ith column of the identity matrix $\mathbf{I}_{Q+L+1}$. Substituting (2.25) into (2.23), the MSE can be reformulated as

$$\begin{aligned} \mathbb{E}\left[\|\mathbf{s}[n-\nu]-\tilde{\mathbf{s}}[n]\|_2^2\right] &= \text{tr}(\mathbf{R}_{ss}) - \Re\left(\text{tr}\left(g\boldsymbol{S}^{(\nu)}\mathbf{HPR}_{ss}\right)\right) \\ &\quad + |g|^2\,\text{tr}(\mathbf{R}_{vv}) + |g|^2\,\mathbf{HPR}_{ss}\mathbf{P}^{\text{H}}\mathbf{H}^{\text{H}}, \end{aligned} \tag{2.27}$$

while the transmit power required for the constraint in 2.23 is given by

$$\mathbb{E}\left[\|\mathbf{x}[n]\|_2^2\right] = \mathrm{tr}\left(\mathbf{P}\mathbf{R}_{ss}\mathbf{P}^{\mathrm{H}}\right) . \tag{2.28}$$

Using the Lagrangian multiplier method, the optimised solution for $\mathbf{P}$ and g based on ν is derived in [48] and given in [17], respectively, as:

$$\mathbf{P}(\nu) = \frac{1}{g(\nu)}\mathbf{H}^{\mathrm{H}}\mathbf{A}^{-1}\mathbf{S}^{(\nu),T} \in \mathbb{C}^{N_t(L+1)\times N}, \tag{2.29a}$$

$$g(\nu) = \sqrt{\mathrm{tr}\left(\mathbf{H}\mathbf{H}^{\mathrm{H}}\mathbf{A}^{-2}\mathbf{S}^{(\nu),T}\mathbf{R}_{ss}\mathbf{S}^{(\nu)}\right)/P_{\mathrm{budget}}}\,, \tag{2.29b}$$

$$\nu_{\mathrm{opt}} = \underset{\nu\in\{0,\cdots,Q+L\}}{\mathrm{argmin}} \ \mathrm{tr}\left(\mathbf{S}^{(\nu)}\mathbf{A}^{-1}\mathbf{S}^{(\nu),T}\mathbf{R}_{ss}\right), \tag{2.29c}$$

where

$$\mathbf{A} = \mathbf{H}\mathbf{H}^{\mathrm{H}} + \xi\mathbf{I}_{N(Q+L+1)} \quad \text{and} \quad \xi = \frac{\mathrm{tr}\left(\mathbf{R}_{vv}\right)}{P_{\mathrm{budget}}}\,. \tag{2.30}$$

Note that optimisation of the decision delay (latency time) ν has to consider all possible values of $\{0,\cdots,Q+L\}$ and select the one that minimises the MSE according to (2.29c). Once ν_{opt} is obtained, both optimum precoder $\mathbf{P}_{\mathrm{opt}}$ and optimum scalar receive filter g_{opt}, which is restricted to be a positive real number, can be found be substituting (2.29c) into (2.29a) and (2.29b), respectively.

2.3.4 Broadband SVD

Another non-block based approach to jointly equalise the broadband MIMO channel can be achieved by considering a broadband singular value decomposition (BSVD) algorithm detailed in [19]. The application of the BSVD algorithm to the channel matrix $\mathbf{H}(z)$ in (2.1) leads to a decomposition

$$\mathbf{H}(z) = \mathbf{U}(z)\mathbf{\Sigma}(z)\tilde{\mathbf{V}}(z) \tag{2.31}$$

with paraunitary matrices $\mathbf{U}(z)$ and $\tilde{\mathbf{V}}(z)$ and an approximately diagonalised and spectrally majorised matrix $\mathbf{\Sigma}(z)$. This decomposition is achieved by an iterative algorithm, which in each step eliminates the largest off-diagonal element by a delay step and a Jacobi rotation [19]. The algorithm has been shown to converge by transferring the energy of the channel matrix onto the main diagonal, and the approximation is due to limiting the number of algorithmic steps and the order of the resulting polynomial matrices $\mathbf{U}(z)$, $\mathbf{V}(z)$ and $\mathbf{\Sigma}(z)$. The iteration steps

are defined such that both $\mathbf{U}(z) \in \mathbb{C}^{N_t \times N_r}$ and $\mathbf{V}(z) \in \mathbb{C}^{N_t \times N_t}$ are paraunitary (or lossless) by definition, i.e.

$$\mathbf{U}(z)\,\tilde{\mathbf{U}}(z) = \mathbf{U}(z)\,\mathbf{U}^{\mathrm{H}}(z^{-1}) = \mathbf{I} \tag{2.32}$$

$$\tilde{\mathbf{U}}(z)\,\mathbf{U}(z) = \mathbf{I}\,. \tag{2.33}$$

The matrix $\mathbf{\Sigma}(z) \in \mathbb{C}^{N_r \times N_t}(z)$ is in the limit diagonal,

$$\mathbf{\Sigma}(z) = \mathrm{diag}\left(\mathbf{\Sigma}_0(z), \mathbf{\Sigma}_1(z), \cdots \mathbf{\Sigma}_{N-1}(z)\right), \tag{2.34}$$

where N is defined in (2.13). The diagonalisation can be ambiguous and has to be tied down by an additional constraint. As an extension of the ordering of singular values in a standard SVD, the algorithm in [19] aims to spectrally majorise $\mathbf{\Sigma}(z)$, such that

$$\mathbf{\Sigma}_0(e^{j\Omega}) \geq \mathbf{\Sigma}_1(e^{j\Omega}) \geq \cdots \geq \mathbf{\Sigma}_{N-1}(e^{j\Omega}) \quad \forall\Omega\,. \tag{2.35}$$

Note that due to the iterative nature and the finite number of steps of the algorithm in [19], (2.34) and (2.35) may only be approximately fulfilled.

Fig. 2.8 demonstrates the BSVD algorithm through an example of a 4×4 MIMO channel with individual responses drawn from a Saleh-Valenzuela indoor channel model [60]. This channel model produces an average power profile for each individual subchannel, while the actual channel coefficients are then drawn from a complex Gaussian distribution with prescribed variance. The Saleh-Valenzuela model simulates an indoor environment with clusters of rays, and average inter-arrival times between both clusters and individual rays. The model parameters have been adjusted to yield impulse responses which can be truncated without loss of significant energy after 11 coefficients. Further, the overall MIMO channel has been normalised to create a frequency-selective non-fading scenario such that

$$\|\mathbf{H}(z)\|_F = \sqrt{\sum_{m=1}^{M}\sum_{n=1}^{N}\sum_{l=0}^{L} |h_{mn}(l)|^2} = 1\,. \tag{2.36}$$

Fig. 2.8(a) shows the magnitude of the MIMO channel impulse responses for one ensemble probe. Assuming CSI to be available at both Tx and Rx ends of the link, the BSVD can be applied to $\mathbf{H}(z)$. The iterative algorithm in [19] stops if 99.9% of channel energy is located on the main diagonal. The resulting diagonalised matrix approximating (2.31) is truncated in its order to suppress tails of coefficients with a size less than 0.1% of the largest coefficient in $\mathbf{\Sigma}(z)$ [61, 62]. The approximate diagonalisation of $\mathbf{H}(z)$ according to (2.31) is presented in Fig. 2.8(b), where

almost all energy from off-diagonal elements has been transferred onto the main diagonal. The magnitude responses $|\Sigma_i(e^{j\Omega})|, i = 0, 1, \cdots, 3$, of the decoupled impulse responses along the main diagonal of $\mathbf{\Sigma}[n]$ are depicted in Fig. 2.8(c), demonstrating the ordering due to spectral majorisation in (2.35).

2.4 Summary

Linear precoding and equalisation schemes for narrowband and broadband MIMO systems have been introduced. These schemes include block-based and non-block based methods to deal with both ISI and CCI interferences in the case of broadband MIMO channels. However, it is well-known that linear equalisation suffers from noise amplification and therefore has a poor power efficiency. This problem becomes serious in situations of rank-deficient MIMO channel matrices. Moreover, the design of linear precoders and equalisers has less degrees of freedom (DoF) in terms of precoding or detection ordering which can only be optimised under non-linear approaches. In fact, ordering plays an important role in performance improvement of non-linear systems with successive interference cancellation (SIC) which can be achieved either in the receiver or at the transmit side. In Chapter 3 non-linear precoding and equalisation approaches will be explored aiming to achieve better performances with a reasonable processing complexity.

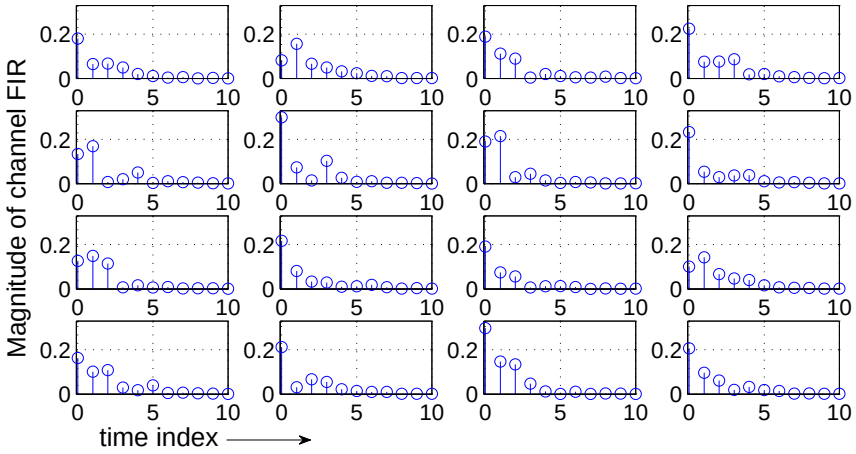

(a)

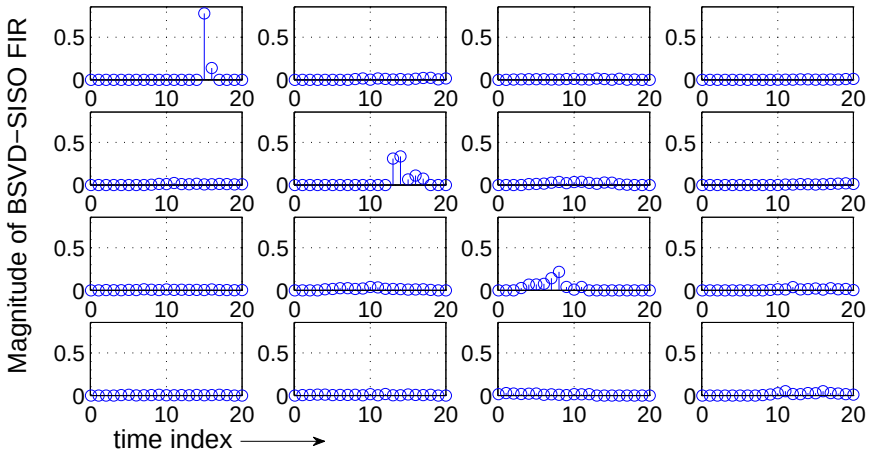

(b)

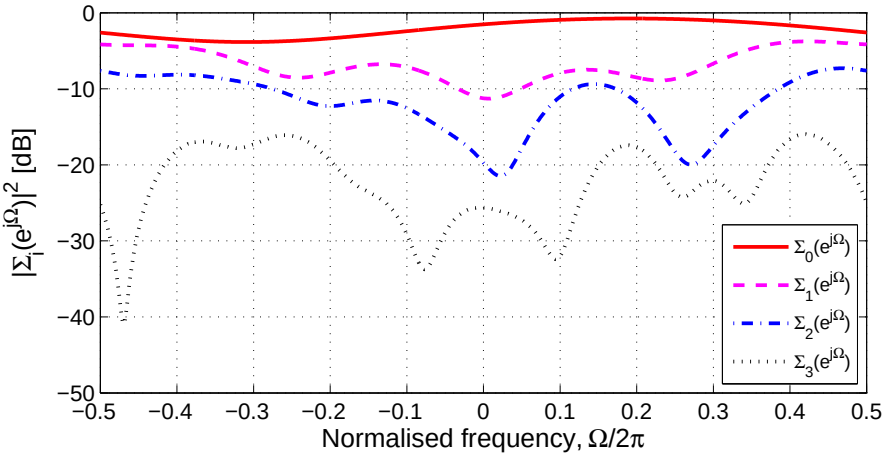

(c)

Figure 2.8: An ensemble probe of $\mathbf{H}[n]$ for a 4×4 MIMO Saleh-Valenzuela indoor channel model [60] in (a) and its approximately diagonalised system based on the BSVD algorithm in (b), while spectral majorisation property of the BSVD is shown in (c).

Chapter 3

Non-Linear Precoding and Equalisation Approaches

In this chapter, non-linear approaches are firstly studied for narrowband MIMO systems comprising both receive processing and transmit preprocessing scenarios. The impact of ordering on performance measures in both cases is investigated and highlighted by simulation results. Secondly, for the more realistic transceiver systems of a broadband MIMO channel, a novel approach based on the recently developed BSVD presented in Sec. 2.3.4 is proposed. This approach utilises the decomposition of a polynomial MIMO channel matrix into a number of independent frequency-selective SISO subchannels that is achieved by the BSVD technique, thereby cancelling the co-channel-interference (CCI). The remaining ISI caused by these individual SISO subchannels is mitigated using some of the non-linear precoding and equalisation schemes presented throughout this chapter. Furthermore, the BSVD spectral majorisation property which results in SISO subchannels with different qualities is exploit by a heuristic bit loading approach.

Results of our proposed scheme are benchmarked against a state-of-the-art broadband MIMO technique in [17] demonstrating that an improved BER performance can be achieved under the constraints of identical data throughput and transmit power.

3.1 MIMO Narrowband with Rx Processing

In this section we will address non-linear equalisation schemes for the MIMO narrowband case where, beside channel noise, spatial interference contributed from data streams transmitted in parallel exists. This interference, known also

as multiuser interference, can be mitigated to reliably detect data on a symbol-by-symbol basis rather than a vector of symbols as in the case of linear schemes. Assuming knowledge of CSI at the receiver, receive processing of data is considered, highlighting the prominent role of ordering if better performance is to be attained.

3.1.1 Maximum-Likelihood Detection

The optimum detection scheme of data transmitted over a MIMO narrowband channel $\mathbf{H} \in \mathbb{C}^{N_r \times N_t}$ of N_t transmitting antennas and N_r receiving antennas is achieved by the maximum-likelihood (ML) detector [63] as it optimally takes into account the properties of noise and interference [64]. ML receivers detect transmitted data symbols $\mathbf{s} \in \mathcal{S}^{N_t}$ on a per-vector basis by estimating the most probable transmitted data vector $\hat{\mathbf{s}}$ amongst all possible combinations $\mathcal{S}^{N_t}$ upon receiving $\mathbf{y} \in \mathbb{C}^{N_r}$such that

$$\hat{\mathbf{s}} = \underset{\mathbf{s} \in \mathcal{S}^{N_t}}{\operatorname{argmin}} \|\mathbf{y} - \mathbf{H}\mathbf{s}\|_2^2 , \tag{3.1}$$

where the set $\mathcal{S}$ denotes the used symbol alphabet which can be defined for a constellation size (or order) M as [16]

$$\mathcal{S} \stackrel{d}{=} \left\{ s^I + j s^Q \mid s^I, s^Q \in \left\{ \pm 1, \pm 3, \cdots, \pm \left(\sqrt{M} - 1 \right) \right\} \right\} \tag{3.2}$$

Obviously, for the ML detector it is required to initiate an exhaustive search of possible M^{N_t} different data vectors to find the solution in (3.1) for every single vector detection. This of course restricts the application of the ML scheme for practical use as the complexity increases rapidly with the number of antennas and the constellation size. In other words, ML detection is not feasible for large orders of MIMO systems even with smaller modulation orders such as BPSK. Therefore, although ML detection is the best detection method for equiprobable input symbols, its complexity of the subspace search is prohibitive for practical systems [65, 64].

3.1.2 Decision Feedback Equalisation

The complexity burden encountered with ML estimation motivates for suboptimal detection schemes with reasonable complexity. To this end decision feedback equalisation (DFE) [13, 66], a simple and popular conventional nonlinear technique, is established to separate data streams at the receiver of MIMO systems

using successive interference cancellation. This is shown to overcome the disadvantages of noise enhancement associated with linear equalisation [50] at the cost of extra complexity. DFE was originally developed to combat ISI of SISO systems (see e.g. [67, 68]) where previously detected symbols are used to assist in subsequent symbols detection. This is referred to as temporal equalisation as detection is performed in the discrete time index of the data sequence. Spatial DFE, in contrast, arises for MIMO system to deal with the multiuser interference — forming the basis behind the optimal BLAST detection algorithm [45, 69], as will be shown in Sec. 3.1.3 — which is the interest of this Section.

A typical DFE system model is depicted in Fig. 3.1 where the received data vector $\mathbf{y}$ is linearly processed by the feedforward filter matrix $\mathbf{F}$ before being considered by the non-linear feedback loop. The undecided symbol $\tilde{\mathbf{s}}$ of the feedback loop is then given by

$$\begin{aligned} \tilde{\mathbf{s}} &= \mathbf{F}\mathbf{y} + \mathbf{B}\hat{\mathbf{s}}, \\ &= \mathbf{F}\mathbf{H}\mathbf{s} + \mathbf{F}\mathbf{v} + \mathbf{B}\hat{\mathbf{s}}, \end{aligned} \tag{3.3}$$

where $\hat{\mathbf{s}}$ combines the decided estimates of $\mathbf{s}$ using the appropriate quantisation or decision device $q(\cdot)$. For feasible realisability and to ensure spatial causality, the feedback filter matrix $\mathbf{B}$ must be of strictly triangular structure. This can be achieved using the well-known QR factorisation of the channel matrix $\mathbf{H}$, that is $\mathbf{H} = \mathbf{Q}\mathbf{R}$ where $\mathbf{Q} \in \mathbb{C}^{N_r \times N_r}$ is a unitary matrix (i.e., $\mathbf{Q}\mathbf{Q}^{\mathrm{H}} = \mathbf{Q}^{\mathrm{H}}\mathbf{Q} = \mathbf{I}$) and $\mathbf{R} \in \mathbb{C}^{N_r \times N_t}$ an upper triangular matrix. Noticeably QR factorisation is not an optimal technique, however it is still widely used due to its numerical stability and it is easy to implement [70].

For the sake of brevity we consider a MIMO system with equal numbers of transmit and receive antennas $N_t = N_r = N$. Assuming perfect decisions of $\tilde{\mathbf{s}}$, i.e. $\hat{s}_i = q(\tilde{s}_i) = s_i, 1 \leq i \leq N$, which is a common assumption in DFE systems [71] called a "genie-aided" approach, the ZF solution can be formulated using (3.3) as

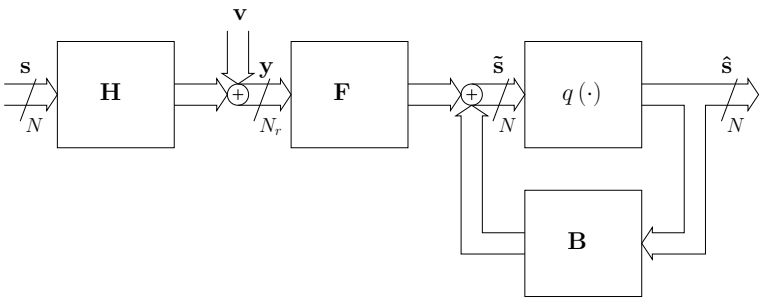

Figure 3.1: DFE system model.

$$\begin{aligned} \mathbf{FH} + \mathbf{B} &= \mathbf{I}, \\ \mathbf{FQR} + \mathbf{B} &= \mathbf{I}\,. \end{aligned} \tag{3.4}$$

Setting the feedforward filter $\mathbf{F} = \mathbf{GQ}^{\mathrm{H}}$ in (3.4), results in the feedback filter $\mathbf{B} = \mathbf{I} - \mathbf{GR}$ where $\mathbf{G}$ is a diagonal matrix that is used to set the diagonal entries of $\mathbf{R}$ to unity, i.e.

$$\mathbf{G} = \mathrm{diag}\left(r_{11}^{-1}, \cdots, r_{NN}^{-1}\right)\,. \tag{3.5}$$

With the absence of noise and by substituting these filter settings for $\mathbf{F}$ and $\mathbf{B}$ into (3.3) yields $\tilde{\mathbf{s}}$ as

$$\tilde{\mathbf{s}} = \begin{bmatrix} 1 & -b_{12} & \cdots & -b_{1N} \\ 0 & \ddots & \ddots & \vdots \\ \vdots & \ddots & \ddots & -b_{N-1N} \\ 0 & \cdots & 0 & 1 \end{bmatrix} \mathbf{s} + \begin{bmatrix} 0 & b_{12} & \cdots & b_{1N} \\ \vdots & \ddots & \ddots & \vdots \\ \vdots & & \ddots & b_{N-1N} \\ 0 & \cdots & \cdots & 0 \end{bmatrix} \hat{\mathbf{s}}\,. \tag{3.6}$$

Using (3.6), it is easy to note that the last-indexed symbol s_N of the transmitted vector $\mathbf{s}$ is an error-free symbol. This is utilised in detecting the spatially previous symbol s_{N-1} by subtracting out its interference signature on the statistics of $\tilde{s}_{N-1}$. Proceeding further, both s_N and s_{N-1} are used to cancel their interference contributions from $\tilde{s}_{N-2}$ and so forth up to detecting the first-indexed symbol s_1. The design of the DFE system according to the MMSE criterion can be obtained via Cholesky factorisation [69].

DFE systems can also be formulated for jointly dealing with CCI and ISI interferences for MIMO ISI systems, see for example [72, 45]. However it is important to point out that DFE analysis is difficult to formulate because of the non-linear operation of their feedback loop. Linearised DFE models can only be attained if past decisions are assumed correct as discussed above. This assumption, in fact, is not a realistic assumption as it fails to account for the so-called error propagation. The error propagation problem arises when wrong decisions are made on past symbols and consequently used in detecting other received symbols. This, in turn, adds disturbances in deciding on other symbols in subsequent next layers. The overall performance of DFE systems may be seriously deteriorated by the inherent error propagation problem. Decision ordering of subsequent symbols can be used to significantly improve the performance of DFE systems by partially overcoming, or reducing, the effect of the error propagation problem. This can be considered either for MIMO frequency-flat systems [7, 39] referred to as spatial ordering or for MIMO frequency selective systems [14, 17] known as spatio-temporal ordering, both of which will be addressed in subsequent

sections. To this end, an obvious consequence of spatial DFE systems leads to the development of the vertical Bell laboratories layered space-time (V-BLAST) architecture as will be discussed in the next section. Another drawback generated for DFE systems is the delay in processing required by immediate decisions [50].

3.1.3 V-BLAST

Motivated by the study of layered space-time architecture of a MIMO system in [73, 4, 5], decoupling between distinct spatial modes can result in a system in which capacity increases linearly with min (N_t, N_r) for fixed bandwidth and total transmit power. Consequently, V-BLAST architecture was proposed [74, 7, 6] to realise the capacity advantage promised on MIMO channels with reasonable complexity [39]. This architecture is, in fact, a layered detection scheme based on the DFE method [75, 50, 76] presented in Sec. 3.1.2 in which a received data vector is detected on a symbol-by-symbol basis, i.e. layer-by-layer. The successive detection ordering of the V-BLAST is optimised in the sense of maximising the worst post-detected SNR [7]. This leads to detecting weak layer components of the data vector more reliably. Indeed the overall detection performance is dominated by the signature of weak layers if the obvious order of antenna labelling is selected as in the case of the DFE system. The optimum detection ordering strategy of the V-BLAST is shown to minimise the symbol error ratio (SER) by detecting at each iteration the component associated with the highest SNR [74], an approach that is known as "best first" [46]. This can be viewed as a virtual relabelling of the transmit antennas. Detection proceeds by nulling out the interference of other layers in a successive manner which is a popular method of equalising interference and achieving parallel AWGN subchannels.

In Table 3.1, the pseudo code of the V-BLAST algorithm is presented for both ZF [7] and MMSE [77, 42] criteria, which can be briefly summarised by the following four steps:

1. *Ordering*: determine the most reliable symbol component position (order) k_i according to the criterion in (c);

2. *Nulling*: compute its corresponding ZF or MMSE nulling vector $\mathbf{w}_{k_i}$ using (d), then obtain the decision statistic $\tilde{s}_{k_i}$ as in (e);

3. *Slicing*: or quantising to the nearest alphabet according to the used constellation as in (f);

4. *Cancellation*: subtracting out its interference contribution from the received vector $\mathbf{y}$ using (g).

Finally, the updates (h)-(j) are required to proceed with the next component.

Note that the difference between ZF and MMSE V-BLAST algorithms as listed in Table 3.1 lies only in computing the position of the highest SNR symbol component in (c). For ZF this is achieved by obtaining the minimum row-norm of $\mathbf{G}$, while for MMSE this is associated with the smallest diagonal entry [44] of

$$\mathbf{D} = \left[\mathbf{H}^{\mathrm{H}}\mathbf{H} + \xi \mathbf{I}_{N_t}\right]^{-1}, \tag{3.7}$$

with the MMSE filter given by

$$\mathbf{G}_{\mathrm{MMSE}} = \mathbf{D}\mathbf{H}^{\mathrm{H}}, \tag{3.8}$$

where ξ is, as in (2.30), the reciprocal of the SNR. As in linear filter systems, the detection performance of the V-BLAST under the MMSE criterion outperforms the ZF one. In order to confirm this, simulations are conducted for a 4×4 MIMO system using QPSK transmission averaged over 300 realisations of a channel matrix normalised such that $\|\mathbf{H}\|_F = 1$. Results are compared with the ML detection scheme described in Sec. 3.1.1 showing advantages of more than 5 dB at BER $= 10^{-3}$ gained by V-BLAST MMSE detection over its ZF counterpart while less than 3 dB is lost compared to the ML detection.

The main computational bottleneck of the V-BLAST architecture lies in the repeated pseudo-inverse or normal inverse in the ordering step of both ZF and MMSE V-BLAST algorithms [78]. Suboptimal ordering approaches based on computationally efficient algorithms for the QR decomposition are proposed in [79, 25, 80, 81], however with slight performance degradation compared to the original V-BLAST. It is also shown in [82] that the V-BLAST algorithm is suboptimum in scenarios with spatial loading[1] when compared to the optimum water-filling algorithm. It is noteworthy that the original V-BLAST performs well when $N_r > N_t$ due to the possibly high diversity level in the first stage that can reduce the error propagation effect [37]. However, unsatisfactory performance is obtained when equal numbers of antennas are used [76].

[1]The allocation of bits per subchannel and transmit power are made according to subchannel conditions for maximum sum-capacity.

Table 3.1: V-BLAST ZF and MMSE detection algorithms.

	ZF V-BLAST	MMSE V-BLAST
	Initialisation:	
a.	$\mathbf{G}_{\text{ZF}}^{(1)} = \mathbf{H}^{+} = \left[\mathbf{H}^{\text{H}}\mathbf{H}\right]^{-1}\mathbf{H}^{\text{H}}$	Compute $\mathbf{D}^{(1)}$ and then $\mathbf{G}_{\text{MMSE}}^{(1)}$ using (3.7) and (3.8), respectively
b.	$i = 1$	$i = 1$
	Recursion:	
c.	$k_i = \underset{j \notin \{k_1,\ldots,k_{i-1}\}}{\text{argmin}} \left\| \left(\mathbf{G}_{\text{ZF}}^{(i)}\right)_j \right\|_2^2$	$k_i = \underset{j \notin \{k_1,\ldots,k_{i-1}\}}{\text{argmin}} \mathbf{D}_j^{(i)}$
d.	$\mathbf{w}_{k_i} = \left(\mathbf{G}_{\text{ZF}}^{(i)}\right)_{k_i}$	$\mathbf{w}_{k_i} = \left(\mathbf{G}_{\text{MMSE}}^{(i)}\right)_{k_i}$
e.	$\tilde{s}_{k_i} = \mathbf{w}_{k_i}\mathbf{y}^{(i)}$	$\tilde{s}_{k_i} = \mathbf{w}_{k_i}\mathbf{y}^{(i)}$
f.	$\hat{s}_{k_i} = q\left(\tilde{s}_{k_i}\right)$	$\hat{s}_{k_i} = q\left(\tilde{s}_{k_i}\right)$
g.	$\mathbf{y}^{(i+1)} = \mathbf{y}^{(i)} - \hat{s}_{k_i}\left[\mathbf{H}\right]_{k_i}$	$\mathbf{y}^{(i+1)} = \mathbf{y}^{(i)} - \hat{s}_{k_i}\left[\mathbf{H}\right]_{k_i}$
h.	$\mathbf{G}_{\text{ZF}}^{(i+1)} = \mathbf{H}_{\overline{k_i}}^{+}$	$\left[\mathbf{H}\right]_{k_i} = \mathbf{0}_{N_r \times 1}$
i.	$i = i + 1$	Compute $\mathbf{D}^{(i)}$ then $\mathbf{G}_{\text{MMSE}}^{(i)}$ using (3.7) and (3.8), respectively
j.		$i = i + 1$

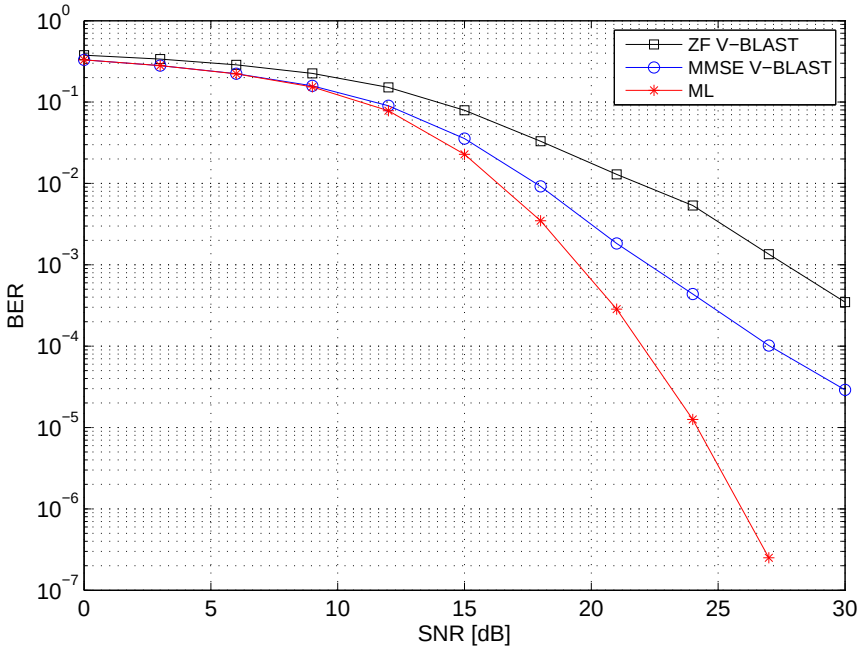

Figure 3.2: BER performance of V-BLAST ZF and MMSE against ML detection for a 4×4 MIMO system with QPSK modulation.

3.2 MIMO Narrowband with Tx Processing

So far the task of non-linear separation of data streams by removing the distortion effect of the communication channel and minimising the received noise is performed at the receiver. Beside point-to-point communications, the earlier discussed methods are also suitable for uplink scenarios, i.e. multipoint-to-point communications, where a common receiver can serve multiple decentralised mobile terminals that do not cooperate [46]. An obvious drawback of receive processing is the increased complexity required by the receiver to mitigate the channel interference and to provide reliable replicas of data streams [48]. The downlink communication part of such systems is a challenging problem or even unfeasible if channel equalisation resides at the individual receivers. To this end transmit processing, assuming availability of CSI at the transmitter, is the proper strategy for dealing with such scenarios and achieving transmission with high-quality performance while enabling low complexity receivers [53].

Dirty paper coding (DPC) [83, 84] represents the optimal transmit strategy which permits a transmitter to send information so that each receiver can see no interference from other receivers. The DPC technique has proven its optimality in the achievable-rate sense that coincides with the theoretical capacity boundary region [85], although it does not directly lead to a realisable transmission strategy [52]. An alternative practical implementation of DPC can be achieved by Tomlinson-Harashima Precoding (THP), which is strongly related to DPC and represents, in fact, a suboptimal realisation of DPC [17, 38]. THP was originally and independently proposed in [22] and [23] to remove ISI in a SISO transmission over frequency selective channels. Recently it has been also proposed for the equalisation of multiuser interference in MIMO systems (see for example [86, 87, 39]) where it performs spatial pre-equalisation instead of temporal pre-equalisation for ISI channels. In other words, THP in SISO systems cancels ISI caused by already detected symbols by subtracting out their contribution from the received signal, while in spatial THP interference from symbols sent at the same time instance but designated for different receiving antennas is mitigated.

THP has also been applied to MIMO ISI systems [45, 88, 17], where in addition to interference from already precoded past data symbols, interference from spatially already precoded symbols can be eliminated. In this case the optimum precoding order — in time, space, or a mixture thereof — is important if a good performance is to be attained. A number of sub-optimum schemes have also been developed, which provide only a small performance degradation while seeking optimum precoding in only temporal or spatial dimensions. The consideration

of the temporal dimension has been shown to have a greater impact in order to approach the optimum performance than spatial ordering [53, 17].

THP is typically a DFE system operated at the transmitter, whereby the feedback loop is transferred from the receiver to the transmitter as shown in Fig. 3.3. With the THP structure, the major drawback of error propagation encountered in DFE systems is eliminated since the feedback loop is placed at the transmitter where the signals are perfectly known [16]. Furthermore, with precoding, no immediate decisions at the receiver are required. As a consequence it is expected that a THP system, in general, has better performance than its DFE receiver version [89] as will be supported by simulation results in Sec. 3.2.2.

Note that since the feedback loop is now located at the transmitter, its summation point suggests that the transmitted signal is unboundedly increased beyond its original constellations $\mathcal{S}$ leading to a total transmit power increase as a result. In order to limit the transmit power, the modulo operator $\mathcal{M}(\cdot)$ is introduced with its essential role to bring the signal amplitude back inside the boundaries of $\mathcal{S}$. For M-QAM modulation, the modulo operator is defined as

$$\mathcal{M}(x) = x - \left\lfloor \frac{\Re(x)}{\tau} + \frac{1}{2} \right\rfloor \tau - j \left\lfloor \frac{\Im(x)}{\tau} + \frac{1}{2} \right\rfloor \tau, \tag{3.9}$$

where τ is a constant depending on the used modulation scheme. For QPSK $\tau = 2\sqrt{2}$, while for a square M-QAM constellation, $\tau = 2\sqrt{M}$. Despite its original function to control the transmit power, the redistribution by the modulo operator in (3.9) over the interval $\left[-\sqrt{M}, \sqrt{M}\right)$ leads to a small increase in transmit power known as a *precoding loss* given by [90]

$$\frac{\mathbb{E}\left[\|\mathbf{s}\|_2^2\right]}{\mathbb{E}\left[\|\mathbf{u}\|_2^2\right]} = \frac{M}{M-1}. \tag{3.10}$$

3.2.1 System Model

We consider a point-to-point flat-fading MIMO THP system with $N_t = N$ transmitting antennas and N_r receiving antennas as shown in Fig. 3.3, where the data vector to be transmitted is denoted by $\mathbf{s} = [s_1, s_2, \cdots, s_N]^{\mathrm{T}}$. It is assumed that all data symbols are spatially and temporally uncorrelated, i.e., $\mathbb{E}\left[\mathbf{s}\mathbf{s}^{\mathrm{H}}\right] = \sigma_s^2 \mathbf{I}_N$. These data streams are pre-processed by the feedback loop and then passed through the permutation matrix $\mathbf{\Pi} \in \{0,1\}^N$ prior to transmission. The permutation matrix $\mathbf{\Pi}$ is an orthogonal matrix that contains 1 in each row or column and zeros elsewhere, which used to designate the precoding ordering of the data

streams $\mathbf{s}$, i.e.

$$\mathbf{\Pi}\mathbf{\Pi}^{\mathrm{T}} = \mathbf{\Pi}^{\mathrm{T}}\mathbf{\Pi} = \mathbf{I}_N\,. \tag{3.11}$$

Letting $\mathbf{x}$ be the $N \times 1$ transmit signal vector, the received signal vector $\mathbf{y}$ with dimension $N_r \times 1$ is given by

$$\mathbf{y} = \mathbf{H}\mathbf{x} + \mathbf{v}, \tag{3.12}$$

where $\mathbf{v}$ is an $N_r \times 1$ additive white Gaussian noise (AWGN) vector that corrupts the received signal vector $\mathbf{y}$ and has zero-mean and variance $\mathbb{E}\left[\mathbf{v}\mathbf{v}^{\mathrm{H}}\right] = \sigma_n^2\mathbf{I}_{N_r}$.

Assuming CSI availability at the transmitter, the role of the feedback filter $\mathbf{B}$ is to successively pre-distort streams of $\mathbf{s}$ in such a way that annihilates, at the receiver, the interference that would be experienced by propagation over the channel. It is evident that the error propagation problem encountered with DFE systems is now avoided because the transmitter has exact knowledge of the symbols to be transmitted.

Based on the QR decomposition of the channel matrix $\mathbf{H}$, the design of feedback and feedforward filter matrices $\mathbf{B}$ and $\mathbf{W}$ can be obtained for the ZF solution and different precoding ordering in $\mathbf{\Pi}$. Starting by finding out an equivalent linear model of the element-wise modulo operator $\mathcal{M}(\cdot)$, the non-linear feedback loop at the transmitter can be linearised [90, 46] as demonstrated in Fig. 3.4. This can be achieved if we consider a new complex vector $\boldsymbol{a}$ with entries $a_k, 1 \leq k \leq N$ defined as $a_k \in \{\tau\beta^I + j\tau\beta^Q \,|\, \beta^I, \beta^Q \in \mathbb{Z}\}$ and chosen such that the real and imaginary parts of the elements of the effective output data vector $\mathbf{u}$ of the feedback loop are constrained in the square region $\left[-\sqrt{M}, \sqrt{M}\right)$, i.e. $\Re(u_k), \Im(u_k), 1 \leq k \leq N \in \left[-\sqrt{M}, \sqrt{M}\right)$. With this arrangement the feedback loop is now linearised and its output $\mathbf{u}$ can be given as

$$\mathbf{u} = \left(\mathbf{I}_N - \mathbf{B}\right)^{-1}\left(\mathbf{s} + \boldsymbol{a}\right), \tag{3.13}$$

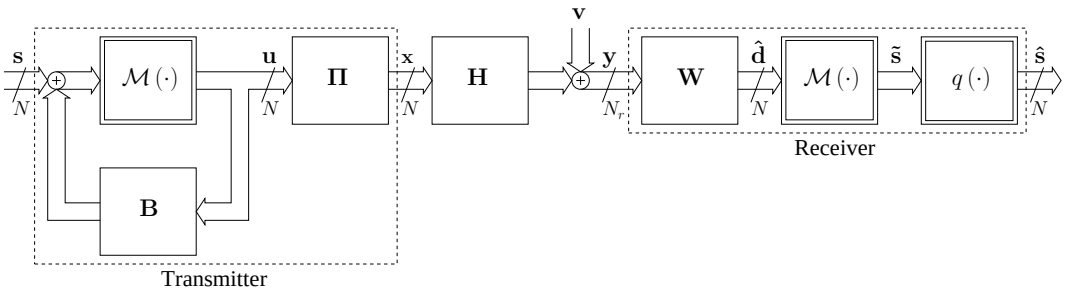

Figure 3.3: THP MIMO communication system with precoding order $\mathbf{\Pi}$.

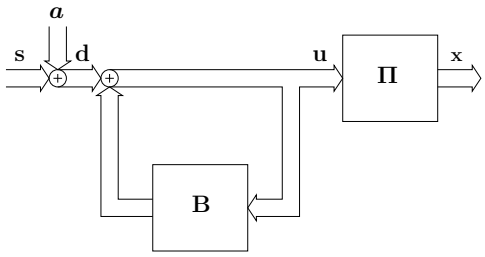

Figure 3.4: Linearised model of the modulo operator in Fig. 3.3.

which is equivalent to

$$u_k = s_k + a_k + \sum_{l=1}^{N} b_{kl} u_l, \quad k = 1, \ldots, N\,. \tag{3.14}$$

Equation (3.14) can be viewed as periodically expanding the initial signal constellation in $\mathbf{s}$ into more and more discrete levels that lie in the same regular two-dimensional grid of the initial constellation. This is due to the effect of adding a_k in (3.14) which is exactly the function of the modulo operator in (3.9). Therefore, this suggests that the same modulo operation has to be used at the receiver just before the slicer (quantiser) q as shown in Fig. 3.3 and highlighted by Fig. 3.5. Accordingly, some known drawbacks of THP systems which mainly arise from the signature of the modulo operator will be summarised in Sec. 3.2.3. Since the selection of a_k depends on the corresponding symbol s_k of $\mathbf{s}$, it is clear that the vector $\mathbf{u}$ is still wide-sense stationary (WSS) i.e., $\mathbb{E}\left[\mathbf{u}\mathbf{u}^{\mathrm{H}}\right] = \frac{M}{M-1}\sigma_s^2\mathbf{I}_N$ or simply $\sigma_u^2 = \frac{M}{M-1}\sigma_s^2$. Defining an equivalent data vector $\mathbf{d} = \mathbf{s} + \boldsymbol{a}$, the equalised received vector $\hat{\mathbf{d}}$ is given as

$$\hat{\mathbf{d}} = \mathbf{W}\mathbf{H}\boldsymbol{\Pi}\left(\mathbf{I}_N - \mathbf{B}\right)^{-1}\mathbf{d} + \mathbf{W}\mathbf{v}, \tag{3.15}$$

the ZF solution can be formulated to perfectly remove interference, i.e.

$$\begin{aligned} \mathbf{W}\mathbf{H}\boldsymbol{\Pi}\left(\mathbf{I}_N - \mathbf{B}\right)^{-1} &= \mathbf{I}_N, \\ \Rightarrow \mathbf{B} &= \mathbf{I}_N - \mathbf{W}\mathbf{H}\boldsymbol{\Pi}\,. \end{aligned} \tag{3.16}$$

As in DFE systems the QR decomposition of $\mathbf{H}\boldsymbol{\Pi}$ can be used to solve for the ZF THP filters $\mathbf{B}$ and $\mathbf{W}$ in (3.16). Although the QR decomposition is possible for non-square matrices, for the sake of simplicity, we will restrict ourselves to systems with an equal number of transmit and receive antennas, i.e. $N_r = N$. Applying the QR decomposition of the permuted channel

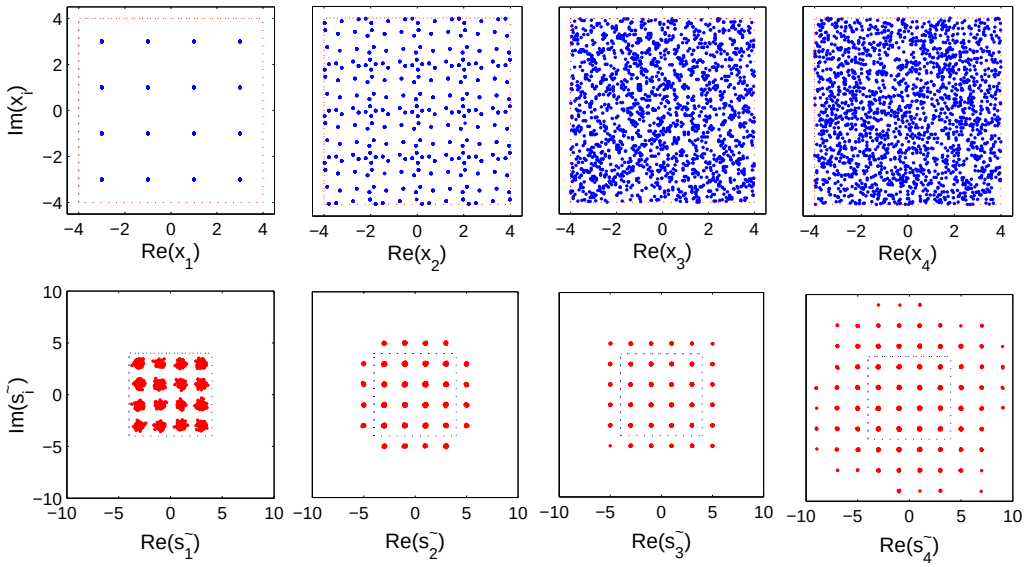

Figure 3.5: Individual scatter plots of channel inputs x_k and filtered received outputs $\tilde{s}_k$ for a 4×4 MIMO THP system using 16-QAM modulation at SNR $= 30$ dB.

$$\mathbf{QR} = \mathbf{H\Pi}, \tag{3.17}$$

results in $\mathbf{R} = \mathbf{Q}^{\mathrm{H}}\mathbf{H\Pi}$ and leads to the system implementation shown in Figure 3.3. In order to have a strictly triangular structure of the feedback filter $\mathbf{B}$, which is necessary to assure spatial causality, a diagonal matrix $\mathbf{G}$ as defined in (3.5) is used to scale all the entries of the main diagonal of $\mathbf{R}$ to unity. Therefore, $\mathbf{W}$ and $\mathbf{B}$ in (3.16) can be obtained as

$$\begin{aligned} \mathbf{W} &= \mathbf{G}\mathbf{Q}^{\mathrm{H}}, \\ \mathbf{B} &= \mathbf{I}_N - \mathbf{G}\mathbf{R} \end{aligned} \tag{3.18}$$

for the ZF solution.

3.2.2 THP Vs. DFE Performance Comparison

Computer simulations are conducted to investigate the performance improvement of a THP system compared to its DFE counterpart under the ZF condition and no ordering, i.e. $\mathbf{\Pi} = \mathbf{I}_N$. For both the ZF and MMSE linear equalisers that were presented in Sections 2.2.1 and 2.2.2, respectively, results are provided for comparison. A 4×4 MIMO system with flat-fading channel where $h_{ij} \in \mathcal{CN}(0, 1)$ is considered and results are averaged over 1000 different channel realisations.

In Fig. 3.6, QPSK transmission is assumed while in Fig. 3.7, both 16-QAM and 64-QAM modulations are examined. It can be clearly noted from Fig. 3.6 that both DFE and THP systems outperform ZF linear equalisation with a small advantage of DFE over THP at low SNR regions owing to the modulo loss defined in Sec. 3.2.3, and for the whole SNR range due to the precoding loss defined in (3.10), which is almost 1.28 dB for QPSK.

When higher modulation orders are considered, it is clearly evident in Fig. 3.7 that both THP and DFE systems outperform linear equalisation for both the 16-QAM and 64-QAM modulation schemes. However, the respective performance of THP is much better than DFE owing to the absence of error propagation in the case of THP. Error propagation deteriorates the performance of the DFE down to the level of linear equalisation. Note that the mitigation of error propagation can be confirmed by comparing THP with the error-free DFE version, namely "DFE g-a", revealing very close performance between each of them with a small disadvantage for THP. This degradation agrees with the precoding loss of approximately 0.28 dB and 0.07 dB for 16-QAM and 64-QAM modulation orders, respectively, according to (3.10).

The relative difference between BER curves for 64-QAM appears reduced w.r.t. some of the curves for QPSK and 16-QAM. This is likely to be caused by the BER performance of the worst subchannel, which dominates the overall BER. This performance would be worst for 64-QAM and may be poor enough to lead to little distinguish between the different precoding/equalisation schemes.

3.2.3 THP Drawbacks

As highlighted earlier in Sec. 3.2.1 due to the necessity to incorporate a modulo operator in both transmitter and receiver of THP systems, some system drawbacks arise, which can be summarised as follows [91, 92, 93]:

- THP systems perform well because of their inherent non-linear structure, however they are very sensitive to errors in CSI that result in saturation in received SNR as the transmitted power increases [94]. This of course requires robust designs that take into account a combined optimisation of THP and channel estimation [95, 96], or based on constrained power loading [97, 98].

- The modulo operator at the transmitter reshapes the probability density function of the transmitted signal away from the capacity-achieving Gaussian distribution as demonstrated by Fig. 3.5, resulting in a *shaping loss*

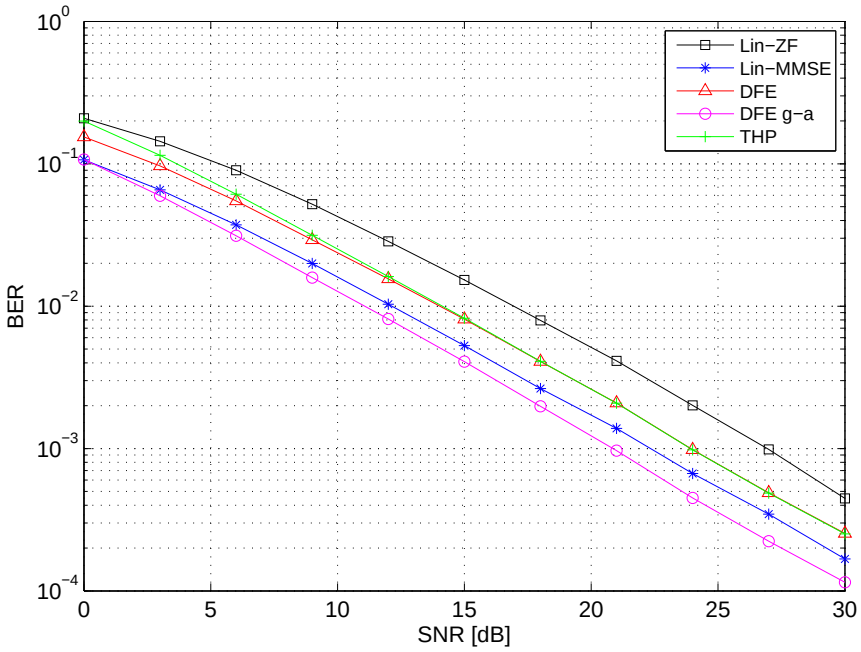

Figure 3.6: DFE and THP performance Vs. Linear ZF and MMSE for a 4×4 MIMO system and QPSK transmission.

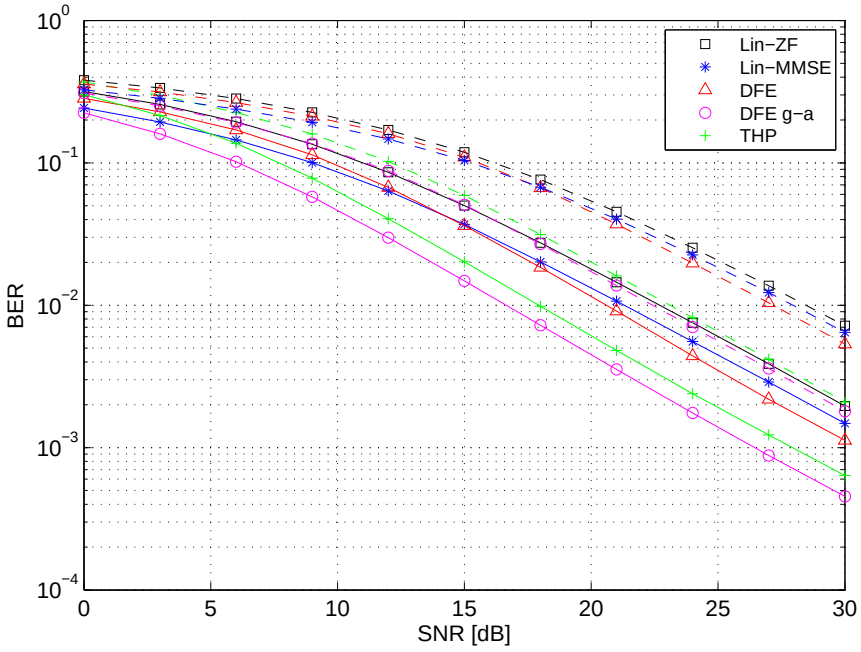

Figure 3.7: DFE and THP performance Vs. Linear ZF and MMSE for a 4×4 MIMO system using 16-QAM (solid line) and 64-QAM (dashed line) transmissions.

of 1.53 dB (or equivalently 0.255 bits loss in capacity) for pulse amplitude modulation (PAM) or square QAM with higher modulation orders M [99, 100, 91].

- Another problem associated with the transmit modulo operator is the *precoding loss* described by (3.10) and the deviation from the standard QAM constellation demonstrated in Fig. 3.5 causes an increase in transmit power which is more prominent for small constellation orders [90].

- Finally, *modulo loss* can occur and is caused by the modulo operator located at the receiver, which is required to remove the distortion effect of its transmitter counterpart. This modulo operator affects the received noise leading to erroneous decisions of constellation points that are estimated near the constellation boundary. This error becomes very serious at low SNRs and small constellation sizes [93] (cf. Fig 3.6).

3.3 Ordering using QR Decomposition

The performance of the THP system presented in Sec. 3.2.2 is evaluated for the case of no precoding ordering, $\mathbf{\Pi} = \mathbf{I}_N$. However, systems with non-linear precoding or equalisation suffer from different error rates for different transmitted data streams [71]. Therefore it is better to order data streams in a manner that reduces the error propagation problem in DFE systems or enhances the performance of THP systems. In this Section, we will focus on the effect of precoding ordering on the THP performance. Intuitively, since finding the optimal ordering involves an exhaustive search over $N!$ possible permutations of $\mathbf{\Pi}$, a suboptimal ordering strategy is usually employed [97], the most important subset of which will be investigated in the following. Thereafter the performance improvement attained by these precoding ordering on the THP system analysed in Sec. 3.2.1 will be examined by simulations.

3.3.1 No and Arbitrary Ordering

In the case of no ordering, the permutation matrix $\mathbf{\Pi}$ in (3.17) is equal to the identity matrix $\mathbf{I}_N$. Like in V-BLAST detection [6], this natural ordering does not lead to improved performance. With arbitrary ordering we randomly select $\mathbf{\Pi}$ from all possible permutation matrices, which should lead to the same result as no ordering and hence is employed as a checking mechanism. Noteworthy, in order to reach fair simulation results we aim to run our simulations over a sufficient

number of channel realisations. The consequence of results for both methods can later act as a measure to ensure that such a sufficient number of simulations has been reached.

3.3.2 QR Implementation of V-BLAST Ordering

In Table 3.2, the QR algorithm that implements V-BLAST ordering is summarised assuming a square channel matrix $\mathbf{H}$ of size N, where $\bar{\mathbf{H}}_k$ denotes the matrix consisting of the remaining columns of $\mathbf{H}$ after deleting its kth column $[\mathbf{H}]_k$ and $\bar{\mathbf{H}}_{k_1,k_2,\cdots,k_i}$ is the same as $\bar{\mathbf{H}}_k$ but with columns $k_1, k_2, \cdots, k_i$ deleted instead. This algorithm achieves V-BLAST ordering by following the signal space spanned by the column vectors of $\mathbf{H}$ and selecting, at each iteration, the column position that maximises the difference between itself and its projection as in steps (1) and (4) [70].

Once all positions $k_i, 1 \leq i \leq N$ are determined, the columns of the permutation matrix are formulated as $\mathbf{\Pi}_{VB} = [\boldsymbol{e}_{k_1}, \cdots, \boldsymbol{e}_{k_N}]$, where $\boldsymbol{e}_i$ is the ith column of the identity matrix $\mathbf{I}_N$. The $\mathbf{Q}$ matrix is formulated by arranging the orthonormal column vectors $\mathbf{q}_i, 1 \leq i \leq N$, i.e. $\mathbf{Q} = [\mathbf{q}_1, ..., \mathbf{q}_N]$. The special QR decomposition that implements the V-BLAST ordering is then $\mathbf{H\Pi}_{VB} = \mathbf{QR}$ with the R factor calculated as in step (7).

3.3.3 QR Efficient Ordering

The V-BLAST ordering obtained above using Table 3.2 requires high computational complexity as will be demonstrated in Sec. 3.3.4. A much simpler approach is to order the diagonal entries of the R factor of the QR decomposition. It is straightforward to note that the statistics of the error covariance matrix of the THP system are characterised by the noise term in (3.15). Substituting with the feedforward filter $\mathbf{W}$ in (3.18) and matrix $\mathbf{G}$ in (3.5), the error covariance matrix is given by

$$\mathbf{\Phi}_{ee} = \sigma_v^2 \mathbf{G}^2 = \sigma_v^2 \cdot \mathrm{diag}\left(\left| \frac{1}{\mathrm{r}_{11}} \right|^2, \cdots, \left| \frac{1}{\mathrm{r}_{\mathrm{NN}}} \right|^2 \right), \tag{3.19}$$

with its diagonal entries inversely proportional to the square of the diagonal entries of $\mathbf{R}$ [81, 40, 101]. This means that if diagonal entries of $\mathbf{R}$ are sorted in a descending order very poor performance will result, however, if this order is reversed, an enhanced performance can be expected.

An even more efficient ordering can be obtained if $|r_{kk}|$ is maximised in each precoding step. This can be achieved with the modified Gram-Schmidt QR de-

Table 3.2: QR implementation algorithm for V-BLAST ordering.

	Initialisation:
1.	Find k_N such that $k_N = \underset{1\leq k\leq N}{\operatorname{argmax}} \left\| \left(\mathbf{I} - \bar{\mathbf{H}}_k \bar{\mathbf{H}}_k^{+}\right) [\mathbf{H}]_k \right\|_2^2$
2.	Compute $\boldsymbol{a}_N = \left(\mathbf{I} - \bar{\mathbf{H}}_{k_N} \bar{\mathbf{H}}_{k_N}^{+}\right) [\mathbf{H}]_{k_N}$
3.	Then obtain $\mathbf{q}_N = \boldsymbol{a}_N / \left\|\boldsymbol{a}_N\right\|_2^2$
	Recursion:
	for $i = N-1, N-2, \cdots, 1$
4.	Find k_i such that $k_i = \underset{\substack{1\leq k\leq N \\ k\neq k_{i+1},\ldots,k_N}}{\operatorname{argmax}} \left\| \left(\mathbf{I} - \bar{\mathbf{H}}_{k,k_{i+1},\ldots,k_N} \bar{\mathbf{H}}_{k,k_{i+1},\ldots,k_N}^{+}\right) [\mathbf{H}]_k \right\|_2^2$
5.	Compute $\boldsymbol{a}_i = \left(\mathbf{I} - \bar{\mathbf{H}}_{k_i,k_{i+1},\ldots,k_N} \bar{\mathbf{H}}_{k_i,k_{i+1},\ldots,k_N}^{+}\right) [\mathbf{H}]_{k_i}$
6.	Then obtain $\mathbf{q}_i = \boldsymbol{a}_i / \left\|\boldsymbol{a}_i\right\|_2^2$
	end
	Conclusion:
7.	Calculate $\mathbf{Q} = [\mathbf{q}_1, ..., \mathbf{q}_N]$, $\boldsymbol{\Pi}_{VB} = [\boldsymbol{e}_{k_1}, \cdots, \boldsymbol{e}_{k_N}]$, and $\mathbf{R} = \mathbf{Q}^{\mathrm{H}} \mathbf{H} \boldsymbol{\Pi}_{VB}$.

composition given in Table 3.3 [25]. Once all iterations in Table 3.3 are completed, the output matrices $\mathbf{Q}$ and $\mathbf{R}$ of this efficient QR decomposition are reached as $\mathbf{QR} = \mathbf{H}\boldsymbol{\Pi}_E$, where $\boldsymbol{\Pi}_E$ denotes the efficient ordering obtained as $\boldsymbol{\Pi}_E = [\boldsymbol{e}_{\pi_1}, \cdots, \boldsymbol{e}_{\pi_N}]$. These efficient ordering schemes avoid the computation of a pseudo-inverse and hence achieve a lower computational complexity than the V-BLAST approach in Table 3.2.

3.3.4 Ordering Complexity Evaluation

The computational costs of different QR decomposition schemes presented above are derived and compared in Table 3.4 in terms of multiply accumulate (MAC) operations. It is obvious that a reduction in computational costs from $\mathcal{O}(N^5)$ to $\mathcal{O}(N^3)$ can be achieved with the sorted QR algorithms over the V-BLAST QR scheme, where the computational cost of the pseudo inverse of an N-dimension square matrix is assumed to be of order N^3 MAC [102].

Table 3.4: Computational complexity comparison of the different ordering algorithms using QR decomposition for $N_t = N_r = N$.

algorithm	normal QR	efficient-order QR [25]	V-BLAST QR [70]
cost, [MAC]	$\frac{1}{2}(N^3 + N^2)$	N^3	$\frac{5}{6}N^5 + N^4 + \frac{2}{3}N^3 + \frac{1}{2}N^2$

Table 3.3: QR efficient ordering algorithm.

	Initialisation:
1.	$\mathbf{Q} = \mathbf{H}$, $\mathbf{R} = \mathbf{0}$, $\boldsymbol{\pi} = [1, 2, \cdots, N]$
	Recursion:
	for $i = 1, 2, \cdots, N$
2.	Find k_i such that $k_i = \underset{i \le k \le M}{\operatorname{argmin}} \left\| [\mathbf{Q}]_k \right\|_2^2$
3.	Interchange columns i and k_i in $\mathbf{Q}$, $\mathbf{R}$ and $\boldsymbol{\pi}$
4.	$r_{ii} = \left\| [\mathbf{Q}]_i \right\|_2$
5.	$[\mathbf{Q}]_i = [\mathbf{Q}]_i / r_{ii}$
	for $k = i + 1, \cdots, N$
6.	$r_{ik} = [\mathbf{Q}]_i^{\mathrm{H}} \cdot [\mathbf{Q}]_k$
7.	$[\mathbf{Q}]_k = [\mathbf{Q}]_k - r_{ik} \cdot [\mathbf{Q}]_i$
	end
	end

3.3.5 Performance of THP with Ordering

A 4×4 MIMO system with channel entries $h_{ij} \in \mathcal{CN}(0, 1)$ is examined in order to investigate the performance of a THP system with different precoding ordering as discussed above. Results are shown in Fig. 3.8 for 2000 channel realisations, for which the BER performances of both "no order" and "arbitrary order" cases are sufficiently similar as discussed earlier. Although the original V-BLAST ordering represents the optimal detection ordering for the DFE, its application in the precoding case does not lead to improved performance and performs even worse than the "no order" case. Contrarily, reverse V-BLAST ordering is the optimum in this case (cf. Fig. 3.8) since late precoded layers have more constraints to avoid interference with previously precoded layers, therefore working with the "best last" ordering strategy [51]. With a very small increase in computational complexity (cf. Table 3.4), both "descending-reverse order" and "efficient order" can greatly improve performance by achieving a gain in SNR of $\simeq 2$ and 3 dB at BER $= 10^{-2}$, respectively, compared to the THP systems without ordering. In particular, the "efficient order" QR decomposition [25] loses only 0.5 dB in BER performance compared to the optimum reverse V-BLAST ordering, but achieves this at a cost that is almost two orders of magnitude lower.

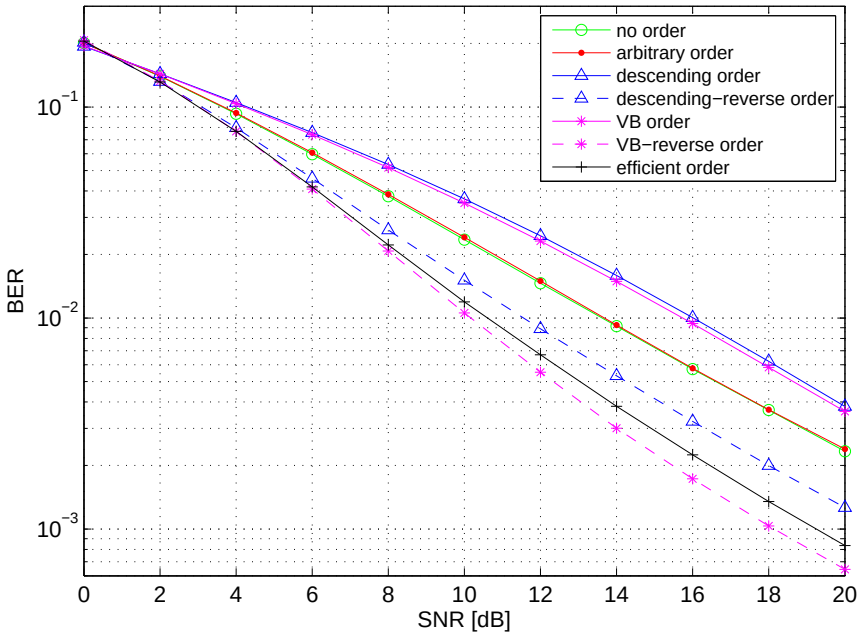

Figure 3.8: Effect of different precoding ordering on BER performance for a 4×4 MIMO THP ZF system.

3.4 Existing MIMO Broadband Approaches

The detection order in the THP and particularly the DFE case are important for the robustness of the transmission scheme. For narrowband MIMO systems, the optimal detection order is provided by the V-BLAST algorithm, a successive interference cancellation (SIC) method that has been adopted for the broadband case in [14]. In a reduced approach, termed partially connected ordered SIC DFE, data streams are successively extracted in the MIMO receiver, detected, and their contributions subtracted out from the received signal to eliminate interference from subsequently detected data streams. The ordering is determined by means of identifying at each stage the best performing MMSE receiver for each data stream. Thus, the strongest contributions, which are more resilient to interference, are detected first, while weak data streams can subsequently be detected more reliably [14]. A fully connected algorithm achieves only a marginal performance improvement in terms of BER at a significantly higher computational effort.

3.4.1 THP with Joint Spatio-Temporal Ordering

Fig. 3.9 shows a MIMO-THP transceiver model designed to combat spatio-temporal interference that is incurred by the ISI MIMO channel $\mathbf{H}[n]$ of order Q shown in Fig 2.1 and described by (2.1) with N_t transmit antennas and $N_r = N$ receive antennas. Joint spatio-temporal interference mitigation optimised w.r.t. the MSE is presented in [17], whereby spatial precoding ordering, as presented in Sec. 3.3 for the narrowband case, is considered here designated by the permutation matrix

$$\mathbf{\Pi}_\nu = \sum_{i=1}^{N} \boldsymbol{e}_i \boldsymbol{e}_{o_i}^{\mathrm{T}} \in \{0,1\}^{N\times N}, \tag{3.20}$$

with precoding ordering $\mathcal{O} = (o_1, \ldots, o_N)$, where $\{o_1, \ldots, o_N\} = \{1, \ldots, N\}$, while decision delay or latency time is signified by ν. Referring to Fig. 3.9, two feedback filters are considered namely the spatial feedback filter $\mathbf{B}$ and the temporal feedback filter $\mathbf{T}[n]$, which have to assure system causality by restricting $\mathbf{B} \in \mathbb{L}^{N\times N}$. Here, $\mathbb{L}$ is the set of strictly lower left triangular matrices and $\mathbf{T}[n]$ is defined as

$$\mathbf{T}[n] = \sum_{i=1}^{L_T} \mathbf{T}_i \delta[n-i], \tag{3.21}$$

where $\mathbf{T}_i \in \mathbb{C}^{N\times N}$ and L_T is the filter order. The precoder or feedforward filter is denoted by $\mathbf{P}[n]$. Prior to the modulo operation in the receiver a gain g is applied to compensate for any scaling applied by the channel matrix $\mathbf{H}[n]$.

The equivalent data vector $\mathbf{d}[n]$ using the linearised transmit modulo model of Fig. 3.9 (b) can be obtained from $\mathbf{u}[n]$ as

$$\begin{aligned} \mathbf{u}[n] &= \mathbf{\Pi}_\nu \mathbf{d}[n] + \mathbf{B}\mathbf{u}[n] + \mathbf{T}[n] \star \mathbf{u}[n] \\ \Rightarrow \mathbf{d}[n] &= \mathbf{\Pi}_\nu^{\mathrm{T}} (\mathbf{I}_N - \mathbf{B})\, \mathbf{u}[n] - \mathbf{\Pi}_\nu^{\mathrm{T}} \sum_{i=1}^{L_T} \mathbf{T}_i \mathbf{u}[n-i], \end{aligned} \tag{3.22}$$

note that $\mathbf{\Pi}_\nu^{-1} = \mathbf{\Pi}_\nu^{\mathrm{T}}$. By analogy with the linear precoding system depicted in Fig. 2.7 and using the same definition for $\mathbf{P}$ and $\mathbf{H}$ as in (2.24) and for $\boldsymbol{S}^{(i)}$ as in (2.26), the observation $\hat{\mathbf{d}}[n]$ can similarly be given by

$$\hat{\mathbf{d}}[n] = g \sum_{i=0}^{Q+L} \boldsymbol{S}^{(i)} \mathbf{H}\mathbf{P}\mathbf{u}[n-i] + g\mathbf{v}[n]\ . \tag{3.23}$$

To simplify the derivation of the MMSE MIMO-THP filters given in [17], a block

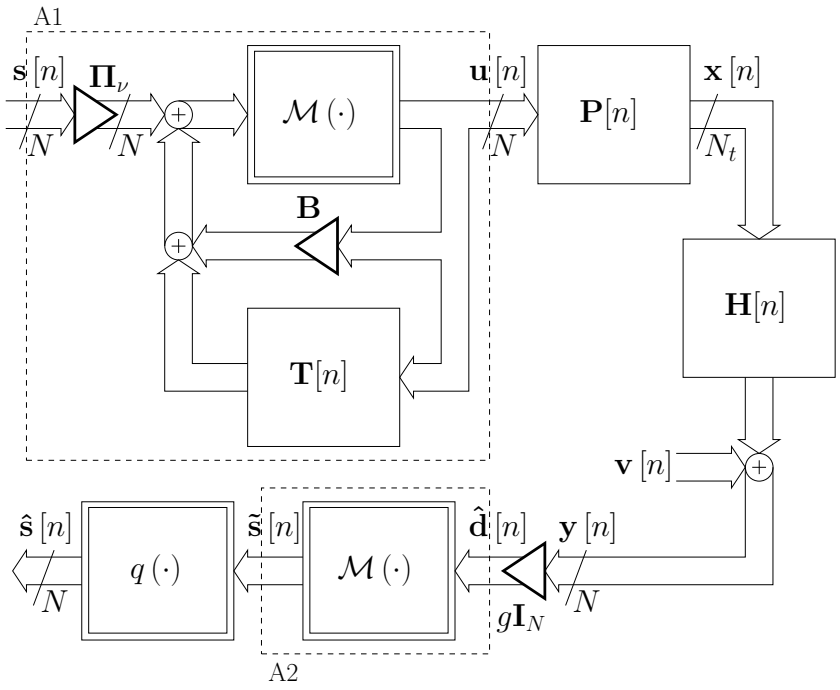

(a)

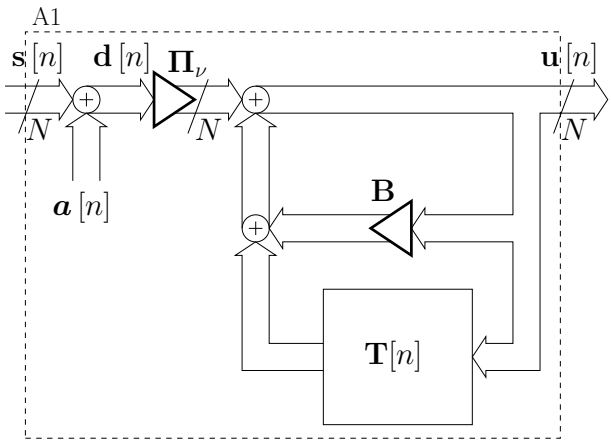

(b)

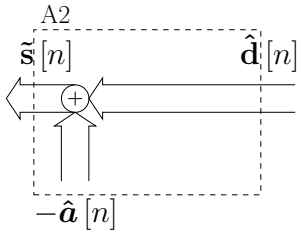

(c)

Figure 3.9: MIMO THP with spatio-temporal ordering optimisation; (a) shows the complete transceiver model, (b) its linearised transmit modulo model, and (c) its linear receive modulo model.

diagonal permutation matrix blkdiag $(\mathbf{\Pi}_0, \ldots, \mathbf{\Pi}_{Q+L})$ is defined such that

$$\mathbf{C} = \text{blkdiag}\left(\mathbf{\Pi}_0, \ldots, \mathbf{\Pi}_{Q+L}\right)\mathbf{H} \in \mathbb{C}^{N(Q+L+1)\times N_t(L+1)} \tag{3.24}$$

is a permuted block Toeplitz channel matrix, where the $Q+L+1$ blocks of dimension $N \times N_t\,(L+1)$ of $\mathbf{H}$ are now differently permuted according to the corresponding permutations $\mathbf{\Pi}_i, 0 \leq i \leq Q+L$. It is important to note that since we are seeking the precoding ordering provided by the permutation matrix $\mathbf{\Pi}_\nu$, i.e. at a latency time ν, therefore all other permutations $\mathbf{\Pi}_i, i \neq \nu$ are not affecting the solution and hence can be arbitrarily selected ($\mathbf{I}_N$ for example). With this arrangement and by noting that

$$\mathbf{\Pi}_i \boldsymbol{S}^{(i)} = \boldsymbol{S}^{(i)}\text{blkdiag}\left(\mathbf{\Pi}_0, \ldots, \mathbf{\Pi}_{Q+L}\right), \tag{3.25}$$

(3.23) can be reformulated as

$$\begin{aligned}\hat{\mathbf{d}}\,[n] &= g\sum_{i=0}^{Q+L}\mathbf{\Pi}_i^{\mathrm{T}}\mathbf{\Pi}_i\boldsymbol{S}^{(i)}\mathbf{H}\mathbf{P}\mathbf{u}\,[n-i] + g\mathbf{v}\,[n]\,,\\ &= g\sum_{i=0}^{Q+L}\mathbf{\Pi}_i^{\mathrm{T}}\boldsymbol{S}^{(i)}\mathbf{C}\mathbf{P}\mathbf{u}\,[n-i] + g\mathbf{v}\,[n]\;.\end{aligned} \tag{3.26}$$

Similar to the linear precoding case in (2.23), the MMSE MIMO-THP solution can now be written as

$$\begin{aligned}&\{\mathbf{P}_{\text{THP}}, \mathbf{B}_{\text{THP}}, \mathbf{T}_{\text{THP},1}, \ldots, \mathbf{T}_{\text{THP},L_T}, g_{\text{THP}}, \nu_{\text{THP}}, \mathcal{O}_{\text{THP}}\}\\ &= \left\{\begin{array}{cc} \underset{\{\mathbf{P},\mathbf{B},\mathbf{T}_1,\ldots,\mathbf{T}_{L_T},g,\nu,\mathcal{O}\}}{\text{argmin}} & \mathbb{E}\left[\left\|\mathbf{d}\,[n-\nu] - \hat{\mathbf{d}}\,[n]\right\|_2^2\right] \\ \text{subject to} & \mathbf{B} \in \mathbb{L}^{N\times N} \text{ and } \mathbb{E}\left[\|\mathbf{x}\,[n]\|_2^2\right] = P_{\text{budget}}\,.\end{array}\right.\end{aligned} \tag{3.27}$$

Using (3.22), (3.26) and making use of $\sum_{i=0}^{Q+L}\boldsymbol{S}^{(\nu),\mathrm{T}}\boldsymbol{S}^{(\nu)} = \mathbf{I}_{N(Q+L+1)}$, the MSE in (3.27) can be given as

$$\begin{aligned}\mathbb{E}\left[\left\|\mathbf{d}\,[n-\nu] - \hat{\mathbf{d}}\,[n]\right\|_2^2\right] = \;& \sigma_u^2\text{tr}\left(\mathbf{I}_N + \mathbf{B}\mathbf{B}^{\mathrm{H}}\right) + \sigma_u^2\textstyle\sum_{i=1}^{L_T}\text{tr}\left(\mathbf{T}_i\mathbf{T}_i^{\mathrm{H}}\right)\\ &+ |g|^2\,\text{tr}\left(\mathbf{R}_{vv}\right) + \sigma_u^2\,|g|^2\,\text{tr}\left(\mathbf{C}\mathbf{P}\mathbf{P}^{\mathrm{H}}\mathbf{C}^{\mathrm{H}}\right)\\ &-2\sigma_u^2\Re\left(\text{tr}\left(g\boldsymbol{S}^{(\nu)}\mathbf{C}\mathbf{P}\left(\mathbf{I}_N - \mathbf{B}\right)^{\mathrm{H}}\right)\right)\\ &+2\sigma_u^2\textstyle\sum_{i=1}^{L_T}\Re\left(\text{tr}\left(g\mathbf{\Pi}_{\nu+i}^{\mathrm{T}}\boldsymbol{S}^{(\nu+i)}\mathbf{C}\mathbf{P}\mathbf{T}_i^{\mathrm{H}}\mathbf{\Pi}_\nu\right)\right),\end{aligned} \tag{3.28}$$

where as in Sec. 3.2.1 $\mathbf{u}\,[n]$ is assumed spatially and temporally uncorrelated, i.e.

$\mathbb{E}\left[\mathbf{u}\left[n\right]\mathbf{u}^{\mathrm{H}}\left[n+\nu\right]\right] = \sigma_u^2\mathbf{I}_N\delta\left[\nu\right]$, in (3.28). The power constraint in (3.27) can simply be rephrased as

$$\mathbb{E}\left[\left\|\mathbf{x}\left[n\right]\right\|_2^2\right] = \sigma_u^2\mathrm{tr}\left(\mathbf{P}\mathbf{P}^{\mathrm{H}}\right) = P_{\mathrm{budget}}, \tag{3.29}$$

since $\mathbf{x}\left[n\right] = \mathbf{P}\left[n\right]\star\mathbf{u}\left[n\right]$ and $\sum_{i=0}^{L}\mathrm{tr}\left(\mathbf{P}\left[i\right]\mathbf{P}^{\mathrm{H}}\left[i\right]\right) = \mathrm{tr}\left(\mathbf{P}\mathbf{P}^{\mathrm{H}}\right)$. Also the constraint on $\mathbf{B}$ in (3.27) can be rewritten as

$$\boldsymbol{S}_i\mathbf{B}\boldsymbol{e}_i = \mathbf{0}_{i\times 1}, \quad i = 1,\ldots,N, \tag{3.30}$$

where another selection matrix $\boldsymbol{S}_i$ is introduced as

$$\boldsymbol{S}_i = \left[\mathbf{I}_i, \mathbf{0}_{i\times N-i}\right] \in \left\{0,1\right\}^{i\times N}\ . \tag{3.31}$$

Incorporating (3.28), (3.29), and (3.30) into the optimisation in (3.27) and using the Lagrangian multiplier method as in (2.23), the solutions for the MMSE MIMO-THP filters are given by [17]

$$\mathbf{P}_{\mathrm{THP}} = \frac{1}{g_{\mathrm{THP}}}\sum_{i=1}^{N}\mathbf{C}^{\mathrm{H}}\mathbf{A}_{\nu_{\mathrm{THP}},i}^{(\mathcal{O}_{\mathrm{THP}}),-1}\boldsymbol{S}^{(\nu_{\mathrm{THP}}),\mathrm{T}}\boldsymbol{e}_i\boldsymbol{e}_i^{\mathrm{T}}, \tag{3.32a}$$

$$\mathbf{B}_{\mathrm{THP}} = -g_{\mathrm{THP}}\sum_{i=1}^{N}\left(\mathbf{I}_N - \boldsymbol{S}_i^{\mathrm{T}}\boldsymbol{S}_i\right)\boldsymbol{S}^{(\nu_{\mathrm{THP}})}\mathbf{C}\mathbf{P}_{\mathrm{THP}}\boldsymbol{e}_i\boldsymbol{e}_i^{\mathrm{T}}, \tag{3.32b}$$

$$\mathbf{T}_{\mathrm{THP},i} = \begin{cases} -g_{\mathrm{THP}}\boldsymbol{\Pi}_{\nu_{\mathrm{THP}}}\boldsymbol{\Pi}_{\nu_{\mathrm{THP}}+i}^{\mathrm{T}}\boldsymbol{S}^{(\nu_{\mathrm{THP}}+i)}\mathbf{C}\mathbf{P}_{\mathrm{THP}} \\ \qquad \text{for } i = 1,\ldots,Q+L-\nu_{\mathrm{THP}}, \\ \mathbf{T}_{\mathrm{THP},i} = \mathbf{0}_{N\times N} \qquad \text{otherwise}, \end{cases} \tag{3.32c}$$

$$g_{\mathrm{THP}} = \sqrt{\frac{\sigma_u^2}{P_{\mathrm{budget}}}\sum_{i=1}^{N}\boldsymbol{e}_i^{\mathrm{T}}\boldsymbol{S}^{(\nu_{\mathrm{THP}})}\mathbf{C}\mathbf{C}^{\mathrm{H}}\mathbf{A}_{\nu_{\mathrm{THP}},i}^{(\mathcal{O}_{\mathrm{THP}}),-2}\boldsymbol{S}^{(\nu_{\mathrm{THP}}),\mathrm{T}}\boldsymbol{e}_i}, \tag{3.32d}$$

where

$$\mathbf{A}_{\nu,i}^{(\mathcal{O})} = \boldsymbol{S}_{\nu,i}^{\mathrm{T}}\boldsymbol{S}_{\nu,i}\mathbf{C}\mathbf{C}^{\mathrm{H}}\boldsymbol{S}_{\nu,i}^{\mathrm{T}}\boldsymbol{S}_{\nu,i} + \xi\mathbf{I}_{N(Q+L+1)}\,. \tag{3.33}$$

The selection matrix $\boldsymbol{S}_{\nu,i}$ returns the first $N\nu+i$ rows of a matrix with $N\left(Q+L+1\right)$ rows when applied from the left, defined as

$$\boldsymbol{S}_{\nu,i} = \left[\mathbf{I}_{N\nu+i}, \mathbf{0}_{N\nu+i\times N(Q+L-\nu+1)-i}\right]\ . \tag{3.34}$$

Note that the optimum values for the latency and the precoding order are needed to compute the filters in (3.32a)-(3.32d) which can be obtained according to the

optimisation [17]

$$\{\nu_{\text{THP}}, \mathcal{O}_{\text{THP}}\} = \underset{\{\nu,\mathcal{O}\}}{\operatorname{argmin}} \sum_{i=1}^{N} \boldsymbol{e}_i^{\text{T}} \boldsymbol{S}^{(\nu)} \mathbf{A}_{\nu,i}^{(\mathcal{O}),-1} \boldsymbol{S}^{(\nu),\text{T}} \boldsymbol{e}_i \,. \tag{3.35}$$

In fact, (3.35) represents the computational bottleneck of the MMSE MIMO-THP filter solution since for every latency value, which is found to lie in the interval $\nu \in \{L, \ldots, Q+L\}$ [17], all precoding orders $\mathcal{O}$ of a total number of $N!$ have to be considered resulting in a complexity burden in computing the inversion of a size of $N\,(Q+L+1) \times N\,(Q+L+1)$ for the matrix $\mathbf{A}_{\nu,i}^{(\mathcal{O})}$ in (3.35). In the following, a simplification in computation of (3.35) is derived as follows [17].

Using (3.25), the l.h.s. of (3.35) can be rephrased as

$$\begin{aligned} &\sum_{i=1}^{N} \boldsymbol{e}_i^{\text{T}} \boldsymbol{\Pi}_\nu \boldsymbol{\Pi}_\nu^{\text{T}} \boldsymbol{S}^{(\nu)} \mathbf{A}_{\nu,i}^{(\mathcal{O}),-1} \boldsymbol{S}^{(\nu),\text{T}} \boldsymbol{\Pi}_\nu \boldsymbol{\Pi}_\nu^{\text{T}} \boldsymbol{e}_i \\ &\qquad = \sum_{i=1}^{N} \boldsymbol{e}_{o_i}^{\text{T}} \boldsymbol{S}^{(\nu)} \boldsymbol{\Gamma}_{\nu,i}^{(\mathcal{O}),-1} \boldsymbol{S}^{(\nu),\text{T}} \boldsymbol{e}_{o_i}, \end{aligned} \tag{3.36}$$

where $\boldsymbol{\Gamma}_{\nu,i}^{(\mathcal{O}),-1} = \boldsymbol{\Pi}_{\nu,i}^{(\mathcal{O})} \mathbf{H}\mathbf{H}^{\text{H}} \boldsymbol{\Pi}_{\nu,i}^{(\mathcal{O})} + \xi \mathbf{I}_{N(Q+L+1)} \in \mathbb{C}^{N(Q+L+1)\times N(Q+L+1)}$ with a projector matrix $\boldsymbol{\Pi}_{\nu,i}^{(\mathcal{O})} \in \{0,1\}^{N(Q+L+1)\times N(Q+L+1)}$defined as

$$\begin{aligned} \boldsymbol{\Pi}_{\nu,i}^{(\mathcal{O})} &= \text{blkdiag}\left(\boldsymbol{\Pi}_0^{\text{T}}, \ldots\right) \boldsymbol{S}_{\nu,i}^{\text{T}} \boldsymbol{S}_{\nu,i} \text{blkdiag}\left(\boldsymbol{\Pi}_0, \ldots\right) \\ &= \sum_{j=0}^{\nu} \boldsymbol{S}^{(j),\text{T}} \boldsymbol{S}^{(j)} - \boldsymbol{S}^{(\nu),\text{T}} \boldsymbol{\Pi}_\nu^{\text{T}} \left(\mathbf{I}_N - \boldsymbol{S}_i^{\text{T}} \boldsymbol{S}_i\right) \boldsymbol{\Pi}_\nu \boldsymbol{S}^{(\nu)} \\ &= \sum_{j=0}^{\nu} \boldsymbol{S}^{(j),\text{T}} \boldsymbol{S}^{(j)} - \begin{cases} \mathbf{0}_{N(Q+L+1)\times N(Q+L+1)}, & i = N \\ \boldsymbol{S}^{(\nu),\text{T}} \sum\limits_{j=i+1}^{N} \boldsymbol{e}_{o_j} \boldsymbol{e}_{o_j}^{\text{T}} \boldsymbol{S}^{(\nu)}, & \text{otherwise}\,. \end{cases} \end{aligned} \tag{3.37}$$

Interestingly, it is clear from (3.37) that the computation of $\boldsymbol{\Pi}_{\nu,i}^{(\mathcal{O})}$ depends only on the indices $o_{i+1}, \ldots, o_N$ of the precoding order $\mathcal{O}$, which means that if $i = N$ no precoding order is required to compute $\boldsymbol{\Pi}_{\nu,i}^{(\mathcal{O})}$. This therefore motivates to start with computing o_N that minimises (3.36) and then successively compute the remaining orders $o_i, i = N-1, \ldots, 1$ by minimising the ith summand of (3.36) for fixed $o_{i+1}, \ldots, o_N$. In other words, the precoding order can be achieved using (3.37) and (3.36) according to

$$\begin{aligned} \text{Find}\, \mathcal{O}_{\text{THP}} &= (o_1, \ldots, o_N) \\ \text{such that} \quad o_i &= \underset{o \in \mathcal{O}_i'}{\operatorname{argmin}}\; \boldsymbol{e}_o^{\text{T}} \boldsymbol{S}^{(\nu)} \boldsymbol{\Gamma}_{\nu,i}^{(\mathcal{O}),-1} \boldsymbol{S}^{(\nu),\text{T}} \boldsymbol{e}_o, \quad i = N, \ldots, 1, \end{aligned} \tag{3.38}$$

where $\mathcal{O}_i' = \{1, \ldots, N\} \setminus \{o_{i+1}, \ldots, o_N\}$ is the set of possible values for o_i (i.e. the values that have not been selected yet), with obviously $\mathcal{O}_N' = \{1, \ldots, N\}$.

Now the precoding order $\mathcal{O}_{\text{THP}}$ is locally optimised for a given value of the latency time ν. Consequently for a joint optimisation of both $\{\nu, \mathcal{O}\}$ as in (3.35), the above arrangements have to be considered for every $\nu \in \{L, \ldots, Q + L\}$ and ν has to be chosen to globally optimise (3.35) in conjunction with $\mathcal{O}_{\text{THP}}$, i.e. $\{\nu_{\text{THP}}, \mathcal{O}_{\text{THP}}\}$ that minimises (3.35).

3.5 Proposed Methods

In this section we introduce a number of non-linear precoding and equalisation techniques, which aim to remove IBI (as well as ISI) by means other than the redundancy-incurring methods of linear block-based processing addressed in Sections 2.3.1 and 2.3.2, which subsequently lead to reduced spectral efficiency. Non block-based approaches with linear [17, 13] or non-linear processing [45, 88, 17, 72], on the other hand, lack the optimality gained by rate-loading schemes as all subchannels have to be loaded with identical rate and power, therefore performance is dominated by poor subchannels. Moreover, an exhaustive search is required in the case of non-linear processing to jointly optimise ordering in space and time for transmitted data precoding [17] or received signal equalisation [14], or to provide a mixture thereof [15].

In our proposed methods, the joint equalisation and precoding of a broadband MIMO system is based on a two-step approach, whereby first the MIMO channel is decoupled into a number of independent SISO subchannels using the the BSVD technique [19] presented in Sec. 2.3.4 thereby mitigating the CCI discussed in Sec. 3.5.1. The remaining SISO subchannels are still dispersive and cause ISI, whose mitigation is addressed in Sec. 3.5.2.

3.5.1 Mitigation of Co-Channel Interference

If channel state information is available at both receiver and transmitter, then the paraunitary matrices $\mathbf{U}(z) \in \mathbb{C}^{N_t \times N_r}$ and $\mathbf{V}(z) \in \mathbb{C}^{N_t \times N_t}$ arising from a broadband SVD [103, 19] of the channel matrix $\mathbf{H}(z) \rightleftharpoons \mathbf{H}[n]$ as $\mathbf{H}(z) = \mathbf{U}(z)\mathbf{\Sigma}(z)\tilde{\mathbf{V}}(z)$ can be utilised to obtain a linear equaliser and precoder as depicted in Fig. 3.10, where $N = \min(N_t, N_r)$. If

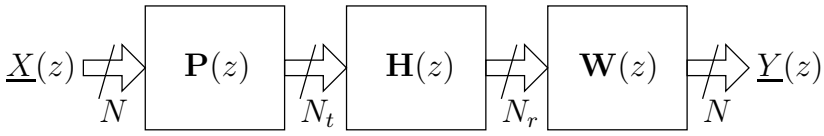

Figure 3.10: Co-Channel interference mitigation with precoder $\mathbf{P}(z)$ and equaliser $\mathbf{W}(z)$.

$$\mathbf{U}(z) = \left[\begin{array}{cccc} \underline{U}_0(z) & \underline{U}_1(z) & \cdots & \underline{U}_{N_r-1}(z) \end{array} \right], \tag{3.39}$$

$$\text{and} \quad \mathbf{V}(z) = \left[\begin{array}{cccc} \underline{V}_0(z) & \underline{V}_1(z) & \cdots & \underline{V}_{N_t-1}(z) \end{array} \right], \tag{3.40}$$

then the precoder and equaliser are defined, respectively, as

$$\mathbf{P}(z) = \left[\begin{array}{cccc} \underline{V}_0(z) & \underline{V}_1(z) & \cdots & \underline{V}_{N-1}(z) \end{array} \right], \tag{3.41}$$

$$\text{and} \quad \mathbf{W}(z) = \left[\begin{array}{c} \tilde{U}_0(z) \\ \tilde{U}_1(z) \\ \vdots \\ \tilde{U}_{N-1}(z) \end{array} \right], \tag{3.42}$$

to obtain

$$\tilde{\mathbf{V}}(z)\mathbf{P}(z) = \begin{cases} \mathbf{I}_{N_t} & N_r \geq N_t, \\ \left[\begin{array}{c} \mathbf{I}_{N_r} \\ \mathbf{0}_{(N_t-N_r)\times N_r} \end{array} \right] & N_r < N_t, \end{cases} \tag{3.43}$$

$$\text{and} \quad \mathbf{W}(z)\mathbf{U}(z) = \begin{cases} \left[\mathbf{I}_{N_t} \ \mathbf{0}_{N_t\times(N_r-N_t)} \right] & N_r \geq N_t, \\ \mathbf{I}_{N_r} & N_r < N_t, \end{cases} \tag{3.44}$$

such that

$$\underline{Y}(z) = \mathbf{\Sigma}(z)\underline{X}(z), \tag{3.45}$$

where the channel noise $\mathbf{v}[n]$ is omitted in (3.45) for the sake of brevity. With $\mathbf{\Sigma}(z)$ being approximately diagonal, the MIMO system has been decoupled and co-channel interference is suppressed.

3.5.2 Mitigation of Inter-Symbol Interference

The transmission over each decoupled SISO subchannel of (3.45)

$$Y_i(z) = \Sigma_i(z)X_i(z)$$

is still subject to ISI, which we here aim to remove by non-linear methods. Different from standard transmission channels, even if the FIR components of the channel matrix $\mathbf{H}(z)$ are minimum-phase, $\Sigma_i(z)$ is generally non-minimum phase. Either the DFE or THP system can be used to independently mitigate these individual ISI (temporal) interferences generated by $\Sigma_i(z), 1 \leq i \leq N$. However, the performance of a DFE/THP for a SISO subchannel depends on the subchannel SNR, i.e. the performance of the various transmission subsystems drops with subchannel index i due to thespectral majorisation property in (2.35)of the BSVD algorithm. This motivates the application of power or bit loading approaches to distribute transmission rates according to the individual qualities of $\Sigma_i(z)$as will be discussed in Sec. 3.5.2.2.

If an incorrect decision is incurred in a DFE, then this error may propagate to degrade subsequent detections. For this reason, the DFE can be operated in the transmitter instead, whereby the transmitted signal is shaped such that interference annihilates at the receiver. Since the decision feedback is performed in the transmitter in the absence of channel noise, no incorrect decisions or error propagation can be incurred as in the spatial interference case in Section 3.2. The combination of a DFE operated in the transmitter with the limitation of the transmit power by a modulo-extended constellation pattern leads to the original THP [22, 23] system. For a QAM constellation map of K-bit symbols, the standard constellation pattern consists of the values $a + jb$ with $a, b \in \{-K+1, -K+3, \cdots, K-3, K-1\}$ while for THP the transmit signal amplitude will be distributed over the larger interval $[-K, K)$ for both real and imaginary part of the transmitted samples, leading to a small increase in transmit power (cf. Fig. 3.5).

3.5.2.1 Temporal DFE

A DFE operates on the CCI-mitigated signal $Y_i(z)$ in the receiver, and contains a linear feedforward filter to suppress all maximum phase components of the SISO subchannel, and a feedback filter fed by detected symbols up to sampling period $n-1$ in order to remove the remaining minimum-phase part of the combined response of subchannel $\Sigma_i(z)$ and the feedforward filter. The parameters to be selected for this DFE comprise of the lengths of both feedforward and feedback filters, as well as the decision delay of the system, which is usually coupled to the feedforward system [104]. Here, the parameters are selected in order to provide an overall minimised MSE.

In the following, a SISO-DFE model optimised for MMSE is derived for the ge-

neral system model outlined in Fig 3.11 with channel impulse response $h[n] \in \mathbb{C}^Q$, feedforward filter $f[n] \in \mathbb{C}^{L_f}$, feedback filter $b[n] \in \mathbb{C}^{L_b}$ and decision delay Δ defined such that $q(y[n]) = x[n-\Delta]$. Whereby Fig. 3.11(a) describes the actual system while Fig. 3.11(b) represents a simplified model assuming the correctness of any decisions being made by the non-linear decision device $q(\cdot)$, which is referred to as a genie-aided system. The simplicity of the genie-aided system is due to the fact that instead of a system with feedback, the problem reduces to the design of a two-channel system.

In matrix formulation, the equaliser output $y[n]$ prior to any decision in Fig. 3.11(b) is given by

$$y[n] = \mathbf{f}^{\mathrm{H}} \left(\boldsymbol{\mathcal{H}}\mathbf{x}_n + \mathbf{v}\right) - \mathbf{b}^{\mathrm{H}}\mathbf{D}\mathbf{x}_n \,,$$

whereby

$$\mathbf{f}^{\mathrm{H}}=[f_0,\ f_1, \cdots, f_{L_f-1}]$$

contains the coefficients of the feedforward and

$$\mathbf{b}^{\mathrm{H}}=[b_0,\ b_1, \cdots, b_{L_b-1}]$$

the coefficients of the feedback filter. Note that when no constraints are placed on filter length, the optimal DFE filters generally have infinite length. To reduce complexity, improve stability, or allow adaptability, however, many designs use FIR filters in both the feedforward and feedback sections [104]. The convolutional matrix $\boldsymbol{\mathcal{H}} \in \mathbb{C}^{L_f \times K}$ with $K = \max\{L_f+Q-1, L_b+\Delta+1\}$ contains the coefficients of the channel impulse response,

$$\boldsymbol{\mathcal{H}} = \left[\begin{array}{cccccc|c} h_0 & h_1 & \cdots & h_{Q-1} & & & \\ & h_0 & h_1 & \cdots & h_{Q-1} & & \\ & & \ddots & & & \ddots & \mathbf{0}_{L_f \times K-L_f-Q+1} \\ & & & h_0 & h_1 & \cdots \; h_{Q-1} & \end{array}\right] ,$$

while the matrix $\mathbf{D} \in \mathbb{C}^{L_b \times K}$

$$\mathbf{D} = \left[\mathbf{0}_{L_b \times (\Delta+1)} \;\; \mathbf{I}_{L_b} \;\; \mathbf{0}_{L_b \times (K-L_b-\Delta-1)}\right]$$

imposes the delay of $\Delta + 1$ samples imposed onto the input signal organised in a

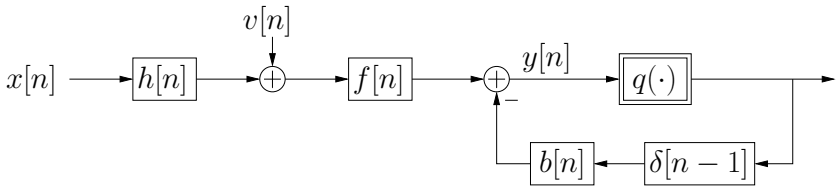

(a)

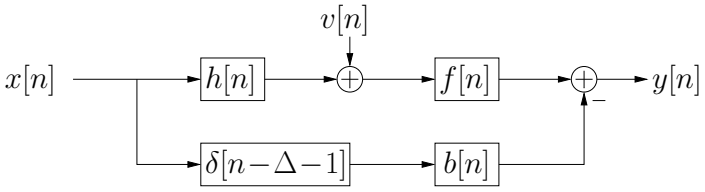

(b)

Figure 3.11: SISO-DFE system with channel impulse response $h\,[n]$, feedforward filter $f\,[n]$, feedback filter $b\,[n]$ and decision delay Δ: (a) true system, (b) genie-aided version.

tap delay line vector $\mathbf{x}_n \in \mathbb{C}^K$,

$$\mathbf{x} = \begin{bmatrix} x[n] \\ x[n-1] \\ \vdots \\ x[n-K+1] \end{bmatrix}.$$

The error can be formulated as

$$e[n] = y[n] - x[n] = y[n] - \mathbf{d}^{\mathrm{T}}\mathbf{x}_n \tag{3.46}$$

incorporating the decision delay of Δ samples by means of a pinning vector

$$\mathbf{d} = \begin{bmatrix} \mathbf{0}_{1\times\Delta} & 1 & \mathbf{0}_{1\times(K-\Delta-1)} \end{bmatrix}^{\mathrm{T}}.$$

Squaring and taking expectations of (3.46) yields

$$\xi_{\mathrm{DFE}} = \left(\mathbf{f}^{\mathrm{H}}\boldsymbol{\mathcal{H}} - \mathbf{b}^{\mathrm{H}}\mathbf{D} - \mathbf{d}^{\mathrm{T}}\right)\mathbf{R}_{xx}\left(\boldsymbol{\mathcal{H}}^{\mathrm{H}}\mathbf{f} - \mathbf{D}^{\mathrm{H}}\mathbf{b} - \mathbf{d}\right) + \mathbf{f}^{\mathrm{H}}\mathbf{R}_{vv}\mathbf{f}$$

as the mean squared error of the genie-aided DFE system of Fig. 3.11(b). There-

fore the MSE-optimal solution, can be found as

$$\mathbf{w}_{\text{opt}} = \left(\underbrace{\begin{bmatrix} \boldsymbol{\mathcal{H}} \\ \mathbf{D} \end{bmatrix} \mathbf{R}_{xx} \begin{bmatrix} \boldsymbol{\mathcal{H}} \\ \mathbf{D} \end{bmatrix}^{\text{H}} + \begin{bmatrix} \mathbf{R}_{vv} & \mathbf{0}_{L_f \times L_b} \\ \mathbf{0}_{L_b \times L_f} & \mathbf{0}_{L_b \times L_b} \end{bmatrix}}_{\mathcal{R}} \right)^{-1} \begin{bmatrix} \boldsymbol{\mathcal{H}} \\ \mathbf{D} \end{bmatrix} \mathbf{R}_{xx} \mathbf{d}, \quad (3.47)$$

where

$$\mathbf{w} = \begin{bmatrix} \mathbf{f} \\ -\mathbf{b} \end{bmatrix} \in \mathbb{C}^{L_f + L_b}. \quad (3.48)$$

For a detailed derivation, please refer to Appendix A.2.

As an illustrative example for the above solution in (3.47), a 5-tap SISO channel of complex entries and a power delay profile for both minimum phase and non-minimum phase cases as shown by the left-most of Figs. 3.12(a) and (b), is utilised. The role of the feedforward filter $\mathbf{f}$ and feedback filter $\mathbf{b}$ are apparent from Fig. 3.12 as discussed above for both ZF (obtained from (3.47) by ignoring the second term of $\mathcal{R}$, i.e. $\mathbf{R}_{vv} = \mathbf{0}$) and MMSE solutions with two different SNR values of 10 and 20 dB. Note that the MMSE solution does not perfectly remove the interference as in the ZF counterpart because the noise term is taken into account for the MMSE design.

3.5.2.2 Temporal THP

Alternative to the DFE approach in Sec. 3.5.2.1, THP can be applied. With co-channel interference mitigated by the BSVD step, we end up with a diagonalised system with spectrally majorised individual dispersive SISO subchannels (3.51) as depicted in Fig. 3.13. The next task is to mitigate the effect of dispersion incurred by these SISO subchannels as well as to exploit the spectral majorisation of the BSVD algorithm. To this end, a rate-scaled THP system is proposed whereby individual data layers are fashioned to achieve throughput that best matches their respective SISO subchannels by selecting from different square M-QAM constellations (QPSK, 16-QAM, 64-QAM, or 256-QAM) while the weakest subchannels may or may not be used according to a transmission target throughput.

Given the ith subchannel $\boldsymbol{\Sigma}_i(z)$ which is usually non-minimum phase, the role of the feedforward filter $F_i(z)$ with length $L_f^{(i)}$ is to drive the end-to-end discrete-time response $\boldsymbol{\Sigma}_i(z)F_i(z)$ to a monic minimum phase system, while the task of the $L_b^{(i)}$-tap feedback filter $B_i(z)$ is to completely remove the remaining postcursor of $\boldsymbol{\Sigma}_i(z)F_i(z)$ by the iterative THP feedback loop. These two filters along with the decision delay are computed for each $\boldsymbol{\Sigma}_i(z)$ using spectral factorisation theory,

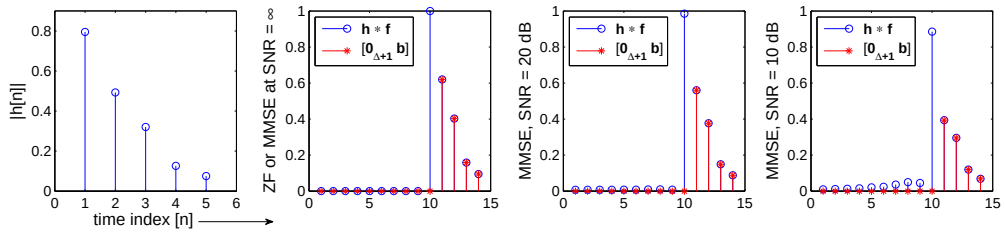

(a)

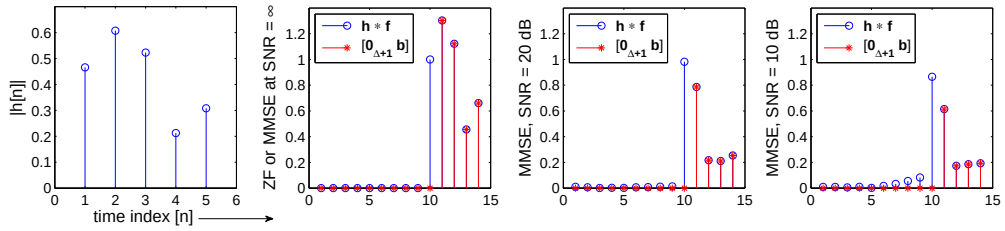

(b)

Figure 3.12: An example of a 5-tap SISO system and its DFE ZF and MMSE filter solutions at different SNR values for (a) minimum phase channel, and (b) non-minimum phase channel.

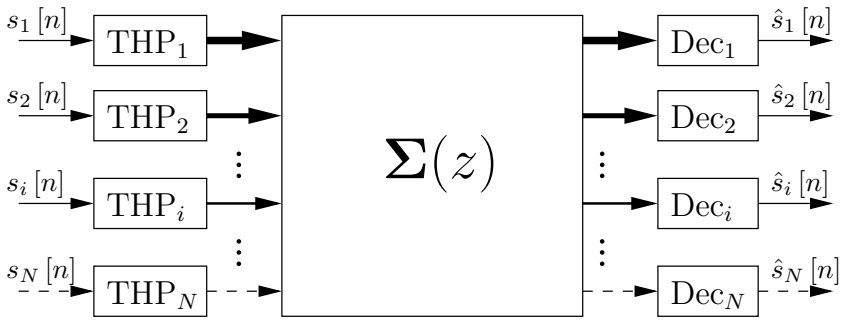

Figure 3.13: Equivalent model to Fig. 3.10 with THP applied for resulting SISO subchannels with details of THP_i and Dec_i blocks are given in Fig. 3.14.

details for which can be found in [13, 105].

A suitable bit loading is applied to each SISO subchannel according to its strength. With the spectral majorisation property (2.35) of the iterative BSVD algorithm, the resulting SISO subchannels appearing in the main diagonal of the decoupled system in (2.34) are ordered in descending gain. The weakest subchannels may be unreliable and hence deselected for transmission. We aim to operate the proposed equivalent SISO system to achieve the same target throughput as its respective original MIMO system. To achieve this, two THP methods are used and described below, namely spectral factorisation and block transmission schemes.

3.5.2.2.1 Spectral Factorisation. Fig. 3.14(a) shows a THP system designed to mitigate ISI of the ith subchannel $\mathbf{\Sigma}_i(z)$ in Fig. 3.13. The filter computations are based on the spectral factorisation method detailed in [13, 105]. Both $F_i(z)$ and $B_i(z)$ along with the decision delay are computed for each $\mathbf{\Sigma}_i(z)$. The decision delay is individually optimised for each SISO subchannel and is generally equivalent to $L_f^{(i)} - 1$.

The importance of the spectral factorisation scheme lies in its capability of establishing serial transmission between transmitter and receiver. In the next section a second method is introduced, which is based on block transmission.

3.5.2.2.2 Block Transmission. THP can also be implemented in a block transmission mode [91, 106]. Given the ith SISO subchannel from Sec. 3.5.1 in its discrete time version $\boldsymbol{\sigma}_i = \left[\sigma_{ii}^{(0)},\ \sigma_{ii}^{(1)}, \cdots, \sigma_{ii}^{(L_i)}\right]$ of order L_i, the block transmission scheme can be formulated following the procedures presented in [91] and with the aid of Fig. 3.14(b) as follows. The block input-output behaviour of this SISO subchannel is formulated as a convolutional matrix

$$\mathbf{\Sigma}_i = \begin{bmatrix} \sigma_{ii}^{(0)} & \sigma_{ii}^{(1)} & \cdots & \sigma_{ii}^{(L_i)} & 0 & \cdots & 0 \\ 0 & \sigma_{ii}^{(0)} & \sigma_{ii}^{(1)} & \cdots & \sigma_{ii}^{(L_i)} & \ddots & \vdots \\ \vdots & \ddots & \ddots & \cdots & \cdots & \ddots & 0 \\ 0 & \cdots & 0 & \sigma_{ii}^{(0)} & \sigma_{ii}^{(1)} & \cdots & \sigma_{ii}^{(L_i)} \end{bmatrix} \in \mathbb{C}^{N_b \times N_b + L_i - 1}, \qquad (3.49)$$

where N_b is the block size of the data streams $\mathbf{s} = [s_{N_b},\ s_{N_b-1}, \cdots, s_1]^{\mathrm{T}}$. This stacking can be easily performed using serial-to-parallel (S/P) and parallel-to-serial (P/S) devices as shown in Fig. 3.14(b). The ZF-THP solution to such a system can be obtained once the feedforward and feedback filter matrices $\mathbf{W}_i$ and

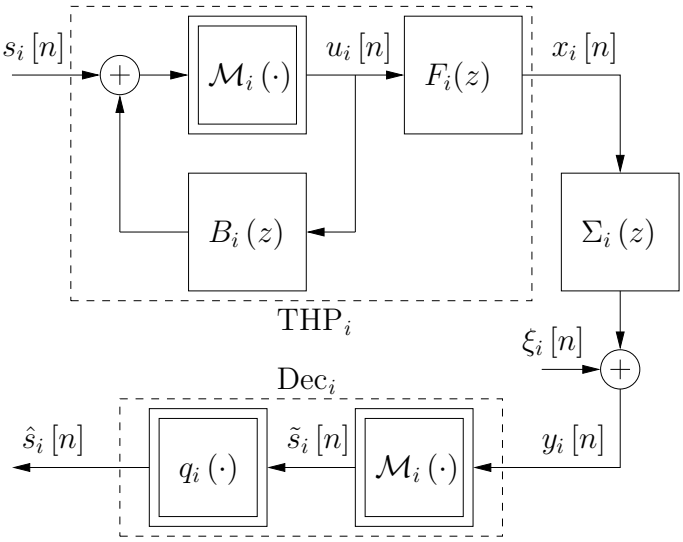

(a)

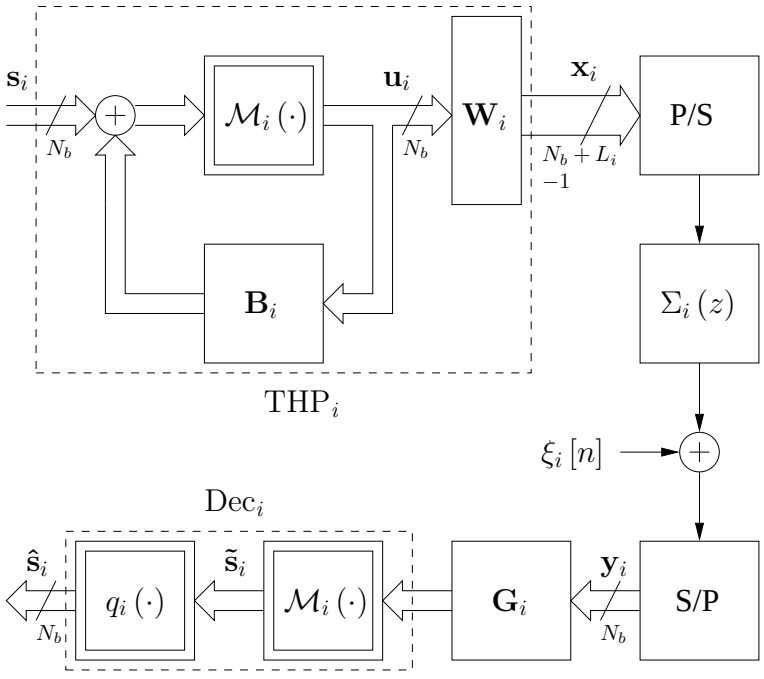

(b)

Figure 3.14: A detailed SISO-THP transceiver for the ith subchannel of Fig. 3.13 using (a) spectral factorisation and (b) block transmission schemes.

$\mathbf{B}_i$, respectively, have been evaluated using the QR decomposition

$$\mathbf{\Sigma}_i^{\mathrm{H}} = \mathbf{Q}_i \begin{bmatrix} \mathbf{R}_i^{\mathrm{H}} & \mathbf{0} \end{bmatrix}^{\mathrm{H}} . \tag{3.50}$$

Here, $\mathbf{Q}_i$ is a unitary matrix of size $N_b + L_i$ and $\mathbf{R}_i \in \mathbb{C}^{N_b \times N_b}$ is an upper triangular matrix. The feedforward filter $\mathbf{W}_i$ is equal to the first N_b columns of $\mathbf{Q}_i$, while the feedback filter is given by $\mathbf{B}_i = \mathbf{I}_{N_b} - \mathbf{G}_i \mathbf{R}_i^{\mathrm{H}}$, where $\mathbf{G}_i = \mathrm{diag}\left(r_{11}^{-1}, r_{22}^{-1}, \cdots, r_{N_b N_b}^{-1}\right)$ with r_{ii} being the ith diagonal element of $\mathbf{R}_i$. This translates ISI into CCI between different elements of the transmitted data block, which can be easily addressed by subspace methods. However, using block transmission sacrifices some redundancy to remove IBI between successive transmit data blocks, and hence reduces the overall system spectral efficiency.

3.5.2.2.3 SISO-THP BER Comparison. The two SISO-THP schemes are compared on the basis of identical transmit power for a 5-tap SISO channel. A total of 300 channel realisations are used whereby channels obey an exponentially decaying power profile with coefficients drawn from complex valued independent Gaussian distributions. The average BER curves are plotted in Fig. 3.15 for the spectral factorisation and block transmission schemes. It can be noted that the block transmission scheme outperforms its spectral factorisation counterpart due to the incorporated extra redundancy of $\frac{L_i}{N_b}$ which in turn reduces the data throughput by a factor of $\frac{N_b}{N_b+L_i}$. Referring to Fig. 3.15, it is also evident that when $N_b \gg L_i$, the redundancy approaches zero while the data throughput reduction factor $\simeq 1$, resulting in both block transmission and spectral factorisation BER performances converging to identical curves.

3.5.3 Approximate Diagonalisation by BSVD

Referring to (3.45), it is shown that the overall MIMO broadband system $\mathbf{H}(z)$ can be reduced to a diagonalised system $\Sigma(z)$ such that for a transmitted data streams $\underline{X}(z)$ the received data is given by

$$\underline{Y}(z) = \Sigma(z)\underline{X}(z) + \underline{\xi}(z)\,, \tag{3.51}$$

where $\underline{\xi}(z)$ represents the AWGN noise at the receiver. Noting that the z-domain representation of a random process does not exist, (3.51) utilises the z-domain for notational convenience only, while all calculations would be performed in the time domain.

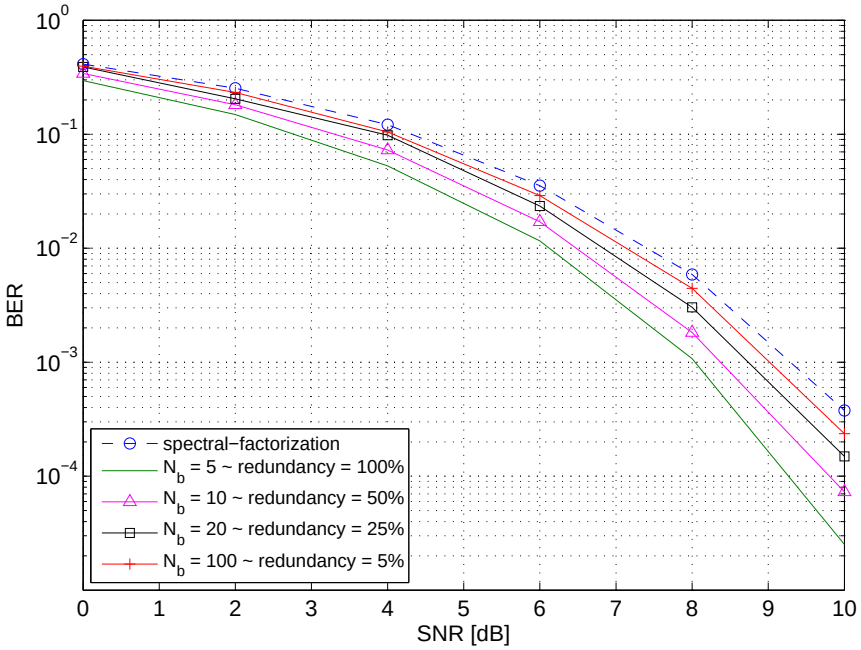

Figure 3.15: BER performance comparison between spectral factorisation and block transmission schemes of a SISO-THP system with 5-tap channel.

The ideal decoupling of the MIMO system in (3.51) such that CCI is perfectly eliminated requires an exact diagonalisation of $\mathbf{H}(z)$ using the BSVD algorithm [19]. However, due to the approximate and iterative nature of the BSVD algorithm this may not sufficiently fulfilled and non-zero off-diagonal elements of finite size may remain in $\Sigma(z)$ as a result (cf. Fig 2.8), which is likely to deteriorate the overall error performance. Therefore, the selection of a reasonable number of iterations (NoI) of the BSVD algorithm that results in a BER performance close to one with a very high NoI of the overall system $\Sigma(z)$ is investigated in this section. The effect of NoI on performance is twofold, as off-diagonal elements consume part of the system energy, and an imperfectly diagonalised $\Sigma(z)$ will admit CCI. Therefore the idealistic approximation in (3.51) can be more correctly described by the time domain formulation for the ith received symbol stream $y_i[l]$, $i = 0, \cdots, N-1$, as

$$y_i[l] = \sum_{\nu=0}^{L_i} \sigma_{ii}[\nu] \cdot x_i[l-\nu] + \sum_{\substack{m=0 \\ m\neq i}}^{N-1} \sum_{\nu=0}^{L_{im}} \sigma_{im}[\nu] \cdot x_m[l-\nu] + \xi_i[l] \ . \tag{3.52}$$

The quantities L_i and L_{im} in (3.52) denote, respectively, the order of the main and off-diagonal polynomials of $\Sigma(z)$, such that the majority of system energy is preserved. In the following, we worked with a figure of 99.9% compared to

the total energy. The second term on the r.h.s. of (3.52) represents the residual CCI contributed by the off-diagonal terms in $\Sigma(z)$. In Section 3.6, the effect of the BSVD NoI on the overall BER performance is investigated in order to admit a BSVD with a potentially lower NoI and lower computational complexity than would otherwise be required.

3.6 Simulation Results

Computer simulations are conducted for a 4×4 MIMO system with a broadband channel of order $Q = 5$ and a power delay profile given in Table 3.5 where the channel coefficients $h_{ij}[n]$ are drawn from a zero-mean uncorrelated complex Gaussian distribution. Results for our proposed method using BSVD with spectral factorisation THP precoding, in the following labelled "BSVD-THP" are benchmarked against both linear MIMO precoding addressed in Sec. 2.3.3 and MIMO THP with spatio-temporal ordering presented in Sec. 3.4.1. We will denote the benchmark system [17] for both linear and THP precoding as MIMO-Lin and MIMO-THP, respectively. The length of the feedforward filter for both MIMO-Lin and MIMO-THP systems as well as BSVD-SISO system is set to twice the channel order i.e., 10 taps for both MIMO systems and $L_f^{(i)} = 2 \times L_i$ for the ith BSVD-SISO subsystem, while the feedback filter length of each BSVD-SISO subsystem is set to the same order as its respective subchannel, i.e., $L_b^{(i)} = L_i$. A comparison between our proposed model and the benchmark systems is set with the aim of achieving the same system throughput. Three cases to achieve a target throughput of 8, 16 and 24 bits are considered. In each case, the overall throughput is achieved with our proposed BSVD-THP model by distributing rates among individual SISO subchannels according to their strength while in the MIMO case it is uniformly allocated by definition. We choose to assign these rates with two constraints: 1) only discrete square-QAM constellations are permitted and 2) transmission over the worst subchannel is avoided unless it is necessary to achieve the target throughput. With these constraints, a reasonable bit loading is proposed in a heuristic fashion as shown in Table 3.6. For the first two cases, the same throughput can be attained with the utilisation of the first three subchannels only while the fourth subchannel is set inactive. However, for the case of 24 bit throughput the fourth subchannel has to be used to achieve the target throughput (cf. Table 3.6).

Results are averaged over a total number of 300 different channel realisations normalised for a frequency-selective non-fading scenario as in (2.36). Fi-

Table 3.5: Channel power delay profile.

path delay (symbol)	1	2	3	4	5	6
relative power (dB)	0	-4	-8	-12	-16	-20

Table 3.6: SISO subchannels bit allocation for same target throughput as a 4×4 MIMO system.

Throughput	Case 1: 8-bits	Case 2: 16-bits	Case 3: 24-bits
MIMO	QPSK	16-QAM	64-QAM
SISO-1	16-QAM	64-QAM	256-QAM
SISO-2	QPSK	64-QAM	256-QAM
SISO-3	QPSK	16-QAM	64-QAM
SISO-4	QPSK	QPSK	QPSK

gures 3.16, 3.17 and 3.18 demonstrate the BER performance comparison between our BSVD-THP and both MIMO-Lin and MIMO-THP for the three target throughput cases, respectively. The BSVD-THP curve that represents the same achieved throughput as the benchmark MIMO systems is highlighted by $(\cdot)^{\mathrm{s}}$ in all of these figures. In Fig. 3.16 it is clear that the average BER for the first two subchannels (marked as "1-2") is much better than both MIMO linear and THP with 2 bits (25%) degradation in the overall throughput. For same achieved throughput comparison the average BER of the first three subchannels (marked as "1:3") is slightly higher than MIMO-THP ($<$ 0.5 dB loss at 10^{-3} BER) and outperforms MIMO-THP for higher SNR (or BER $< 10^{-4}$ performance). If the fourth subchannel is used, the overall throughput can be increased by a factor of 25% at the expense of very poor BER that dominates the overall performance (marked as "all"). Note that for the BSVD-THP system, the mean BER of the first combined k subchannels $\overline{\mathcal{P}}_b$ is given for their individual subchannel BERs $\mathcal{P}_{b,i}$ weighted by their respective allocated number of bits b_i as

$$\overline{\mathcal{P}}_k = \frac{\sum_{i=1}^{k} b_i \mathcal{P}_{b,i}}{\sum_{i=1}^{k} b_i} \,. \tag{3.53}$$

For a higher throughput-achieving operation, the results of "16-bits" and "24-bits" cases are shown in Fig. 3.17 and Fig. 3.18, respectively. In Fig. 3.17, the BSVD-THP system clearly outperforms its MIMO benchmark counterpart over the normal practical operating region (BER < 0.01). It is also noted that averaged BER performances for both first two and first three subchannels are very close to each other which reveals the good choice of individual rates (modulations) that best match SISO subchannels strengths. An extra throughput of 12.5% can

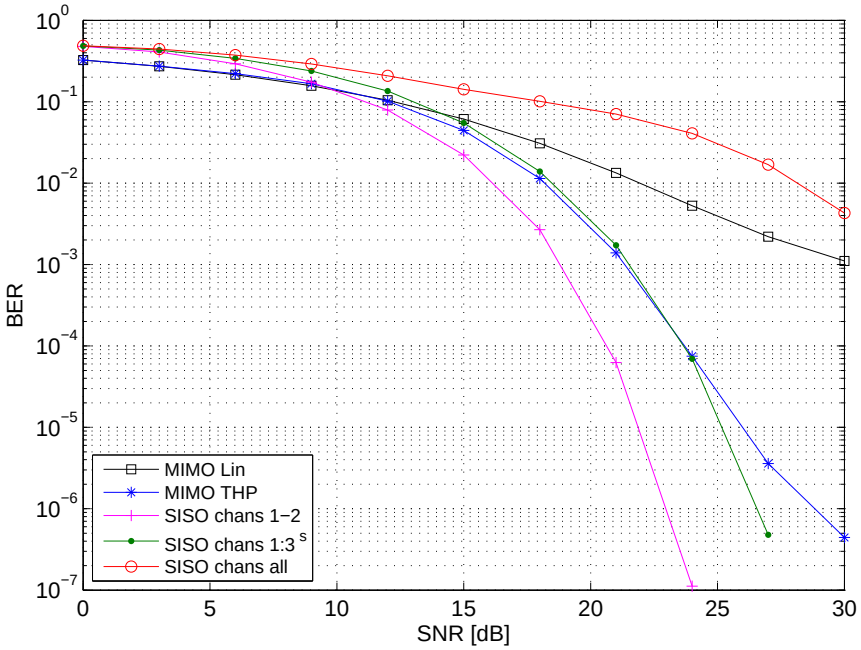

Figure 3.16: Case "8-bits" where the 1st SISO subchannel operates on 16-QAM and all other subchannels on QPSK modulation.

be achieved if the fourth subchannel is used for transmission at the cost of an increase in SNR of $\simeq 1.5\,\mathrm{dB}$ in the medium operation region. Fig. 3.18 shows the performance comparison for the 24-bits throughput case, where all SISO subchannels have to be taken into account to achieve the same target throughput as the MIMO benchmark (see Table 3.6). A gain of more than 2.5 dB in SNR can be achieved at BER ≤ 0.05 , also it is obviously noted the close performance of each combination of BSVD-THP subsystems which again demonstrates the good choice of the individual rates that assigned to each BSVD-THP subchannel.

The results presented above assume near perfect diagonalisation of the BSVD algorithm [19] in (3.51), however, as highlighted in Sec. 3.5.3 the actual BSVD diagonalisation is provided by (3.52) and depends on the BSVD NoI. To investigate the effect of this NoI on the performance of our proposed BSVD-THP method and concentrate on a BSVD with simplified computations, another set of simulation is conducted without considering bit loading. This means that all SISO subchannels are loaded with the same modulation scheme, therefore different subchannel BERs are expected as a result of the spectral majorisation property of the BSVD algorithm. SISO-THP under the spectral factorisation scheme presented in (3.5.2.2.1), with filter parameters as above, is used to mitigate the individual ISI of these SISO subsystems and overcome the error propagation problem which a DFE scheme would experience.

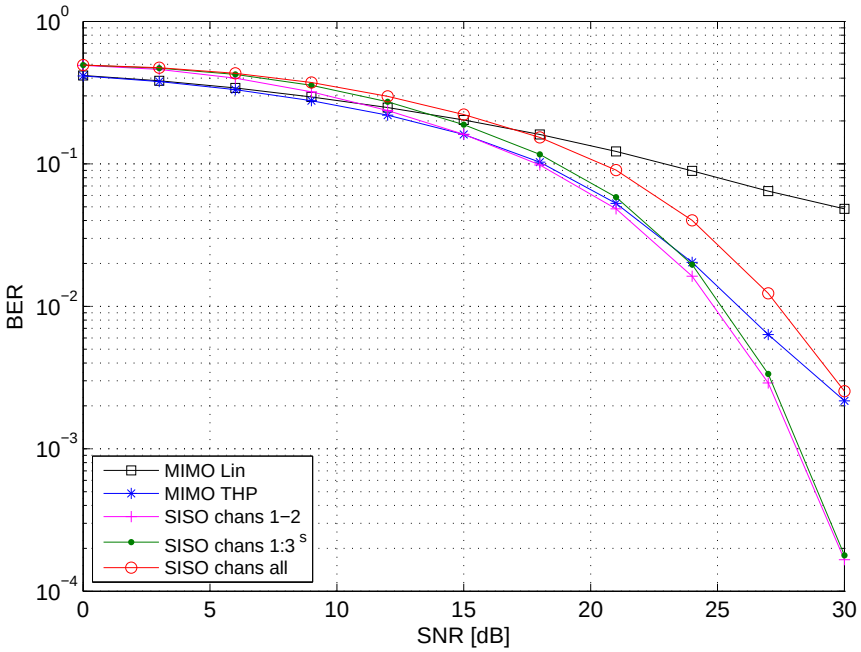

Figure 3.17: Case "16-bits" where the first two SISO subchannels operate on 64-QAM, 3rd one on 16-QAM and last subchannel on QPSK modulation.

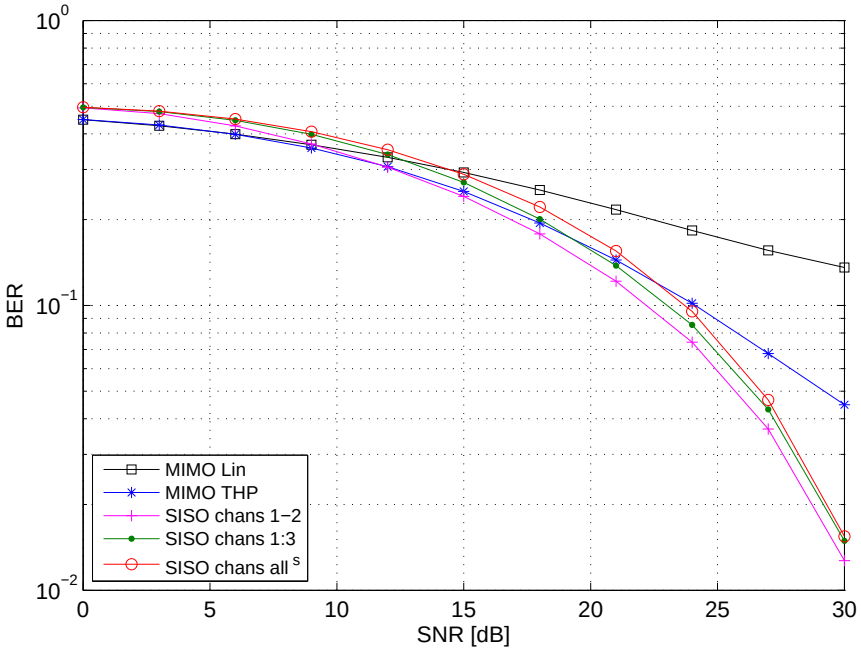

Figure 3.18: Case "24-bits" where the first two SISO subchannels operate on 256-QAM, 3rd one on 64-QAM and last subchannel on QPSK modulation.

A 3×3 MIMO channel instance of order 4 and power profile in Table 3.5 normalised using (2.36) is decoupled into 3 SISO subchannel based on the BSVD algorithm with different NoI values of 20, 60, and 100. In order to investigate the BER performance for different transmission rates, three symbol mappings are considered using square M-QAM modulation with $M = 4$, 16 and 64, i.e. QPSK, 16-QAM, and 64-QAM, respectively.

Figures 3.19, 3.20 and 3.21 demonstrate the BER results of the individual SISO subchannels after applying the BSVD algorithm with the different NoI values for the three transmission rates of QPSK, 16-QAM, and 64-QAM, respectively. Obviously, the NoI determines how well both decoupling (2.34) and spectral majorisation (2.35) can be achieved. The following comments can be drawn from these simulation results:

- For all cases and all subchannels, BER performance is improved by increasing the NoI. Also note that for high NoI, this advantage becomes incremental. This decrease allows for a significant reduction in system complexity by choosing a moderate NoI without any degradation in performance as shown in all of these Figures.

- The stronger the subchannel the more minor the effect of the NoI, as can be easily noted in the 1st subchannel for all cases. Spectral majorisation is a very useful instrument in practical applications since when some of the weaker subchannels are not needed, the NoI can be decreased leading to further reduction in system complexity.

- According to the NoI values conducted in this simulation, it is possible to restrict the complexity of the BSVD algorithm to be run at only NoI = 60 with minimal and negligible degradation in the BER performance for the MIMO transmission channels considered here, i.e. of order 4 and a decaying power profile.

3.7 Conclusion

In this chapter we have addressed non-linear precoding and equalisation methods for both narrowband and broadband MIMO channels. Schemes of decision feedback equalisation (DFE), Tomlinson-Harashima precoding (THP) and V-BLAST detection have been considered which highlight the role of precoding and detection ordering of data substreams on the performance of narrowband systems. In

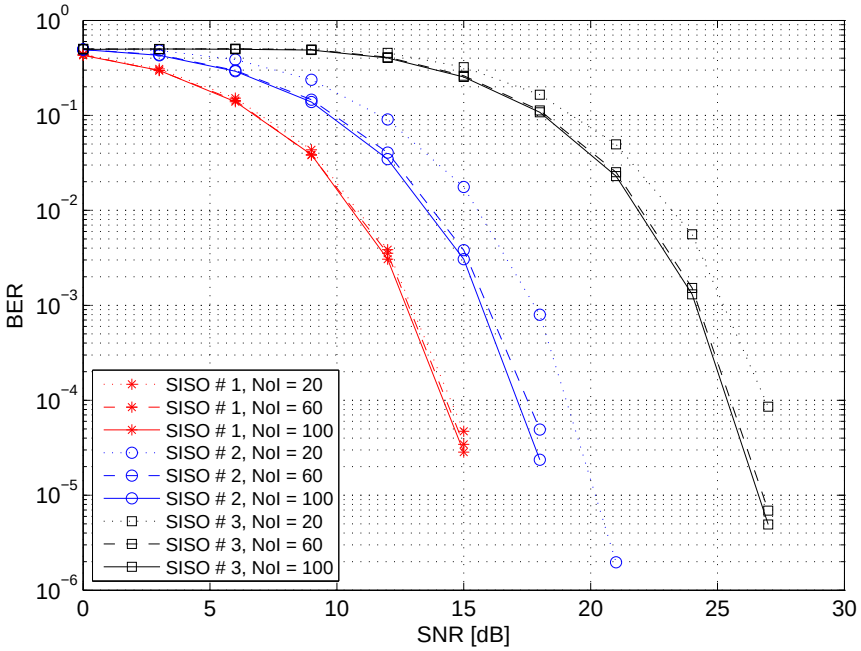

Figure 3.19: SISO-THP performance of the individual subchannels resulting from the application of the BSVD algorithm with varying NoI to a 3×3 MIMO system and QPSK transmission.

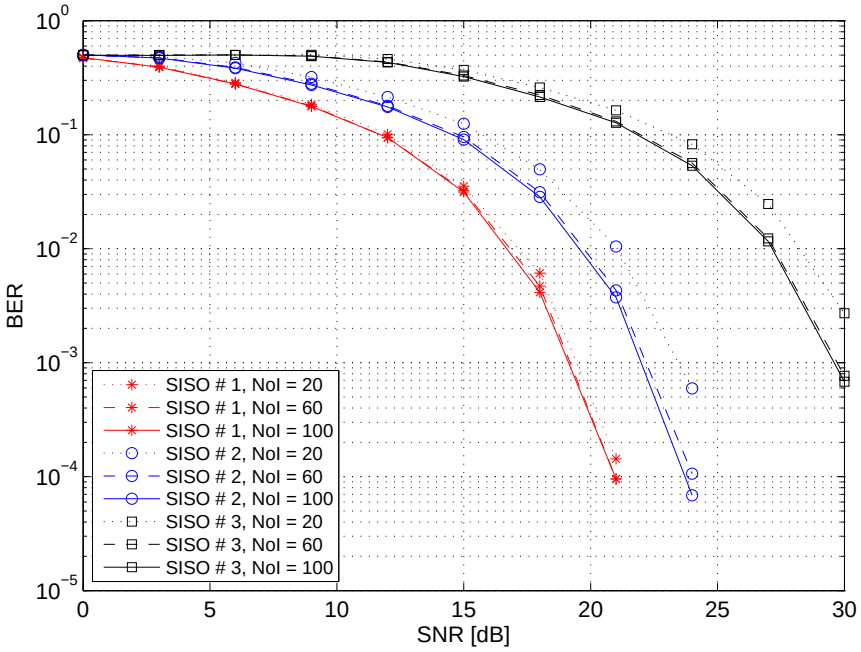

Figure 3.20: SISO-THP performance of the individual subchannels resulting from the application of the BSVD algorithm with varying NoI to a 3×3 MIMO system and 16-QAM transmission.

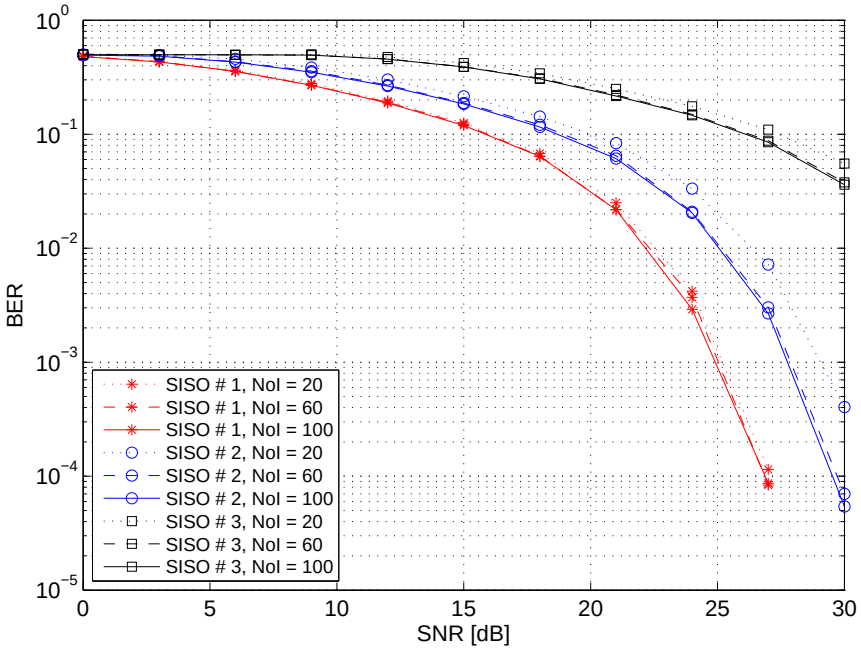

Figure 3.21: SISO-THP performance of the individual subchannels resulting from the application of the BSVD algorithm with varying NoI to a 3×3 MIMO system and 64-QAM transmission.

contrast, for the broadband case both spatial and temporal ordering have to be optimised for improved performance. A novel approach based on a recently developed broadband SVD (BSVD), which can decouple a broadband MIMO channel into a number of frequency selective SISO subchannels, is proposed. This approach shows better BER performance compared to a state-of-the-art method. In order to maximise the data throughput of this scheme or similar multichannel systems, adaptive bit and power loading schemes have to be applied which will be considered in the next chapter.

Chapter 4

Greedy Power and Bit Loading Schemes

Adaptation of transmission resources to channel conditions in multichannel systems has been proved to significantly enhance the overall system performance provided that channel state information (CSI) is known to the transmitter [5, 107]. This includes the achievement of either higher data rates or lower power requirements under one or more practical/design constraints known respectively in the literature as *rate maximisation* [108, 109], or *margin maximisation* [110, 111]. The parameters to be considered in such loading problems are commonly: data rate, bit error ratio (BER) and total transmit power. From a system design point of view, the sum-rate of a multichannel system with different subchannel gains is of particular interest, and can be optimised using power and/or bit loading schemes.

Power and bit allocation problems are usually phrased as closed form expressions with respect to either channel capacity [108, 112] or bit error probability [113, 114]. The optimal standard water-filling based solutions assume infinite modulation orders and real-valued data rates which is realistically infeasible and leads to a final rounding remedy step [109] that degrades the overall performance. Alternatively, so-called incremental or greedy approaches optimising sum-rate using power [115] and bit [116] loading schemes can achieve higher rates at the expense of computational complexity. In this Chapter, we investigate the data rate maximisation using both power and bit loading schemes under the Greedy approach.

4.1 Constrained Optimisation Problem

Rate maximisation of a multichannel system is extensively considered in the literature, see for example [117, 118] for a review. The sum-rate maximisation problem of such systems can be formulated as

$$\textbf{maximise} \quad \sum_{i=1}^{N} b_i \tag{4.1a}$$

$$\textbf{subject to} \quad \sum_{i=1}^{N} P_i \leq P_{\text{budget}}, \tag{4.1b}$$

$$\forall i : 1 \leq i \leq N,$$

$$P_i \geq 0, \tag{4.1c}$$

$$\overline{\mathcal{P}}_b \leq \mathcal{P}_b^{\text{target}}, \tag{4.1d}$$

$$b_i \leq b^{\max}. \tag{4.1e}$$

Where b_i and P_i are, respectively, the number of bits and amount of power allocated to the ith subchannel, while N is the total number of subchannels of the multichannel system and P_{budget} is the total transmit power budget. The mean BER of all subchannels is denoted by $\overline{\mathcal{P}}_b$, while $\mathcal{P}_b^{\text{target}}$ denotes the target BER. We also assume that the system is constrained by a fixed permissible number of bits which cannot be exceeded $b^{\max}$ to be loaded to each subchannel.

Based on the concept of SNR-gap approximation [119, 120], which signifies the loss in SNR of a particular transmission scheme when compared to the theoretical channel capacity, a closed form expression for b_i can be given by [67]

$$b_i = \log_2 \left(1 + \frac{\gamma_i}{\Gamma}\right), \tag{4.2}$$

where γ_i is the SNR of the ith subchannel and Γ denotes the SNR-gap. QAM modulation schemes are considered for which the SNR-gap is given as [121]

$$\Gamma = \frac{1}{3}\left[Q^{-1}\left(\frac{\mathcal{P}_{s,i}}{4}\right)\right]^2, \tag{4.3}$$

where Q^{-1} is the inverse of the well-known Q-function defined as

$$Q(x) = \frac{1}{\sqrt{2\pi}} \int_x^{\infty} e^{-u^2/2} du, \tag{4.4}$$

and $\mathcal{P}_{s,i}$ is the SER of the ith subchannel. It is clear from (4.3) that Γ is not fixed for all subchannels but depends on the subchannel SER, which in turn depends on b_i and γ_i of (4.2). This dependence has to be carefully taken into account whenever the rate or the gain in (4.2) is changed. Nevertheless, this approximation is valid only for very low BER, typically 10^{-6}, and higher QAM orders which is not usually the case for realistic wireless communication applications [109].

Defining the channel-to-noise ratio of the ith subchannel as

$$\mathrm{CNR}_i = \frac{g_i^2}{\mathcal{N}_0}, \tag{4.5}$$

where $\mathcal{N}_0$ is the total noise power at the receiver and g_i is ith subchannel gain[1], the SNR of this subchannel γ_i in (4.2) is given by

$$\gamma_i = P_i \times \mathrm{CNR}_i \,. \tag{4.6}$$

We consider rectangular M-QAM modulation of order $M_k, 1 \leq k \leq K$, where M_K is the maximum QAM constellation that is permissible by the transmission system, i.e., $M_K = 2^{b^{\max}}$. The BER of this modulation scheme is given by [122]

$$\mathcal{P}_{b,i} = \mathcal{F}\left(\gamma_i, M_k\right) = \begin{cases} Q\left(\sqrt{2\gamma_i}\right) & \text{for BPSK,} \\ \frac{1-\left[1-2\left(1-\frac{1}{\sqrt{M_k}}\right)Q\left(\sqrt{\frac{3\gamma_i}{M_k-1}}\right)\right]^2}{\log_2 M_k} & \text{for } M \text{ QAM}\,. \end{cases} \tag{4.7}$$

With the availability of channel state information (CSI) at the transmitter, symbols of b_k-bits, $b_k = \log_2 M_k$ can be loaded to a subchannel with minimum required SNR obtained from (4.7) as

$$\gamma_k^{\mathrm{QAM}} = \mathcal{F}^{-1}\left(\mathcal{P}_{b,i}, M_k\right) = \begin{cases} \frac{1}{2}\left[Q^{-1}\left(\mathcal{P}_{b,i}\right)\right]^2 & \text{for BPSK,} \\ \frac{M_k-1}{3}\left[Q^{-1}\left(\frac{1-\sqrt{1-\mathcal{P}_{b,i}\cdot\log_2 M_k}}{2\left(1-1/\sqrt{M_k}\right)}\right)\right]^2 & \text{for } M \text{ QAM}\,. \end{cases} \tag{4.8}$$

[1]These subchannels gains can be simply obtained for narrowband MIMO systems by considering the SVD of the MIMO channel. While for broadband MIMO systems, OFDM can be used to deduce these gains.

4.2 Uniform Power Allocation (UPA)

The simplest and most straightforward attempt to achieve bit loading and obtain the sum-rate in (4.1a) is to distribute the power budget P_{budget} equally across all subchannels regardless of their CNR_i to obtain the subchannels SNRs as

$$\gamma_i = P_i^{\text{u}} \times \text{CNR}_i = \frac{P_{budget}}{N} \times \text{CNR}_i \,. \tag{4.9}$$

Referred to as uniform power allocation (UPA), this solution disregards the CSI that is assumed to be available at the transmit side. In other wards, no utilisation of the CSI is considered and therefore non-adaptive bit loading is obtained as a result. Fulfilling the mean BER constraint in (4.1d) with equality, the bit loading of the UPA can be achieved with the aid of Fig. 4.1 as follows.

1. Calculate γ_k^{QAM} for all $M_k, 1 \leq k \leq K$ and $\mathcal{P}_{b,i} = \mathcal{P}_b^{\text{target}} \forall i$ using (4.8).

2. For all subchannels $i, 1 \leq i \leq N$, find the modulation order index $k_i \in \{0, 1, 2, \cdots, K\}$ that satisfies

$$k_i : \quad \gamma_i \geq \gamma_{k_i}^{\text{QAM}} \quad \text{and} \quad \gamma_i < \gamma_{k_i+1}^{\text{QAM}} \,. \tag{4.10}$$

3. Load all subchannels $i, 1 \leq i \leq N$ with b_i^{u} bits given by

$$b_i^{\text{u}} = \begin{cases} \log_2 M_{k_i} & \text{for } k_i \neq 0 \\ 0 & \text{for } k_i = 0 \end{cases} \tag{4.11}$$

   to obtain the UPA sum-rate as

$$B_{\text{u}} = \sum_{i=1}^{N} b_i^{\text{u}} \,. \tag{4.12}$$

4.3 Water-Filling Solution

By relaxing the constraint of finite-alphabet constellations in (4.1e) and assuming Gray coded bit mapping $\mathcal{P}_{s,i} \approx \mathcal{P}_{b,i} \times \log_2 M_i$, where $M_i = 2^{b_i}$ is the QAM constellation size of b_i-bits symbols, the optimum solution to the constrained optimisation problem in (4.1a) leads to the well-known water-filling algorithm [123, 5]. This algorithm generally allocates more power to strong subchannels and less power or even no power to weak subchannels.

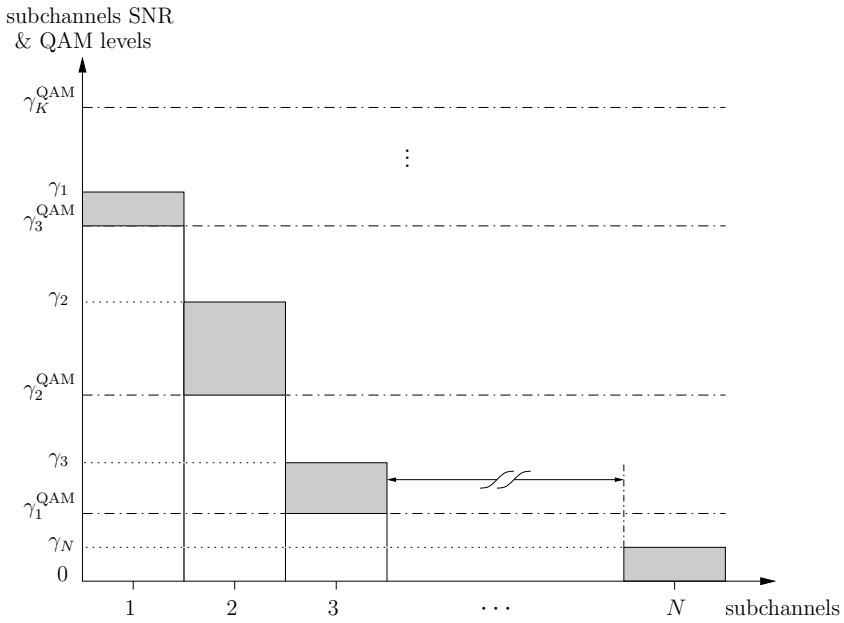

Figure 4.1: Subchannels residing into QAM levels according to their SNRs and UPA.

Defining $\theta_i \overset{d}{=} \frac{\text{CNR}_i}{\Gamma}$ and substituting with (4.6), (4.2) can be rewritten as

$$b_i = \log_2 (1 + P_i \cdot \theta_i) \ . \tag{4.13}$$

Before proceeding further, it is easy to note that if $P_i = \frac{P_{\text{budget}}}{N}$ in (4.13), the UPA solution presented in Section 4.2 will result but, however, it will be continuous and unbounded in the QAM order M. Now, the optimum power allocation that maximises the sum-rate in (4.1a) with the closed-form formula for b_i in (4.13) is given by the water-filling solution

$$P_i^{\text{w}} = \begin{cases} \alpha - \theta_i^{-1} & 1 \leq i \leq N_{\text{w}}, \\ 0 & \text{otherwise} \, . \end{cases} \tag{4.14}$$

In (4.14) N_{w} is the number of active subchannels for transmission and $\alpha \in \mathbb{R}$ is a constant known as "water-level" and selected to fulfil the constraint of the total power budget in (4.1b) with equality as illustrated by Fig. 4.2. For a proof, please refer to Appendix A.3. Obviously by assuming sorting of subchannels with respect to their gains θ_i in a descending order ($\theta_i \geq \theta_{i+1}, \forall i$), α can be determined as

$$\alpha = \frac{P_{\text{budget}} + \sum_{i=1}^{N_{\text{w}}} \theta_i^{-1}}{N_{\text{w}}} \, . \tag{4.15}$$

In computing α, it is easy to determine how many subchannels N_{w} are considered

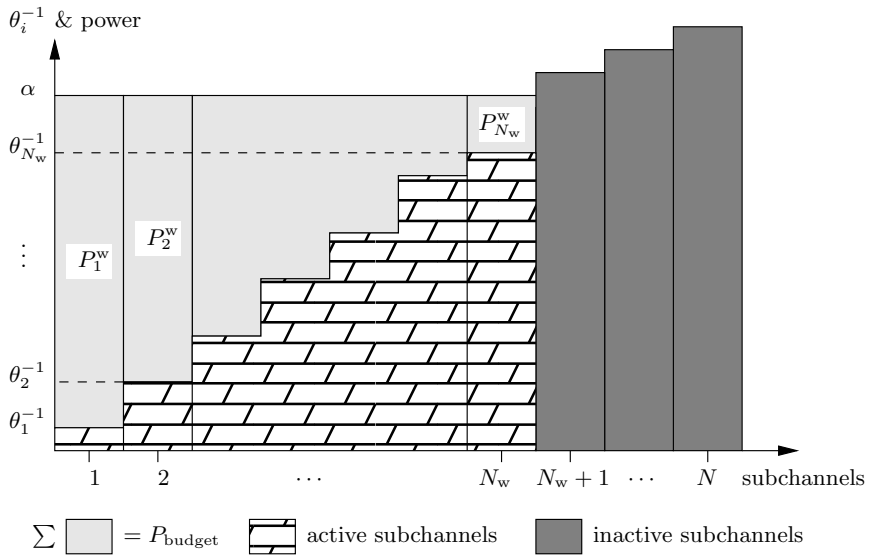

Figure 4.2: Graphical illustration of the water-filling solution given in (4.14).

in (4.15) by picking up all subchannels below the water-level α, i.e.

$$N_\mathrm{w}: \quad \alpha \geq \theta_{N_\mathrm{w}}^{-1} \text{ and } \alpha < \theta_{N_\mathrm{w}+1}^{-1}\,. \tag{4.16}$$

Note that from (4.15), α is dependent on the total transmit power, i.e., if more power is available for transmission, α is consequently increased allowing for more subchannels N_w to be selected for transmission (see Fig. 4.2).

The optimum bit loading using the solution in (4.14) can be obtained by substituting in (4.13) to obtain

$$b_i^\mathrm{w} = \begin{cases} \log_2(\alpha \cdot \theta_i) & 1 \leq i \leq N_\mathrm{w}, \\ 0 & \text{otherwise}\,. \end{cases} \tag{4.17}$$

Noticeably, the resultant bit allocation $b_i^\mathrm{w}, 1 \leq i \leq N_\mathrm{w}$ obtained by (4.17) is real-valued and requires, in practice, a rounding off to the nearest integer value. This quantisation leads to a loss in the sum-rate achieved by this solution, which degrades the overall performance. In order to account for discrete bit allocation, the actual sum-rate B_w can be given by the following discrete formula

$$B_\mathrm{w} = \sum_{i=1}^{N_\mathrm{w}} \lfloor b_i^\mathrm{w} \rfloor\,, \tag{4.18}$$

where $\lfloor \cdot \rfloor$ denotes the floor operator, returning the largest integer less than or equal to its argument.

Fig. 4.3 shows the sum-rate performance of both pure and discrete water-

filling algorithms compared to the non-adaptive (uniform) power allocation case for a 4×4 MIMO system with Rayleigh-fading channel coefficients. The result for the ergodic channel capacity is given by [124]

$$\begin{aligned} C &= \mathbb{E}\left[\log_2\left|\mathbf{I}_{N_r} + \tfrac{P_{\text{budget}}}{N_t \mathcal{N}_0}\mathbf{H}\mathbf{H}^{\text{H}}\right|\right] \\ &= \mathbb{E}\left[\sum_{i=1}^{r}\log_2\left(1 + \tfrac{P_{\text{budget}}}{N_t \mathcal{N}_0}\lambda_i\right)\right], \qquad \text{[bps/Hz]} \end{aligned} \tag{4.19}$$

where r and λ_i are, respectively, the rank and the ith eigenvalue of $\mathbf{H}\mathbf{H}^H$, are also provided for the sake of comparison.

The Greedy Approach

So far, the solutions provided for the constrained optimisation problem given through (4.1a)-(4.1e) are not efficient, in the sense that violating the finite modulation orders constraint in (4.1e) and inevitable rounding in case of the water-filling solution or inefficient power allocation in case of the UPA scheme. Alternatively, the so-called incremental or greedy approaches optimising sum-rate using power [115] and bit [116] loading schemes can achieve higher rates at the expense of computational complexity. In fact, the greedy algorithm offers the rate-optimal solution in case of discrete bit loading [110, 125] like our optimisation problem.

Generally speaking, optimality in greedy approaches is guaranteed by considering an appropriate bit allocation cost function, similar to (4.8), and iteratively assigning one bit (or the smallest possible bit allocation step[2]) at a time to the least cost-expensive subchannel. The greedy algorithm is characterised by two main properties [126]:

- Firstly, at each step, the algorithmic operating point is always moved towards the direction that guarantees the largest possible increment (decrement) to the assigned objective function to be maximised (minimised).
- Secondly, a greedy algorithm proceeds only in a forward way, that is, it never tracks back.

In the following two Sections two greedy algorithms aiming to maximise the sum-rate of a multichannel system by solving (4.1a)-(4.1e) are investigated and

[2]For instance, if only square QAM constellations are allowed by a particular transmission system, a step of two bits is considered instead.

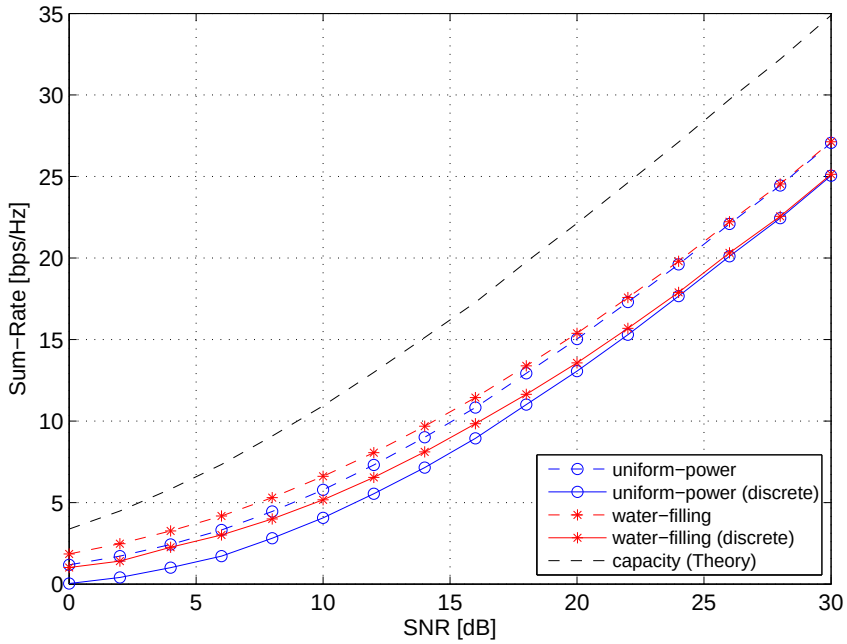

Figure 4.3: Sum-rate results for water-filling and uniform power of a 4×4 MIMO system at SER $= 10^{-3}$ and varying SNR.

compared, namely Greedy Bit Allocation (GBA) and Greedy Power Allocation (GPA).

4.4 Greedy Bit Allocation (GBA) Algorithm

In order to achieve the sum-rate optimality with the constraints given in (4.1b)-(4.1e), the first greedy algorithm, GBA, is introduced by considering (4.7). The bit allocation cost function is selected to accomplish the mean BER constraint given in (4.1d) which is defined for different subchannels BERs as

$$\overline{\mathcal{P}}_b = \frac{\sum_{i=1}^{N} b_i \mathcal{P}_{b,i}}{\sum_{i=1}^{N} b_i}. \tag{4.20}$$

However in order to achieve this, an initial power allocation scheme implementing a simple UPA, i.e., $P_i = \frac{P_{\text{budget}}}{N}$ is defined. Looking at (4.1b) and (4.1d), the key constraints for the GBA algorithm are highlighted by

$$\sum_{i=1}^{N} P_i = P_{\text{budget}} \quad \text{and} \quad \overline{\mathcal{P}}_b \leq \mathcal{P}_b^{\text{target}}. \tag{4.21}$$

Similar to [116], an incremental bit loading approach is presented to maximise the sum-rate by efficiently fulfilling the mean BER in (4.21). Referring to (4.7), the GBA algorithm starts with filling all subchannels with the highest possible QAM modulation order M_K and then proceeds with a bit removal approach [127]. The optimal strategy of the GBA is considered by avoiding the worst bit-loading that violates the condition of $\mathcal{P}_b^{\text{target}}$. In other words, at each algorithmic iteration this algorithm executes the bit removal approach by selecting the subchannel of the highest degradation impact on the mean BER $\overline{\mathcal{P}}_b$ in (4.20).

This solution, however, lacks the benefit of the efficient power distribution as power is assumed to be equally distributed amongst all subchannels. The complete GBA algorithm is given in Table 4.1.

4.5 Greedy Power Allocation (GPA) Algorithm

The second greedy algorithm is introduced by considering the power aspect of the bit allocation cost function. To distribute power more reliably compared to the GBA algorithm which considers a UPA across all subchannels, a sort of optimal power allocation is to be investigated. The water-filling solution addressed in Section 4.3 gives the optimal power allocation in case of continuous bit loading, i.e. $b_i \in \mathbb{R}$. In practice, however, only discrete bit loading is permitted. Towards this end GPA is proposed to optimise the sum-rate under the constraints given in (4.1b)-(4.1e). Expression (4.8) is of particular interest for this goal as it returns the minimum required allocated power ($\frac{\gamma_k^{\text{QAM}}}{\text{CNR}_i}$) for a certain subchannel i of CNR_i to be loaded with a QAM modulation scheme of order M_k. Therefore optimality is guaranteed in terms of saving power [115].

By adjusting the transmit power to exactly fulfil the target BER $\mathcal{P}_b^{\text{target}}$ across all subchannels $\mathcal{P}_{b,i} = \mathcal{P}_b^{\text{target}}$, the GPA algorithm is trying to maximise the sum-rate. Accordingly, the key constraints of the GPA algorithm are

$$\sum_{i=1}^{N} P_i \leq P_{\text{budget}} \quad \text{and} \quad \overline{\mathcal{P}}_b = \mathcal{P}_b^{\text{target}}. \tag{4.22}$$

Note that $\mathcal{P}_{b,i} = \mathcal{P}_b^{\text{target}} \forall i$ guarantees $\overline{\mathcal{P}}_b = \mathcal{P}_b^{\text{target}}$ in (4.22). Furthermore, (4.22) it represents a reasonable assumption in terms of fair QoS across all subchannels compared to the GBA algorithm. To proceed with the GPA algorithm, an initialisation step of a UPA arrangements presented in Section 4.2 has to be performed

Table 4.1: Bit Loading using GBA - Constraint (4.21)

Initialisation:
Calculate γ_i for all subchannels using UPA in (4.9)
Load all subchannels with M_K, i.e., $k_i = K$ and $b_i^{\text{gba}} = \log_2 M_K \quad \forall i$
Calculate $\mathcal{P}_{b,i}$ for all subchannels $1 \leq i \leq N$ using (4.7)
Evaluate $\overline{\mathcal{P}}_b$ using (4.20)
if $\overline{\mathcal{P}}_b \leq \mathcal{P}_b^{\text{target}}$
  Maintain current bit loading
else
Recursion:
  while $\overline{\mathcal{P}}_b > \mathcal{P}_b^{\text{target}}$
    $j = \underset{1 \leq i \leq N}{\text{argmax}} \left(\mathcal{P}_{b,i}\right)$
    $k_j = k_j - 1$
    if $k_j \geq 1$
      $b_j^{\text{gba}} = b_j^{\text{gba}} - \log_2 \left(\frac{M_{k_j+1}}{M_{k_j}}\right)$
      Re-calculate $\mathcal{P}_{b,j}$ with γ_j and M_{k_j} using (4.7)
      Update $\overline{\mathcal{P}}_b$ using (4.20)
    else
      $b_j^{\text{gba}} = 0$, $\mathcal{P}_{b,j} = 0$
      Update $\overline{\mathcal{P}}_b$ using (4.20)
      if $\sum_j b_j^{\text{gba}} = 0$[3]
        $\overline{\mathcal{P}}_b = 0$
      end
    end
  end
end
$B_{\text{gba}} = \sum_{i=1}^{N} b_i^{\text{gba}}$

first. Since in UPA subchannels are assigned QAM modulation orders M_{k_i} that are lower in power than their actual SNRs γ_i as clearly represented by (4.10), some unused (excess) powers from the total budget highlighted by the shadowed areas in Fig. 4.1 arise, and are given by

$$P^{\text{ex,u}} = \sum_{i=1}^{N} \frac{\gamma_i - \gamma_{k_i}^{\text{QAM}}}{\text{CNR}_i} = P_{\text{budget}} - \sum_{i=1}^{N} \frac{\gamma_{k_i}^{\text{QAM}}}{\text{CNR}_i}\,. \tag{4.23}$$

These excess powers along with the UPA bit allocation b_i^{u} in (4.11) are the starting point of the iterative GPA algorithm. Basically, the GPA algorithm achieves optimality by trying to allocate $P^{\text{ex,u}}$, finding at each iteration, the subchannel with the minimum power required to upgrade to the next QAM level. These upgrade powers P_i^{up} are initially computed for all subchannels $1 \leq i \leq N$ in the

UPA initialisation step.

The procedure of the GPA algorithm including the UPA initialisation is illustrated in Fig. 4.1 and stated completely in Table 4.2. The algorithm starts with loading subchannels with bits up to the nearest QAM level that is just less in power than the subchannel SNRs provided by the UPA initialisation. Then the excess power $P^{\text{ex,u}}$ is collected and iteratively allocated, under the greedy approach, to subchannels that have not yet reached their maximum allowable QAM level $M_K = 2^{b^{\max}}$. Finally, the sum-rate of this algorithm B_{gpa} and its final excess power $P^{\text{ex,gpa}}$ are evaluated. The power usage of both UPA and GPA algorithms are therefore

$$P_{\text{used}}^{\text{u}} = P_{\text{budget}} - P^{\text{ex,u}}, \tag{4.24a}$$

$$\text{and} \quad P_{\text{used}}^{\text{gpa}} = P_{\text{budget}} - P^{\text{ex,gpa}}, \tag{4.24b}$$

which is a useful measure of how efficient, in terms of power utilisation, both algorithms are. Note that this quantity is not defined for the GBA algorithm as it uses, by definition, the total power budget, i.e. $P_{\text{used}}^{\text{gba}} = P_{\text{budget}}$.

4.6 BER Improvement via Excess Power Redistribution

Since UPA and GPA algorithms presented in Sections 4.2 and 4.5, respectively, cannot attain the complete usage of the total power budget due to the constraint of fixed modulation orders, in addition to that BER has to be tied to a given target value $\mathcal{P}_b^{\text{target}}$ for mathematical tractability. Therefore our second stage of interest after achieving either the maximum possible sum-rate in case of UPA or optimal sum-rate in case of GPA is to focus on extra possible BER performance improvement from the upper limit of the target BER. This Section proposes to utilise the remaining excess power for this aim. This is achieved by the redistribution of the excess power of both UPA and GPA algorithms given, respectively, by (4.24a) and (4.24b) in two distinctive algorithms namely: Uniform Power Redistribution (UPR) and Fairness-BER Power Redistribution (FPR), both of which are presented in the following.

Table 4.2: Bit Loading using UPA and GPA - Constraint (4.22)

Initialisation:
Calculate γ_k^{QAM} for all M_k with $\mathcal{P}_{b,i} = \mathcal{P}_b^{\text{target}}$ using (4.8)
Equally allocate P_{budget} among subchannels using (4.9)
for $i = 1$ to N
  Find k_i that satisfy: $\gamma_i \geq \gamma_{k_i}^{\text{QAM}}$ and $\gamma_i < \gamma_{k_i+1}^{\text{QAM}}$
  if $k_i = 0$
    $b_i^{\text{u}} = 0$, $P_i^{\text{up}} = \frac{\gamma_1^{\text{QAM}}}{\text{CNR}_i}$
  elseif $k_i < K$
    $b_i^{\text{u}} = \log_2 M_{k_i}$, $P_i^{\text{up}} = \frac{\gamma_{k_i+1}^{\text{QAM}} - \gamma_{k_i}^{\text{QAM}}}{\text{CNR}_i}$
  else
    $b_i^{\text{u}} = \log_2 M_{k_i}$, $P_i^{\text{up}} = +\infty$
  end
end
$B_{\text{u}} = \sum_{i=1}^{N} b_i^{\text{u}}$
Collect the excess power $P^{\text{ex,u}}$ using (4.23)
Initiate GPA bit allocation $b_i^{\text{gpa}} = b_i^{\text{u}}\ \forall i$ & excess power $P^{\text{ex,gpa}} = P^{\text{ex,u}}$
Recursion:
while $P^{\text{ex,gpa}} \geq \min(P_i^{\text{up}})$ **and** $\min(k_i) < K$
1. $j = \underset{1 \leq i \leq N}{\text{argmin}}(P_i^{\text{up}})$
2. Update $k_j = k_j + 1$, $P^{\text{ex,gpa}} = P^{\text{ex,gpa}} - P_j^{\text{up}}$
  if $k_j = 1$
3. $b_j^{\text{gpa}} = \log_2 M_1$, $P_j^{\text{up}} = \frac{\gamma_2^{\text{QAM}} - \gamma_1^{\text{QAM}}}{\text{CNR}_j}$
  elseif $k_j < K$
4. $b_j^{\text{gpa}} = b_j^{\text{gpa}} + \log_2\left(\frac{M_{k_j}}{M_{k_j-1}}\right)$, $P_j^{\text{up}} = \frac{\gamma_{k_j+1}^{\text{QAM}} - \gamma_{k_j}^{\text{QAM}}}{\text{CNR}_j}$
  else
5. $b_j^{\text{gpa}} = b_j^{\text{gpa}} + \log_2\left(\frac{M_{k_j}}{M_{k_j-1}}\right)$, $P_j^{\text{up}} = +\infty$
  end
end
Evaluate $B_{\text{gpa}} = \sum_{i=1}^{N} b_i^{\text{gpa}}$ and $P^{\text{ex,gpa}}$

4.6.1 Uniform Power Redistribution (UPR)

The simplest and straightforward way to redistribute the excess power that is left unused by the UPA and GPA algorithms is to equally allocate these powers across all active subchannels regardless of how much BER improvement is attained by each subchannel. We refer to this power redistribution algorithm as uniform power redistribution (UPR). The excess powers $P^{\text{ex,u}}$ and $P^{\text{ex,gpa}}$ are utilised for BER improvement of both UPA and GPA, respectively. For the UPA, the algorithm can be described as follows.

1. Determine the active subchannels $i : b_i^{\mathrm{u}} \neq 0$ and their respective allocated modulation orders M_{k_i} that are occupied by the UPA, where k_i, as above, is the index of the QAM modulation order M_k that is assigned to the subchannel i.

2. Calculate the minimum required SNR to achieve $\mathcal{P}_b^{\mathrm{target}}$ across these active subchannels using (4.8) as

$$\gamma_{k_i}^{\mathrm{QAM}} = \mathcal{F}^{-1}\left(\mathcal{P}_b^{\mathrm{target}}, M_{k_i}\right)$$

.

3. Equally allocate the excess power $P^{\mathrm{ex,u}}$ among all active subchannels and compute the subchannel new SNRs as

$$\gamma_i^{\mathrm{u}} = \gamma_{k_i}^{\mathrm{QAM}} + \frac{P^{\mathrm{ex,u}}}{N_a^{\mathrm{u}}} \times \mathrm{CNR}_i\,, \tag{4.25}$$

where N_a^{u} is the number of active subchannels under the UPA scheme.

4. Calculate the subchannel new BERs using (4.7) as $\mathcal{P}_{b,i}^{\mathrm{u}} = \mathcal{F}\left(\gamma_i^{\mathrm{u}}, M_{k_i}\right)$ and then the mean BER $\overline{\mathcal{P}}_b^{\mathrm{u}}$ using (4.20).

The same procedures are used for the case of the GPA algorithm to redistribute $P^{\mathrm{ex,gpa}}$ and obtain $\overline{\mathcal{P}}_b^{\mathrm{gpa}}$ but the redistribution in this case should include all active subchannels under the GPA scheme, N_a^{gpa}.

Note that, in general $P^{\mathrm{ex,gpa}} \leq P^{\mathrm{ex,u}}$ due to the improvement in power allocation gained by the GPA algorithm and $N_a^{\mathrm{gpa}} \geq N_a^{\mathrm{u}}$ as a result of the chance to upgrade more inactive subchannels to be involved for transmission with the GPA application. Consequently, $\frac{P^{\mathrm{ex,gpa}}}{N_a^{\mathrm{gpa}}} \ll \frac{P^{\mathrm{ex,u}}}{N_a^{\mathrm{u}}}$ is most likely to be expected and accordingly by substituting in (4.25), the subchannel new SNRs in case of GPA will result in less improvement in the mean BER $\overline{\mathcal{P}}_b^{\mathrm{gpa}}$ of the GPA compared to that obtained by UPA.

4.6.2 Fairness-BER Power Redistribution (FPR)

The UPR presented above equally allocates the excess power among all active subchannels, and results in unequal subchannel BERs that depend on CNR_i and the occupied modulation orders M_{k_i} for each active subchannel i. Therefore, the expected mean BERs $\overline{\mathcal{P}}_b^{\mathrm{u}}$ or $\overline{\mathcal{P}}_b^{\mathrm{gpa}}$ may be dominated by the worst individual subchannel BERs as a result. Moreover, it is desirable to achieve uniform

BER performance across all subchannels for fairness in QoS or link reliability applications. Therefore in this Section we adapt the power redistribution for an algorithm that can achieve this QoS fairness across all active subchannels for both UPA and GPA algorithms; this algorithm is here referred to as fairness-BER power redistribution (FPR). Because derivations are identical for UPA and GPA, superscripts referring to either are omitted in the following.

Compared to the UPR algorithm, a new factor $\mu_i \in \mathbb{R}, 1 \leq i \leq N_a, \sum_i \mu_i = 1$ is introduced to the last term of the r.h.s of (4.25) to adjust the power redistribution conditions for equal BERs across all active subchannels. This can be mathematically formulated as

$$\begin{aligned} \text{solve for} \quad \boldsymbol{\mu} &= [\mu_1, \mu_2, \cdots, \mu_{N_a}] \\ \text{that results in} \quad \gamma_i^F &= \mathcal{F}^{-1}\left(\mathcal{P}_b^F, M_{k_i}\right) \quad \forall i : 1 \leq i \leq N_a, \end{aligned} \tag{4.26}$$

where

$$\gamma_i^F = \gamma_{k_i}^{\text{QAM}} + \mu_i \cdot P^{\text{ex}} \cdot \text{CNR}_i \tag{4.27}$$

are the new subchannel SNRs and $\mathcal{P}_b^F$ is the fair (constant) BER across all active subchannels. From (4.26) and (4.27), the entries of the unknown vector $\boldsymbol{\mu}$ are given by

$$\mu_i = \frac{\mathcal{F}^{-1}\left(\mathcal{P}_b^F, M_{k_i}\right) - \gamma_{k_i}^{\text{QAM}}}{P^{\text{ex}} \cdot \text{CNR}_i}, \quad 1 \leq i \leq N_a\,. \tag{4.28}$$

Since $\sum_{i=1}^{Na} \mu_i = 1$ and by defining the function

$$f\left(\mathcal{P}_b\right) \stackrel{d}{=} \sum_{i=1}^{N_a} \frac{\mathcal{F}^{-1}\left(\mathcal{P}_b, M_{k_i}\right) - \gamma_{k_i}^{\text{QAM}}}{P^{\text{ex}} \cdot \text{CNR}_i} - 1, \tag{4.29}$$

it is possible to find the solution $\mathcal{P}_b^F$ of $f\left(\mathcal{P}_b\right)$ such that $f\left(\mathcal{P}_b\right)|_{\mathcal{P}_b \to \mathcal{P}_b^F} \simeq 0$. The bisection method is used to find this root of $f\left(\mathcal{P}_b\right)$.

The complete FPR algorithm is given as follows.

1. Given the active subchannels $i : 1 \leq i \leq N_a$ and their respective allocated M_{k_i} as well as CNR_i, $\mathcal{P}_b^{\text{target}}$, and P^{ex} for either UPA or GPA algorithm, calculate $\gamma_{k_i}^{\text{QAM}} = \mathcal{F}^{-1}\left(\mathcal{P}_b^{\text{target}}, M_{k_i}\right)$ using (4.8).

2. Locate two possible appropriate BER points that return the function $f\left(\mathcal{P}_b\right)$ in (4.29) with two opposite-sign values that are close to zero. These $\mathcal{P}_b$ points exists in the domain $\left(0, \mathcal{P}_b^{\text{target}} - \epsilon\right]$, where $\epsilon \to 0^+$ while the corresponding domain of $f\left(\mathcal{P}_b\right)$ ranges in $(\infty, -1]$.

3. Use the bisection method to find the root $\mathcal{P}_b^F$ that returns $f\left(\mathcal{P}_b^F\right) \rightarrow 0$. This BER solution is denoted by $\mathcal{P}_b^{F,\mathrm{u}}$ for the UPA algorithm and by $\mathcal{P}_b^{F,\mathrm{gpa}}$ for the GPA algorithm.

Notice that, the complexity of this algorithm is dominated by the root finding search method. While less complex methods may exist in the literature, the bisection approach has been chosen because of its relative simplicity.

Fig. 4.4 demonstrates a simulated example of the function $f\left(\mathcal{P}_b\right)$ against its BER argument $\mathcal{P}_b$ for both UPA and GPA under the FPR algorithm of a 6×6 MIMO system with a channel probe of entries $h_{ij} \in \mathcal{CN}\left(0,1\right)$, $\mathcal{P}_b^{\mathrm{target}} = 10^{-3}$, and SNR = 30 dB. Obviously, the BER improvement of the UPA is much better than that of the GPA as the function root $\mathcal{P}_b^{F,\mathrm{u}} \leq \mathcal{P}_b^{F,\mathrm{gpa}}$ as discussed in Sec. 4.6.1. This is again due to the good expenditure of power attained by the GPA that is used to maximise the sum-rate. It is also clearly noted that $f\left(\mathcal{P}_b\right)$ reaches its solution $\mathcal{P}_b^{F,\mathrm{u}}$ faster than $\mathcal{P}_b^{F,\mathrm{gpa}}$ and its values for both UPA and GPA intersect at $\mathcal{P}_b^{\mathrm{target}}$ of 10^{-3}.

4.7 Simulation Results

Since (4.8) and (4.7) are deduced from each other, a fair comparison between GBA and GPA algorithms in terms of data throughput would be expected. The difference between the algorithms lies in the sense of optimality considered by each of them as highlighted in Sec. 4.4 and Sec. 4.5, respectively plus the key constraints of these two algorithms given, respectively, in (4.21) and (4.22). In order to investigate the performance of both GPA and GBA algorithms, computer simulations are conducted for a 4×4 frequency-flat MIMO system with channel matrix $\mathbf{H} \in \mathbb{C}^{N_r \times N_t}$. The channel matrix entries h_{ij} are drawn from independent identically distributed complex Gaussian distribution with zero mean and unit variance, $h_{ij} \in \mathcal{CN}\left(0,1\right)$. A target BER of $P_b^{\mathrm{target}} = 10^{-3}$ is to be achieved through the bit loading schemes of the GBA and GPA along with the UPA algorithm. Fixed QAM modulation orders of $\left\{2^1, 2^2, \cdots, 2^{b^{\max}}\right\}$, where $b^{\max} =$ 6 bits, are constrained by the system under consideration.

It is shown from the throughput results in Fig. 4.5 that the GPA algorithm performs better than both GBA and UPA algorithms. An explanation of this is as follows: since the power allocation of the GBA algorithm is done using the UPA, which is an inefficient power allocation scheme, therefore wastes power for unnecessary improvement (compared to the requirement of $\mathcal{P}_b^{\mathrm{target}}$) of the mean BER $\overline{\mathcal{P}}_b < \mathcal{P}_b^{\mathrm{target}}$. On the other hand, the GPA algorithm efficiently utilises the

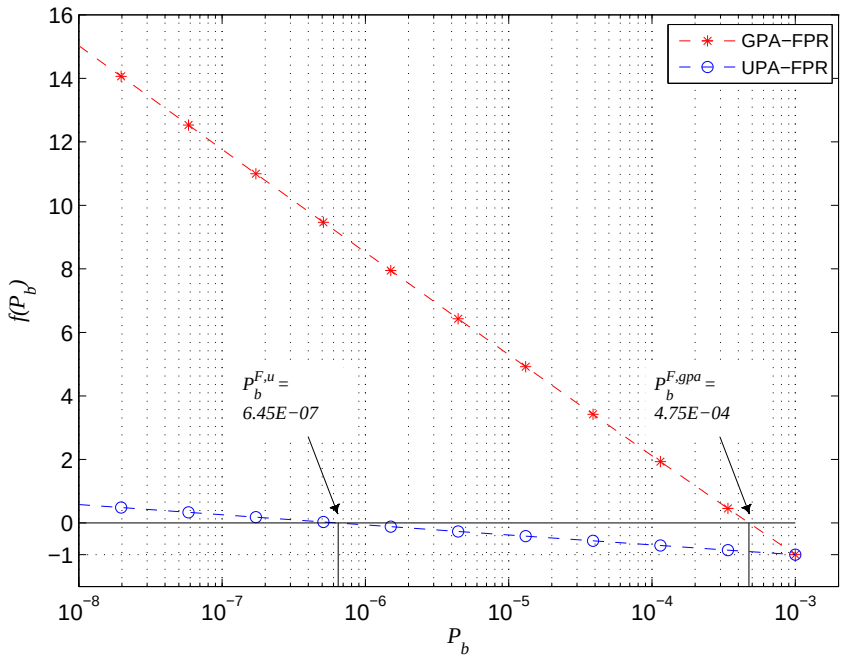

Figure 4.4: The function $f(\mathcal{P}_b)$ defined in (4.29) for both UPA and GPA algorithms of a 6×6 MIMO system at SNR = 30 dB and $\mathcal{P}_b^{\text{target}} = 10^{-3}$.

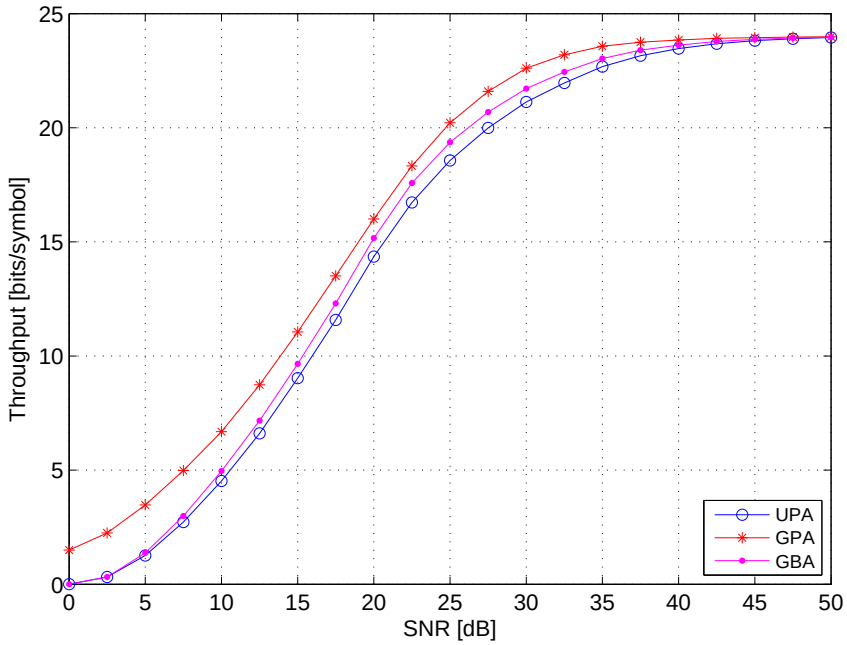

Figure 4.5: Throughput results for a 4×4 MIMO system with $\mathcal{P}_b^{\text{target}} = 10^{-3}$ and varying SNR.

total power budget P_{budget} (power is allocated according to the greedy approach) to maximise the overall throughput while achieving BER to its maximum requirements, $\mathcal{P}_{b,i} = \mathcal{P}_b^{\text{target}}, \forall i$. This means better investment of the total power towards the rate maximisation problem.

Fig. 4.6 shows the throughput versus different target BER values at SNR=25 dB. Intuitively, throughput is increasing with the increase of target BER. The GPA algorithm outperforms its GBA counterpart by more than 1.2 bits/symbol at $\mathcal{P}_b^{\text{target}} = 10^{-7}$ and this improvement gradually decreasing with further increasing of the target BER to reach $\simeq 0.8$ bit at $\mathcal{P}_b^{\text{target}} = 10^{-3}$. A fixed increase of more than 1.6 bits/symbol over the whole target BER range can be noted as an advantage of the GPA algorithm over the UPA scheme.

In Fig. 4.7, the power usage of UPA and GPA algorithms are compared, in conjunction with the achieved rate in Fig. 4.5, which shows better performance of GPA over UPA algorithm. Note that the GBA algorithm (shown as the P_{budget} curve) cannot be compared here as it spends, by definition, the entire power budget to improve the achieved mean BER as will be shown in Fig. 4.8. Once the throughput reaches its expected maximum of 24 bits (6 bits over all 4 subchannels), extra power is no longer required. Therefore, the effective used power for both UPA and GPA algorithms given in (4.24a) and (4.24b), respectively, starts to saturate to the minimum power that is theoretically required to achieve the maximum bit loading $b^{\max}$ for all subchannels, i.e., $\sum_i \frac{\gamma_K^{\text{QAM}}}{\text{CNR}_i}$ which is found to be ≈ 38.17 dB and highlighted by the dashed line in Fig. 4.7.

As proposed in Section 4.6 and demonstrated in Fig. 4.7, the excess power of both UPA and GPA algorithms is redistributed to improve the BER performance. Fig. 4.8 shows these improvements for both power redistribution algorithms UPR and FPR compared to the actual achieved BER of the GBA algorithm. Mean BER is investigated against varying SNR showing BER improvements compared to the target BER (of 10^{-3}) for all algorithms. Interestingly, both UPA and GPA algorithms with excess power redistribution can achieve better mean BER performance than the GBA algorithm of [116]. Again these results should be seen in conjunction with the achieved rate in Fig. 4.5. It is also noted that FPR performs better than UPR if applied to the UPA, while the situation is inverted for the GPA algorithm. This can be attributed to the fact that the excess power of the UPA algorithm is greater than that of the GPA, and hence it is most likely that the mean BER of UPA-UPR is dominated by subchannels of poor CNR_i while the FPR algorithm is advantageous in this case because of its inherently fair BER property. On the other hand, since for the GPA algorithm

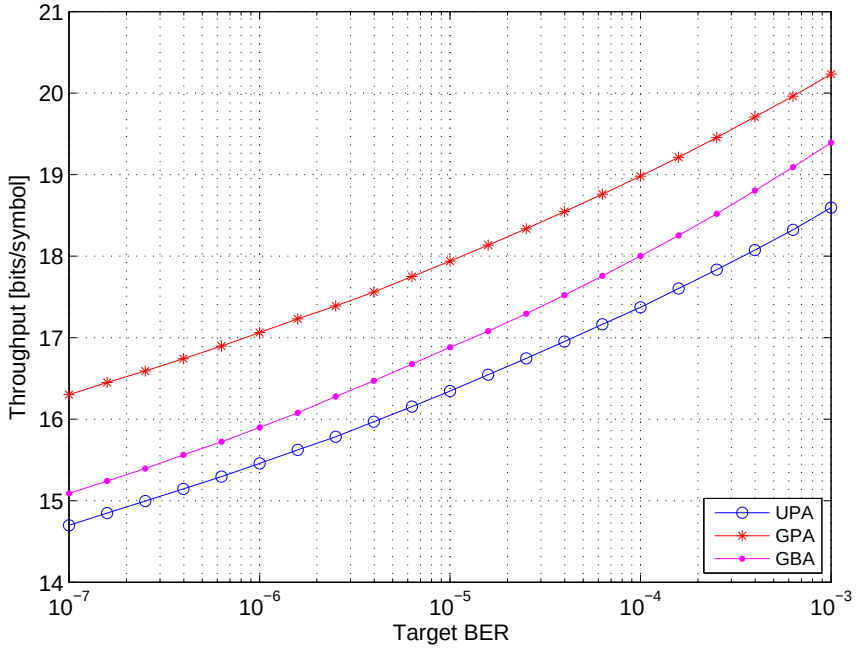

Figure 4.6: Sum-rate results for a 4×4 MIMO system at SNR $= 25$ dB and varying $\mathcal{P}_b^{\text{target}}$.

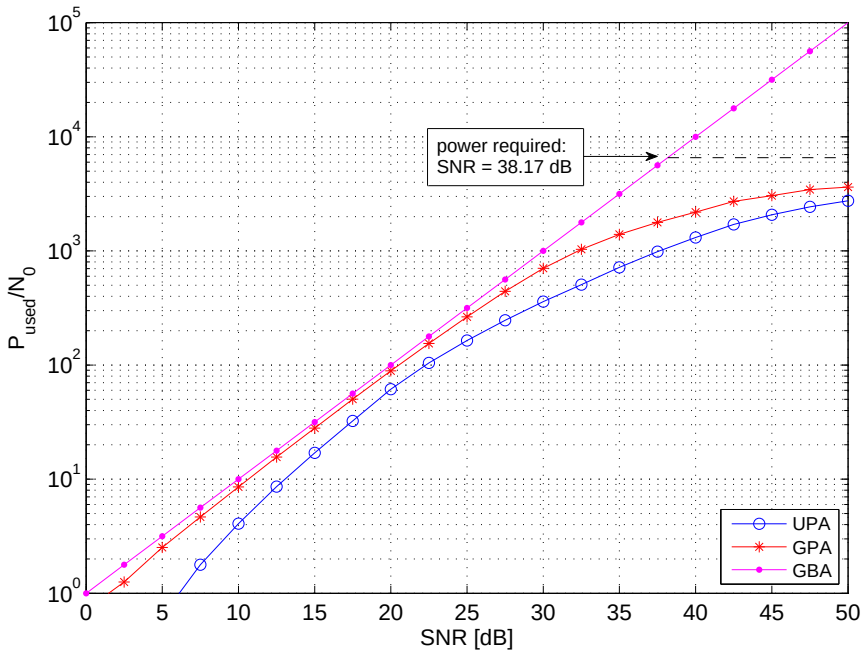

Figure 4.7: Power usage for a 4×4 MIMO system with $\mathcal{P}_b^{\text{target}} = 10^{-3}$ and varying SNR.

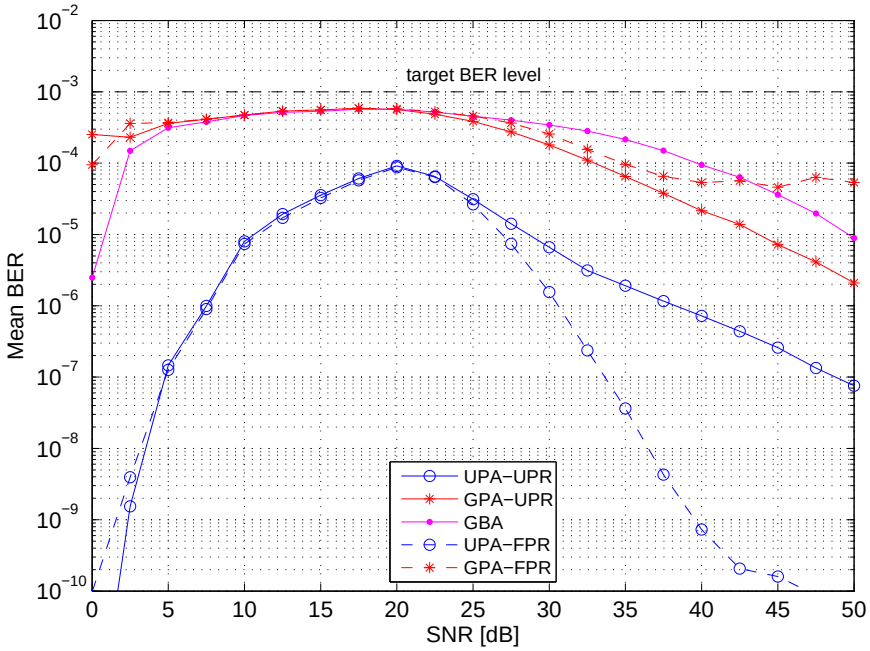

Figure 4.8: BER improvements of UPA and GPA algorithms.

the excess power is relatively small and another constraint of balancing BERs across all active subchannels, most of the redistributed power will be occupied by subchannels in lower QAM levels leading to lower BER performance compared to that obtained by the UPR algorithm.

4.8 Conclusion

In this Chapter, the problem of data rate maximisation has been considered. The inefficient uniform power allocation (UPA) scheme leads to poor throughput performance of multichannel systems with constrained-loading parameters. This can be improved through rate maximisation using greedy power GPA and bit GBA allocation schemes. Both algorithms share the main target of optimising the overall system throughput. The GPA algorithm tackles this from the efficient power utilisation point of view keeping the target BER to its maximum requirements, while the GBA algorithm guarantees a lower average BER than the target is. Since the GBA approach sacrifices power utilisation by adapting UPA for BER improvements, a degradation in the achieved data rate is expected as a result. By optimising power allocation, GPA demonstrates optimal performance in the discrete rate maximisation sense. Another aspect of UPA and GPA schemes is that power can be saved in achieving the target BER, which can be redistributed

for better BER using different design aspects. Simulation results show that both UPA and GPA can achieve much better BER performance compared to the GBA scheme. More importantly, GPA can achieve lower BER compared to the GBA algorithm while keeping the data throughput to its optimal figure. In Table 4.3 power and bit loading schemes discussed in this chapter are briefly summarised.

The different schemes discussed in this chapter are optimal in various senses, such as maximisation of the sum-rate. However, the computational complexity of greedy algorithms is well-known to be excessive [118, 128], therefore the next chapter will consider low-cost suboptimal approaches.

Table 4.3: Summary of power and bit loading schemes considered in this chapter.

scheme	maximisation	constraints	power allocation	bit allocation
UPA	-	$P_i = \frac{P_{\text{budget}}}{N}$ and $\overline{\mathcal{P}}_b = \mathcal{P}_b^{\text{target}}$	uniform	-
GBA	sum-rate	$\sum_{i=1}^{N} P_i = P_{\text{budget}}$ and $\overline{\mathcal{P}}_b \leq \mathcal{P}_b^{\text{target}}$	uniform	greedy, bit-removal
GPA	sum-rate	$\sum_{i=1}^{N} P_i \leq P_{\text{budget}}$ and $\overline{\mathcal{P}}_b = \mathcal{P}_b^{\text{target}}$	greedy	greedy, bit-filling

Chapter 5

Reduced-Complexity Schemes for Greedy Power Allocation

The introduced greedy bit and power allocation algorithms in Chapter 4 share the characteristic of high complexity. Owing to the iterative nature of these algorithms to optimally achieve their respective objective functions, the computational complexity is dramatically increases with the number of subchannels. The situation becomes practically prohibitive for multicarrier systems (e.g. OFDM) as the number of subcarriers is usually high and can reach e.g. up to 2^{13} for digital video broadcasting (DVB) [34] for terrestrial (DVB-T) [35] or handheld (DVB-H) [36] standards. While achieving rate optimality, the family of greedy algorithms is also known to be greedy in terms of computing requirements. Therefore, reduced complexity schemes are either water-filling-based only [123] or aim at simplifications [128]. Seeking for suboptimal greedy power allocation schemes with reduced-complexity is therefore of particular interest.

In this Chapter, reduced-complexity schemes for GPA are explored aiming to achieve near optimum data throughput performance. Compared to the standard GPA, which is optimal in terms of maximising the data throughput, three suboptimal schemes are proposed, which perform GPA on subsets of subchannels only. These subsets are created by considering the minimum SNR boundaries of QAM levels for a given target BER. We demonstrate how these schemes can significantly reduce the computational complexity, especially for large number of subcarriers. Two of the proposed algorithms can achieve near optimal performance by including a transfer of residual power between subsets at the expense of a very small extra cost.

5.1 Multichannel System Models

In OFDM, multiplexing over MIMO channels, or general transmultiplexing techniques a number of independent subcarriers or subchannels arise for transmission, which differ in SNR. Maximising the data throughput over these subcarriers/subchannels under the constraints in (4.1b)-(4.1e) with $\mathcal{P}_{b,i} = \mathcal{P}_b^{\text{target}} \, \forall i : 1 \leq i \leq N$ is provided by the GPA algorithm presented in Section 4.5 as discussed in Chapter 4. The basis over which the GPA achieves its optimal bit allocation is formed by the subchannel gains $g_i, 1 \leq i \leq N$ given generally in (4.5). In the following, we will introduce these subchannel gains for two different system models.

- MIMO Narrowband

In a simple MIMO system of a narrowband channel characterised by a matrix $\mathbf{H} \in \mathbb{C}^{N_r \times N_t}$ of complex coefficients h_{ij} which describe the complex gains between the jth transmit and the ith receive antenna. The SVD can be used to decouple the system $\mathbf{H}$ into $N = \text{rank}\,(\mathbf{H}) \leq \min\,(N_t, N_r)$ subchannels whose gains are equal to the singular values $g_i = \sigma_i, i = 1 \ldots N$ that are ordered such that $\sigma_i \geq \sigma_{i+1} \, \forall i$. The channel-to-noise ratio of the ith subchannel defined previously in (4.5) is therefore

$$\text{CNR}_i = \frac{\sigma_i^2}{\mathcal{N}_0} \,. \tag{5.1}$$

- MIMO-OFDM

For the broadband MIMO case, OFDM can be used to turn a frequency-selective MIMO channel into a set of parallel frequency-flat MIMO channels. Applying again the SVD on these frequency-flat MIMO channels analogous to the MIMO narrowband case above results in an N-subcarrier system with different gains $|H_i|\,, i = 1 \cdots N$, where N here denotes the total number of subcarriers of the resultant OFDM multicarrier system. In severe ISI MIMO channels, N has to be selected large enough to properly satisfy the uncorrelation assumption of these frequency-flat MIMO channels. The channel-to-noise ratio of the ith subcarrier is then

$$\text{CNR}_i = \frac{|H_i|^2}{\mathcal{N}_0} \,. \tag{5.2}$$

In both cases, we result in an N subchannel/subcarrier[1] system whereby data-rate is to be maximised.

5.2 Subchannel Grouping Concept

In Chapter 4, the analysis of both UPA and GPA algorithms assumed that the BER is identical across all subchannels and equal to the target BER $\mathcal{P}_{b,i} = \mathcal{P}_b^{\text{target}}$, therefore the subscript i will be dropped from the BER notation. Based on (4.8), the minimum SNR that is required to allocate $b_k = \log_2 M_k$ bits with the achievement of $\mathcal{P}_b^{\text{target}}$ for any subchannel is

$$\gamma_k^{\text{QAM}} = \begin{cases} \frac{1}{2}\left[Q^{-1}\left(\mathcal{P}_b^{\text{target}}\right)\right]^2 & \text{for BPSK,} \\ \frac{M_k-1}{3}\left[Q^{-1}\left(\frac{1-\sqrt{1-\mathcal{P}_b^{\text{target}}\cdot\log_2 M_k}}{2\left(1-1/\sqrt{M_k}\right)}\right)\right]^2 & \text{for } M \text{ QAM}. \end{cases} \tag{5.3}$$

By equally allocating the transmit power budget across all subchannels, the UPA algorithm described in Section 4.2 can be modified rephrased by considering the division of subchannels into QAM groups. This can be viewed as collectively grouping the subchannels in Fig. 4.1 according to their SNRs $\gamma_i, 1 \leq i \leq N$ resulting in either Fig. 5.1 in case of a multicarrier system or Fig. 5.2 in case of an ordered multicarrier system or after applying the SVD in order to decouple a narrowband MIMO system. With the aid of Figs. 5.1 and 5.2, these groups are created by considering the minimum SNR boundaries of QAM levels for a given target BER. In Sec. 5.2.1, a typical UPA is performed, however, in its subchannels grouping version.

5.2.1 Grouped UPA and Initialisation Setup

The following steps constitute the grouped UPA concept and will form the first stage of any later refinements.

1. Calculate γ_k^{QAM} for all $M_k, 1 \leq k \leq K$ using (5.3).
2. Equally allocate P_{budget} among all subchannels $1 \leq i \leq N$ and compute the subchannel SNRs γ_i using (4.9).

[1] In the sequel, unless otherwise stated, we will use the term "subchannel" to refer to both subchannels or subcarriers.

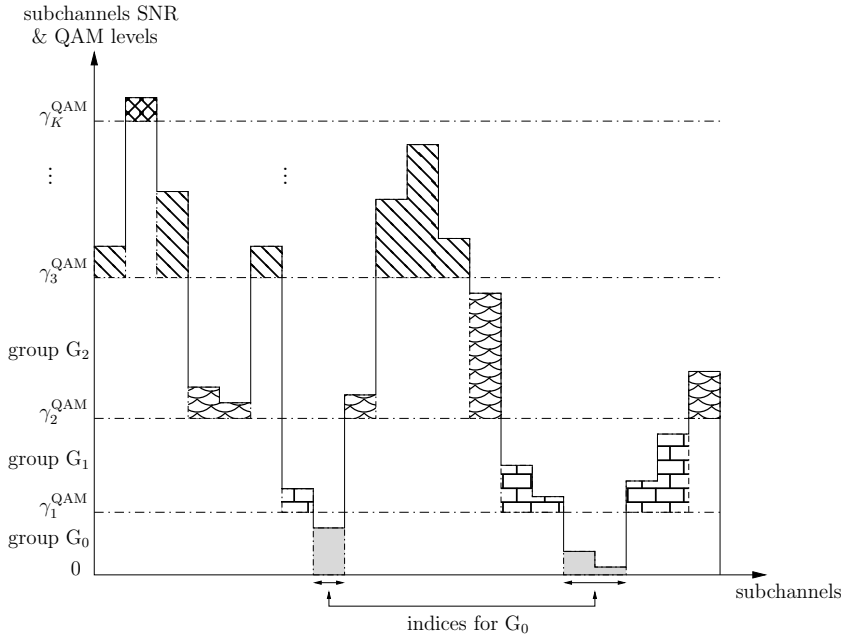

Figure 5.1: Subchannel grouping of a multicarrier system into $K+1$ QAM groups based on their SNRs in (4.9) and step (3) of Sec. 5.2.1.

3. Allocate subchannels according to their SNR γ_i to QAM groups $\mathrm{G}_k, 0 \leq k \leq K$ bounded by QAM levels γ_k^{QAM} and $\gamma_{k+1}^{\mathrm{QAM}}$ with $\gamma_0^{\mathrm{QAM}} = 0$ and $\gamma_{K+1}^{\mathrm{QAM}} = +\infty$ (cf. Figs. 5.1 and 5.2) such that

$$\gamma_i \geq \gamma_k^{\mathrm{QAM}} \quad \text{and} \quad \gamma_i < \gamma_{k+1}^{\mathrm{QAM}} . \tag{5.4}$$

4. For each QAM group G_k, load subchannels within this group with QAM constellation M_k and compute the group's total allocated bits

$$B_k^{\mathrm{u}} = \sum_{i \in \mathrm{G}_k} b_{i,k}^{\mathrm{u}} = \sum_{i \in \mathrm{G}_k} \log_2 M_k, \tag{5.5}$$

with $B_0^{\mathrm{u}} = 0$. The excess (unallocated) power of the QAM group G_k as in (4.23) is given by $P^{\mathrm{ex,u}}$

$$\begin{aligned} P_k^{\mathrm{ex,u}} &= \textstyle\sum_{i \in \mathrm{G}_k} \frac{\gamma_i - \gamma_k^{\mathrm{QAM}}}{\mathrm{CNR}_i} = \sum_{i \in \mathrm{G}_k} P_i - \frac{\gamma_k^{\mathrm{QAM}}}{\mathrm{CNR}_i} \\ &= N_k \tfrac{P_{budget}}{N} - \textstyle\sum_{i \in \mathrm{G}_k} \frac{\gamma_k^{\mathrm{QAM}}}{\mathrm{CNR}_i}, \end{aligned} \tag{5.6}$$

where $N_k, 1 \leq k \leq K$ is the number of subchannels that occupies the QAM group G_k.

5. The overall allocated bits and the used power for the grouped UPA are

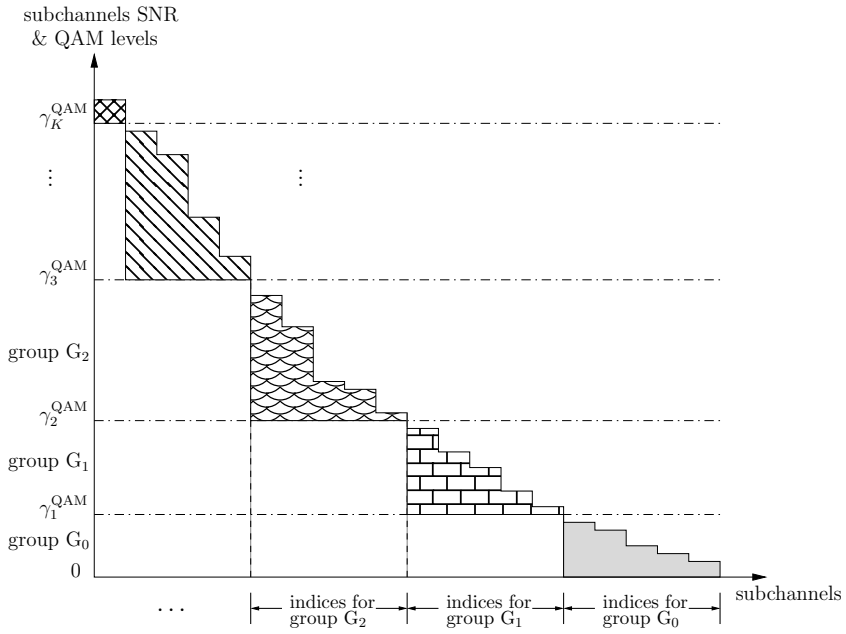

Figure 5.2: Ordered subchannel grouping of a MIMO system into $K+1$ QAM groups based on their SNRs in (4.9) and step (3) of Sec. 5.2.1.

identical to that obtained by the UPA algorithm given in Section 4.2 and are given, respectively, as

$$B_{\text{u}} = \sum_{k=1}^{K} B_k^{\text{u}} \tag{5.7a}$$

$$P_{\text{used}}^{\text{u}} = P_{\text{budget}} - P^{\text{ex,u}}, \tag{5.7b}$$

where the overall excess power $P^{\text{ex,u}}$ in (5.7b), identical to the previous case in (4.23), constitutes the power that remains unallocated in all QAM groups, that is,

$$P^{\text{ex,u}} = \sum_{k=0}^{K} P_k^{\text{ex,u}}. \tag{5.8}$$

Note that the summation in (5.7a) starts from group G_1 since none of the subchannels in G_0 will be loaded in this initialisation.

The difference between the transmit power budget and the overall used power $P_{\text{used}}^{\text{u}}$ represents a useful measure to indicate how well a bit loading scheme utilises the total system transmit power P_{budget}. The closer the used power to P_{budget}, the better is the utilisation of the available transmit power budget achieved by a specific power loading scheme. Therefore, it is clear from (5.7b) that the amount of excess power $P_k^{\text{ex,u}}$ that is left unused has an impact on the performance of the

UPA scheme. The worst cases are $P_0^{\mathrm{ex,u}}$ and $P_K^{\mathrm{ex,u}}$ which reveal inefficient power allocations in situations of low-to-medium and medium-to-high SNRs, respectively, as will be discussed in Section 5.7.

5.2.2 Full GPA Algorithm and Ways Forward

Based on the initialisation step described in the previous section, the full GPA algorithm [115] presented in Table 4.2 performs an iterative re-distribution of the unallocated power of the UPA algorithm $P^{\mathrm{ex,u}}$ by applying the algorithmic steps detailed in the second (recursion) part of Table 4.2. At each iteration, this algorithm achieves bit loading optimality by upgrading (to the next higher QAM level) the subchannel with the least power requirements through an exhaustive search by performing step (1) in Table 4.2 for all subchannels N. When either i) the remaining power cannot support any further upgrades or ii) all subchannels appear in the highest QAM level K, the algorithm stops, resulting in the system allocated bits and used power given, respectively, by

$$B_{\mathrm{gpa}} = \sum_{i=1}^{N} b_i^{\mathrm{gpa}} \tag{5.9a}$$

$$P_{\mathrm{used}}^{\mathrm{gpa}} = P_{\mathrm{budget}} - P^{\mathrm{ex,gpa}}. \tag{5.9b}$$

Given B_k^{u} as defined in (5.5) and $P_k^{\mathrm{ex,u}}$ in (5.6), three low-complexity greedy algorithms are proposed to efficiently utilise the total excess power of the UPA in (5.8) using the QAM grouping concept. More precisely, GPA is separately accomplished for each QAM group G_k aiming to increase the total bit allocation to this group and therefore the overall allocated bits. Based on the way of utilising $P_k^{\mathrm{ex,u}}, 0 \leq k \leq K$, we propose three different algorithms, which below are referred to as (i) grouped GPA (g-GPA), (ii) power Moving-up GPA (Mu-GPA) and (iii) power Moving-down GPA (Md-GPA). In the following sections these algorithms are presented in turns.

5.3 Grouped Greedy Power Allocation (g-GPA)

As discussed in Section 4.5, optimum discrete bit loading constrained by total power and maximum permissible QAM order can be performed by the GPA approach. However, the direct application of the GPA algorithm is computationally

very costly due to the fact that at each iteration an exhaustive searching across all N subchannels is required as is evident from Table 4.2. This searching step (1) of Table 4.2 is, in fact, dominating the computational complexity of practical loading algorithms [118, 128].

A simplification of the GPA algorithm can be achieved if subchannels are firstly divided into QAM groups $\mathrm{G}_k, 0 \leq k \leq K$ according to their SNRs as shown in Fig. 5.1 (for non-ordered[2] subchannels). After ordering or due to the implicit ordering of the singular values in case of SVD-based decoupling of MIMO systems, the grouping as shown in Fig. 5.2 arises. The g-GPA algorithm proceeds by independently applying the GPA algorithm to each group G_k, trying to allocate as much of the excess power $P_k^{\mathrm{ex,u}}$ within this QAM group as possible. This excess power is iteratively allocated to subchannels within this group according to the greedy concept with the aim of upgrading as many subchannels as possible to the next QAM level.

With the aid of Fig. 5.3, the expected reduction in computational complexity that can be gained by the arrangements of the g-GPA algorithm compared to the standard full GPA presented in Section 4.5 is highlighted as follows. Assume that subchannels are sorted in descending order with respect to their CNR_i as shown in Fig. 5.3. Since the GPA algorithm re-distributes the total excess power $P^{\mathrm{ex,u}}$ globally across all subchannels which spread over all QAM groups, it is possible to find two subchannels $i \in \mathrm{G}_v$ and $j \in \mathrm{G}_u$ with the following properties:

$$\begin{aligned} \mathrm{CNR}_i &> \mathrm{CNR}_j, \\ \Delta\gamma_v^{\mathrm{QAM}} = \gamma_{v+1}^{\mathrm{QAM}} - \gamma_v^{\mathrm{QAM}} &> \Delta\gamma_u^{\mathrm{QAM}} = \gamma_{u+1}^{\mathrm{QAM}} - \gamma_u^{\mathrm{QAM}}. \end{aligned} \tag{5.10a}$$

The upgrade powers required to promote subchannels i and j to QAM groups G_{v+1} and G_{u+1}, respectively, are therefore

$$P_i^{\mathrm{up}} = \frac{\Delta\gamma_v^{\mathrm{QAM}}}{\mathrm{CNR}_i} \quad \text{and} \quad P_j^{\mathrm{up}} = \frac{\Delta\gamma_u^{\mathrm{QAM}}}{\mathrm{CNR}_j}, \tag{5.10b}$$

where QAM group G_v is higher than G_u. Obviously from (5.10a) and (5.10b), we cannot assume that all upgrade powers $P_i^{\mathrm{up}}, 1 \leq i \leq N$ are in ascending order as it is possible to find $P_j^{\mathrm{up}} < P_i^{\mathrm{up}}$. Therefore, subchannel ordering does not lead to any improvement in the complexity of the full GPA algorithm as all subchannels N have to be considered in every iteration of power re-distribution. Contrarily,

[2]Ordering here refers to descending order of subchannels with respect to their CNR_i.

for the g-GPA algorithm since $\Delta\gamma_k^{\mathrm{QAM}}$ is fixed for all subchannels in QAM group G_k, ordering subchannels gains $\mathrm{CNR}_i, i \in \mathrm{G}_k$ (the denominators in (5.10b)) either in ascending or descending fashion will lead to an overall ordering of $P_i^{\mathrm{up}}, i \in \mathrm{G}_k$. Accordingly, the allocation of $P_k^{\mathrm{ex,u}}$ within this group can be done sequentially without the need for any sorting, which will significantly simplify the computational complexity of the g-GPA algorithm, as will be discussed in detail in Section 5.6.

The pseudo code of the g-GPA algorithm for the subchannels in the kth QAM group G_k is given in Table 5.1, where subchannels are assumed to be not ordered in their CNR gains. Note that different from the standard GPA, this algorithm permits upgrades to the next QAM level only for a given QAM group, with P_j^{up} set to $+\infty$ in steps (5) and (6) in Table 5.1. Therefore some left-over (LO) power P_k^{LO} may remain for each QAM group G_k, resulting in a total LO power of

$$P_{\mathrm{g}}^{\mathrm{LO}} = \sum_{k=0}^{K-1} P_k^{\mathrm{LO}} + P_K^{\mathrm{ex,u}} \,. \tag{5.11}$$

Intuitively, for the overall operation of the g-GPA algorithm, the algorithm in Table 5.1 has to be executed K times, once for each QAM group, from G_0 to G_{K-1}, resulting in the system allocated bits and used power given, respectively, by

$$B_{\mathrm{g}} = \sum_{k=0}^{K-1} B_k^{\mathrm{g}} + B_K^{\mathrm{u}} \tag{5.12a}$$

$$P_{\mathrm{used}}^{\mathrm{g}} = P_{\mathrm{budget}} - P_{\mathrm{g}}^{\mathrm{LO}} \,. \tag{5.12b}$$

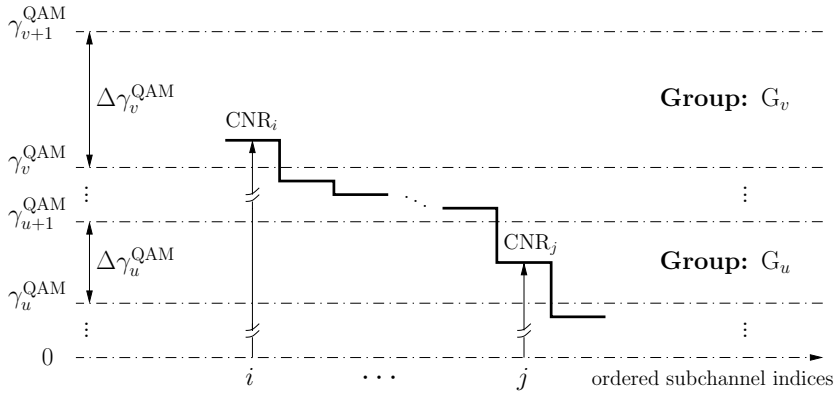

Figure 5.3: Illustration of the reduction in complexity gained by the g-GPA algorithm compared to the standard GPA algorithm.

Table 5.1: g-GPA Algorithm for Subchannels in the kth QAM Group G_k

1.	$\forall i \in \mathrm{G}_k$, calculate the upgrade power $P_i^{\mathrm{up}} = (\gamma_{k+1}^{\mathrm{QAM}} - \gamma_k^{\mathrm{QAM}})/\mathrm{CNR}_i$
2.	Initiate $b_{i,k}^{\mathrm{g}} = b_{i,k}^{\mathrm{u}}$ in (5.5) and $P_k^{\mathrm{LO}} = P_k^{\mathrm{ex,u}}$ in (5.6)
	while $P_k^{\mathrm{LO}} \geq \min(P_i^{\mathrm{up}})$
3.	$j = \underset{i \in \mathrm{G_k}}{\mathrm{argmin}}(P_i^{\mathrm{up}})$
4.	$P_k^{\mathrm{LO}} = P_k^{\mathrm{LO}} - P_j^{\mathrm{up}}$
	if $k = 0$
5.	$b_{j,k}^{\mathrm{g}} = \log_2 M_1$, $P_j^{\mathrm{up}} = +\infty$
	else
6.	$b_{j,k}^{\mathrm{g}} = b_{j,k}^{\mathrm{g}} + \log_2 \frac{M_{k+1}}{M_k}$, $P_j^{\mathrm{up}} = +\infty$
	end
	end
7.	Evaluate $B_k^{\mathrm{g}} = \sum_{i \in \mathrm{G}_k} b_{i,k}^{\mathrm{g}}$ and P_k^{LO}

5.4 Power Moving-up GPA (Mu-GPA)

The g-GPA algorithm presented in Section 5.3 results in unallocated power P_k^{LO} for each QAM group G_k. This residual power can be exploited by a second stage, whereby it is proposed to move power upwards starting from the lowest QAM group G_0 to QAM group G_{K-1} as outlined in Fig. 5.4 and by the flowchart in Fig. 5.5. This modifies the g-GPA algorithm by considering the LO power P_0^{LO} of the QAM group G_0 after running the g-GPA algorithm on that group and assigns this power for re-distribution to group G_1 along with the excess power $P_1^{\mathrm{ex,u}}$. Any LO power after running g-GPA on G_1 is then passed further upwards to G_2, and so forth. At the kth algorithmic iteration, the Mu-GPA algorithm is working with QAM group G_k and tries to allocate the sum of the excess power missed by the UPA algorithm of that group as well as the LO power resulting from the application of the g-GPA algorithm to the previous group G_{k-1}, i.e., $P_k^{\mathrm{ex,u}} + P_{k-1}^{\mathrm{LO}}$ (cf. Fig. 5.4). Finally, the LO power resulting from the QAM group G_{K-1} is added to the excess power of the K^{th} QAM group $P_K^{\mathrm{ex,u}}$ to end up with a final LO power

$$P_{\mathrm{Mu-g}}^{\mathrm{LO}} = P_{K-1}^{\mathrm{LO}}|_{\mathrm{Mu-g}} + P_K^{\mathrm{ex,u}}, \tag{5.13}$$

where $P_{K-1}^{\mathrm{LO}}|_{\mathrm{Mu-g}}$ is the final LO power of the iterative structure of the Mu-GPA algorithm as demonstrated by the flowchart in Fig. 5.5. To distinguish from the individual LO powers of the g-GPA algorithm P_k^{LO} in (5.11), the subscript $|_{\mathrm{Mu-g}}$ is used to declare the Mu-GPA algorithm. The overall number of allocated bits

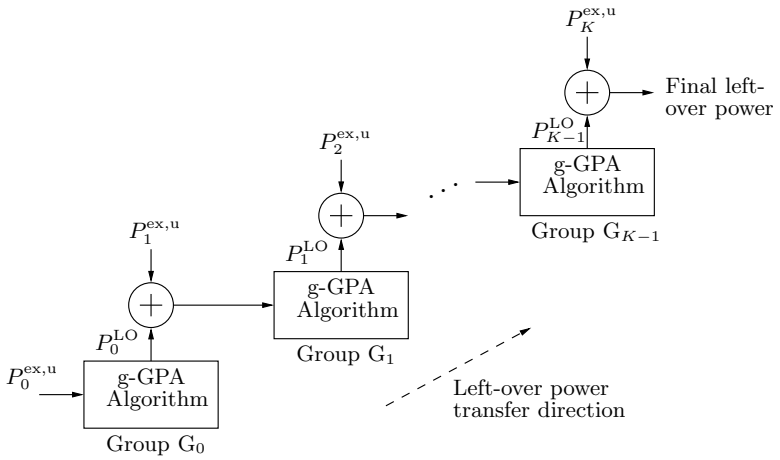

Figure 5.4: Algorithmic arrangements for the Mu-GPA algorithm with final left-over power in (5.13).

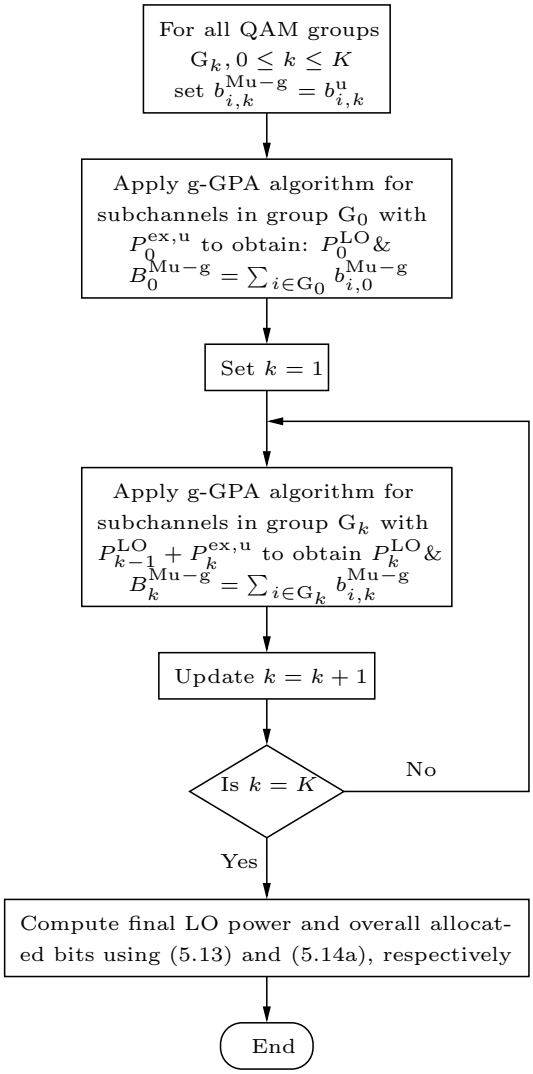

Figure 5.5: Flowchart of the Mu-GPA algorithm.

and the amount of used power for Mu-GPA algorithm are, respectively,

$$B_{\mathrm{Mu-g}} = \sum_{k=0}^{K-1} B_k^{\mathrm{Mu-g}} + B_K^{\mathrm{u}} \tag{5.14a}$$

$$P_{\mathrm{used}}^{\mathrm{Mu-g}} = P_{\mathrm{budget}} - P_{\mathrm{Mu-g}}^{\mathrm{LO}}\,. \tag{5.14b}$$

Note that this final LO power $P_{\mathrm{Mu-g}}^{\mathrm{LO}}$ is of course less than $P_{\mathrm{g}}^{\mathrm{LO}}$ of the g-GPA algorithm as

$$P_{K-1}^{\mathrm{LO}}|_{\mathrm{Mu-g}} \leq \sum_{k=0}^{K-1} P_k^{\mathrm{LO}} \tag{5.15}$$

which emphasises an improvement in bit allocation of the Mu-GPA over that obtained by the g-GPA algorithm.

5.5 Power Moving-down GPA (Md-GPA)

A second algorithm is proposed to exploit the residual power P_k^{LO} of each QAM group of the g-GPA algorithm but in a possibly reverse direction compared to the Mu-GPA algorithm. Starting from the highest-indexed QAM group G_{K-1} downwards to the lowest-indexed QAM group G_0, the Md-GPA algorithm, similar to the Mu-GPA algorithm, tries to improve the bit allocation by efficiently utilising $P_k^{\mathrm{LO}}, K-1 \geq k \geq 1$ plus the excess power $P_K^{\mathrm{ex,u}}$. These procedures are illustrated in Fig. 5.6 which show the direction of the LO power flow. Proceeding downwards, at the kth stage the Md-GPA scheme applies the g-GPA algorithm for the available power that comprises both the excess power missed by the UPA algorithm of the previous QAM group (G_{k+1} in this case) and the LO power of the previous stage, i.e. $P_{k+1}^{\mathrm{ex,u}} + P_{k+1}^{\mathrm{LO}}$, (cf. Fig. 5.6). Therefore, the excess power of the QAM group under consideration along with its LO power is not utilised within this group but is transferred to the next working group. This will finally result in a LO power of

$$P_{\mathrm{Md-g}}^{\mathrm{LO}} = P_0^{\mathrm{LO}}|_{\mathrm{Md-g}} + P_0^{\mathrm{ex,u}}\,. \tag{5.16}$$

The subscript $|_{\mathrm{Md-g}}$ is used, as in Section 5.4, to emphasis the LO power of the Md-GPA algorithm. Again the final LO power $P_{\mathrm{Md-g}}^{\mathrm{LO}}$ is expected to be less than

$P_{\mathrm{g}}^{\mathrm{LO}}$ of the g-GPA algorithm, which can be signified by noting that

$$P_0^{\mathrm{LO}}|_{\mathrm{Md-g}} \ll \sum_{k=1}^{K-1} P_k^{\mathrm{LO}} + P_K^{\mathrm{ex,u}} \tag{5.17}$$

$$P_0^{\mathrm{ex,u}} \geq P_0^{\mathrm{LO}}\,. \tag{5.18}$$

Equation (5.17) demonstrates a straightforward advantage of using Md-GPA compared to g-GPA as all unallocated power terms of the g-GPA appearing in the r.h.s. of (5.17) are efficiently re-distributed under the Md-GPA algorithm. Most particularly $P_K^{\mathrm{ex,u}}$, which is entirely missed by the g-GPA, is allocated by the Md-GPA algorithm. This will prominently improve the bit allocation of this scheme especially for high SNR as will be discussed in Section 5.7. On the other hand the only power term that is unallocated by the Md-GPA is $P_0^{\mathrm{ex,u}}$ in (5.18) which is greater than P_0^{LO} of the g-GPA. By summing analogous sides of (5.17) and (5.18), the final LO powers of both Md-GPA and g-GPA algorithms respectively result. The flowchart of this algorithm is analogous to that of the Mu-GPA algorithm, and hence omitted here. The overall number of the allocated bits and the amount of used power are, respectively,

$$B_{\mathrm{Md-g}} = \sum_{k=0}^{K-1} B_k^{\mathrm{Md-g}} + B_K^{\mathrm{u}} \tag{5.19a}$$

$$P_{\mathrm{used}}^{\mathrm{Md-g}} = P_{\mathrm{budget}} - P_{\mathrm{Md-g}}^{\mathrm{LO}}\,. \tag{5.19b}$$

5.6 Computational Complexity Evaluation

In order to address the significance of the proposed power loading schemes in terms of simplicity compared to the full GPA algorithm, the computational complexity of both the g-GPA and GPA algorithms are evaluated. Instead of jointly applying the GPA algorithm across all subchannels which consequently requires high system complexity especially for large numbers of subchannels, the g-GPA algorithm only addresses a subset of subchannels within a specific QAM group at a time. With the aid of Fig. 5.3 it is obvious that the search step (1) of Table 4.2, which represents the complexity bottleneck of the GPA algorithm, has to include all subchannels N in every iteration regardless of initial subchannel ordering. This is because it is possible to find subchannels in lower QAM levels that require less power to upgrade than others in higher QAM levels as demonstrated in Section

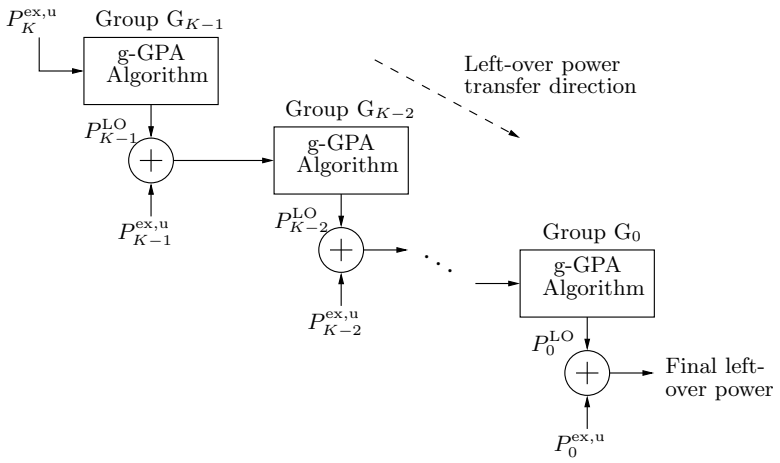

Figure 5.6: Algorithmic arrangements for the Md-GPA algorithm with final left-over power in (5.16).

5.3. Beyond the division of the QAM grouping concept, a further reduction in complexity can be achieved if subchannels are initially ordered by their gains CNR_i. In this case the search step (3) in Table 5.1 can be replaced by a simple incremental indexing.

Referring to Table 4.2 and Table 5.1, the computational complexities of both GPA and g-GPA algorithms are summarised in Table 5.2, whereby the number of operations is computed for each algorithm. We consider the cases where subchannel SNRs are either ordered prior to involving g-GPA, or where the ordering is left to any of the g-GPAs. Note that for the GPA algorithm, ordering of subchannels does not lead to any improvement in complexity as the search step (1) in the while loop has to include all subchannels. This is due to the fact that by relaxing the grouping concept it is possible to find subchannels in lower QAM levels that need less power to upgrade than others in higher QAM levels as highlighted in Section 5.3. Whereas in the case of the g-GPA algorithm, initial sorting of subchannels according to their CNR_i (see Fig. 5.2) is sufficient to avoid the repetitive search (sorting) step (3) of Table 5.1 as this algorithm is independently applied for the subchannels that are bounded by one QAM level only.

The quantities L_1 and L_2^k in Table 5.2 denote, respectively, the number of iterations of the while loops for the GPA (Table 4.2) and the g-GPA (Table 5.1) algorithms. Note that it is expected that $L_1 \geq L_2 = \sum_{k=0}^{K-1} L_2^k$ as $P^{\text{ex,u}}$ in (5.6) collected from all subchannels has to be re-distributed by the GPA algorithm, while $P_k^{\text{ex,u}}$ collected only from subchannels $i \in \text{G}_k$ is considered by the g-GPA algorithm.

Obviously, the number of subchannels that occupies QAM group G_k defined in (5.6) as N_k cannot be easily quantified as it depends on both the CNR_i, which

is a chi-squared distributed random variable, and the operating SNR. Therefore the complexity of the g-GPA algorithm is evaluated in a heuristic fashion. In the worst case and by assuming that subchannels are uniformly distributed across all QAM groups, i.e. $N_k = {}^{N}/_{K}$, the complexity of the g-GPA algorithm can be approximated as given in Table 5.2 which is lower than its GPA counterpart.

5.7 Numerical Results and Discussion

Sections 5.4 and 5.5 have shown that both Mu-GPA and Md-GPA algorithms work very similarly in utilising the power P_k^{LO} that remained unused by the g-GPA algorithm for all groups $k, 0 \leq k \leq K-1$. The two algorithms differ in the direction in which P_k^{LO} is transferred. Below we compare by simulations the bit allocation performance of the two algorithms with the UPA, GPA, and the g-GPA approaches. Two simulation sets of results are conducted to explore the achieved data throughput of the considered algorithms for the case of MIMO narrowband and OFDM-multicarrier systems.

5.7.1 MIMO Narrowband Case

The proposed loading schemes are tested for a 10×10 MIMO narrowband system to investigate bit loading performance. The entries of the channel matrix $\mathbf{H}$ are drawn from a complex Gaussian distribution with zero mean and unit variance, i.e., $h_{ij} \in \mathcal{CN}(0,1)$. Results presented below refer to ensemble averages across 10^4 different channel realisations for a target BER of $\mathcal{P}_b^{\mathrm{target}} = 10^{-3}$ and various levels of SNRs using square QAM modulation schemes $M_k = 2^{2k}, k = 1 \cdots K$ with $K = 4$ being the maximum permissible QAM level of constellation size, i.e., $M_K = 256$ which is equivalent to encoding $b^{\max} = 8$ bits per data symbol.

The total system data throughput is examined and shown in Fig. 5.7 for all proposed algorithms in addition to both UPA and standard GPA algorithms. It

Table 5.2: Computational analysis for both GPA and g-GPA algorithms.

algorithm	number of operations
GPA (order and no order)	$L_1(2N+7)+4N+1$
g-GPA (no order)	$\sum_{k=0}^{K-1} L_2^k(2N_k+4)+2N_k+2$ $\approx L_2(2\frac{N}{K}+4)+2\frac{N}{K}+2$
g-GPA (order)	$\sum_{k=0}^{K-1} L_2^k(N_k+5)+2N_k+2$ $\approx L_2(\frac{N}{K}+5)+2\frac{N}{K}+2$

is evident that UPA represents an inefficient way of bit loading since the performance is approximately 5 to 10 dB below other algorithms for normal operating SNR, and provide approximately half the throughput at 10 dB SNR.

Of the proposed low-complexity greedy algorithms, both Mu-GPA and Md-GPA algorithms outperform the g-GPA without the refinement stage to allocate residual power across QAM groups. Interestingly, Mu-GPA performs better at low SNR, while Md-GPA performs better at higher SNRs. This can be attributed, as discussed in Sections 5.4 and 5.5, to the fact that for low-to-medium SNRs $P_K^{\mathrm{ex,u}}$ (which is missed by the Mu-GPA) in this case will be relatively low and can be allocated without violating the constraint on the maximum QAM level M_K. In contrast, $P_0^{\mathrm{ex,u}}$ which is missed by the Md-GPA is most likely to be high, please see (5.6) and Fig. 5.2. For medium-to-high SNRs $P_K^{\mathrm{ex,u}} > P_0^{\mathrm{ex,u}}$ can be expected to be high, and then Md-GPA is advantageous in its bit allocation, as the maximum QAM level constraint is beginning to be felt and $P_K^{\mathrm{ex,u}}$ is fully utilised by the Md-GPA algorithm.

Finally, for very high SNRs most subchannels will appear in the highest QAM group G_K as their SNRs, γ_i in (4.9), exceed the highest QAM level γ_K^{QAM} in (5.3). As a result, the overall throughput of all different algorithms reaches its expected maximum of $10 \times b^{\max}$ bits/symbol.

The data throughput performance of the various algorithms can also be confirmed when considering the power utilisation. Fig. 5.8 shows the total transmit power budget and the levels of power allocation that are reached by the different algorithms. For Md-GPA and Mu-GPA it can be noted that within their respective superiority regions both are very close to the performance of the standard GPA which demonstrate the efficient utilisation of the LO power missed by the g-GPA algorithm. Nevertheless, at high SNR both g-GPA and Mu-GPA algorithms behaves like the UPA algorithm due to the increase of $P_K^{\mathrm{ex,u}}$ which is missed by both of them and therefore deteriorates their performances. Note that the minimum theoretical transmit power according to (5.3) that is required to load all subchannels with $b^{\max}$ averaged over all 10^4 channel realisations is an approximate SNR of 49.6 dB as shown in Fig. 5.8

5.7.2 OFDM-Multicarrier Case

Another simulation set is conducted to examine the performance of our proposed greedy power allocation schemes for an OFDM-multicarrier system. Here

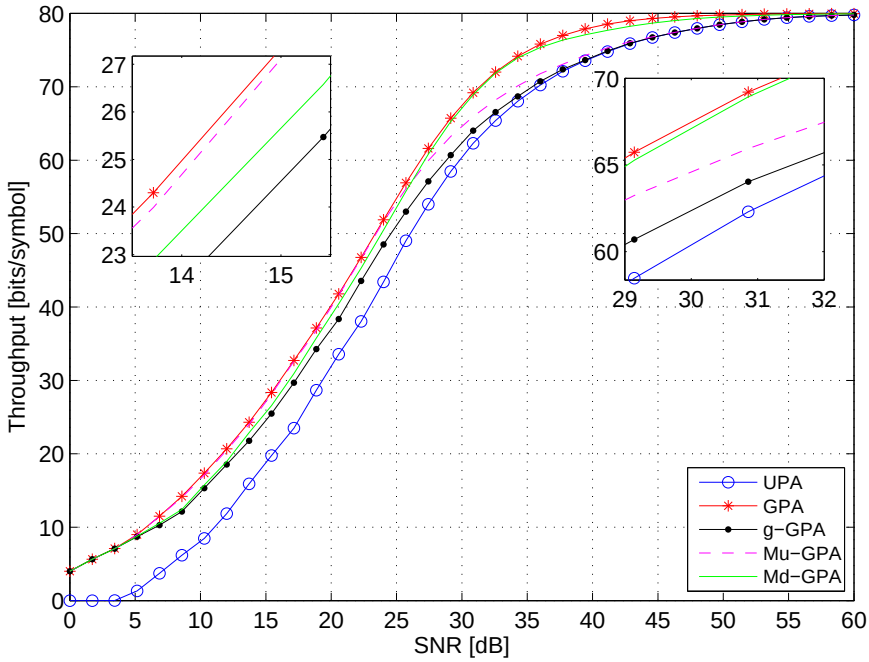

Figure 5.7: Overall throughput for a 10×10 MIMO system with a target BER of $\mathcal{P}_b^{\text{target}} = 10^{-3}$.

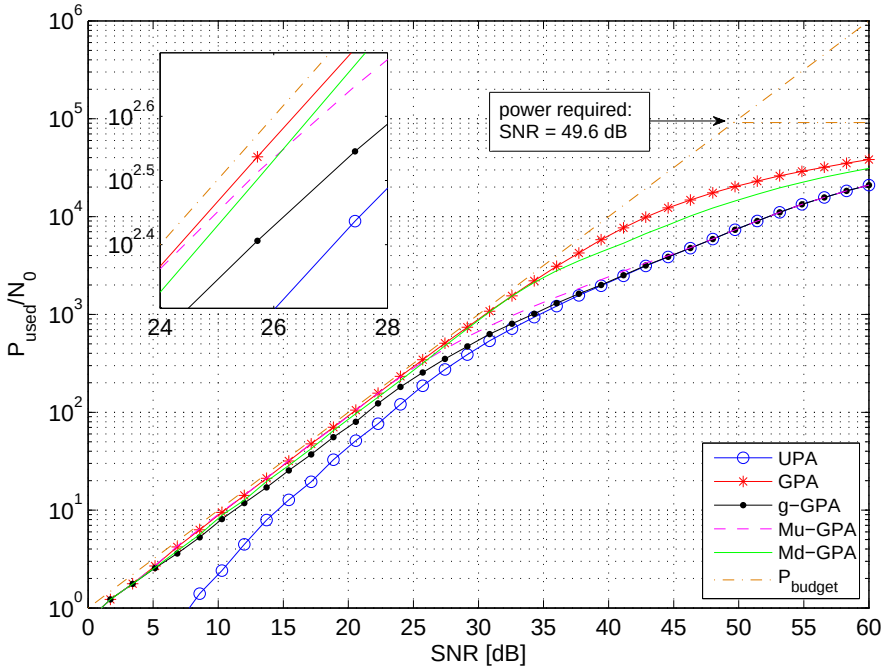

Figure 5.8: Total allocated power by the considered algorithms for a 10×10 MIMO system to achieve their respective throughput in Fig. 5.7 and a target BER of $\mathcal{P}_b^{\text{target}} = 10^{-3}$.

we assume, for simplicity, a SISO-OFDM[3] system, whereby the ISI channel is characterised by an impulse response of order $Q = 5$ organised in a vector $\mathbf{h} = [h_0 \cdots h_Q] \in \mathbb{C}^{Q+1}$ with entries drawn from an independent complex Gaussian process with zero mean and unit variance. Results are considered for a 32-subcarrier system averaged over 10^4 different channel realisations for a target BER of $\mathcal{P}_b^{\text{target}} = 10^{-3}$ and varying SNR using the same QAM modulation schemes of constellation orders $M_k = 2^k, k = 1 \cdots 6$, i.e. rectangular QAM modulations with $b^{\max} = 6$ bits. The total system throughput is shown in Fig. 5.9 for all proposed algorithms in addition to both UPA and standard GPA algorithms. It is clearly shown that both Mu-GPA and Md-GPA algorithms perform very close to the GPA algorithm (with throughput loss ≤ 4 bits) within their SNR favourable regions, which swap approximately at SNR = 25.8 dB. Fig. 5.10 again shows the power usage of all algorithms that is required to reach their respective throughput of Fig. 5.9. Compared to the optimum GPA, the Md-GPA algorithm demonstrates very close power utilisation with some inferior performance due to missing to allocate the final LO power in (5.16). At higher SNRs, both Mu-GPA and g-GPA algorithms converge to the power usage performance of the UPA algorithm as $P_K^{\text{ex,u}}$ dominates other $P_k^{\text{ex,u}}, 0 \leq k \leq K-1$ and therefore only Md-GPA algorithm is advantageous in this region. Note that, similar to Fig. 5.8 the minimum theoretical transmit power according to (4.8) that is required to load all subcarriers with $b^{\max}$ is an approximate SNR of 41.6 dB as shown in Fig. 5.10.

5.7.3 Computational Complexity Results

In order to evaluate the computational complexity of the proposed power allocation schemes compared to the standard GPA algorithm, the number of algorithmic operations presented in the complexity analysis in Section 5.6 is tested and compared for both g-GPA and GPA algorithms using a 1024-subcarrier system. Table 5.3 gives the simulation results of the number of operations (averaged over 10^4 channel instances) for both "no order" and "order" cases of the g-GPA algorithm along with the GPA algorithm at three different values of SNR of 15, 25 and 35 dB. It is clearly noted that $L_2 = \sum_{k=0}^{K-1} L_2^k$ is less than L_1 for all SNR values which validates the complexity analysis of Section 5.6. Furthermore, a reduction of almost half the number of operations can be gained by ordering subchannels of the g-GPA algorithm which results in an overall reduction factor compared to the full GPA algorithm of approximately 2, 3, and an order of magnitude for SNR

[3]The extension to the MIMO-OFDM case is straightforward.

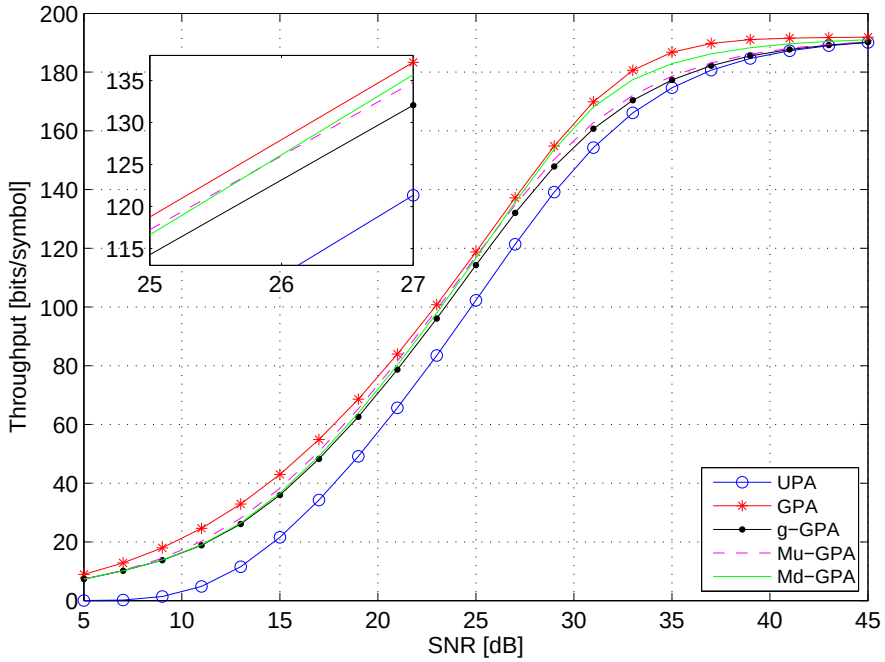

Figure 5.9: Overall throughput for a 32-subcarrier system with a target BER of $\mathcal{P}_b^{\text{target}} = 10^{-3}$.

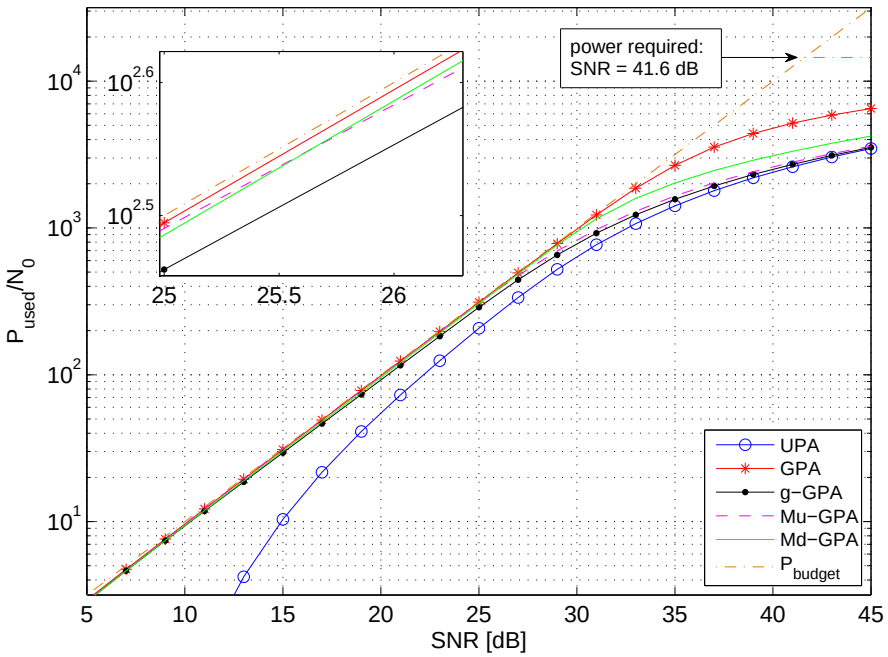

Figure 5.10: Total allocated power by the considered algorithms for a 32-subcarrier system to achieve their respective throughput in Fig. 5.9 and a target BER of $\mathcal{P}_b^{\text{target}} = 10^{-3}$.

values of 15 dB, 25 dB, and 35 dB, respectively (cf. Table 5.3).

The complexity analysis can also be evaluated by investigating the computation time of both GPA and g-GPA algorithms. Fig. 5.11 shows the computation time against the number of subcarriers N for the g-GPA algorithm with both "no order" and "order" cases compared to the GPA algorithm. Two different SNR values of 15 dB and 35 dB that represent the approximate conditions of mobile and fixed wireless communications, respectively, are considered in this simulation. It is clear that the g-GPA algorithm has a higher computational efficiency in particular for large values of N and high SNRs, while the effect of subcarrier ordering is also evident as discussed in Section 5.6. Assuming a close correlation between the number of operations and their computation time, it is noted that at $N = 1024$ subcarriers these results coincide with that of Table 5.3. In a statistical fashion, Fig. 5.12 demonstrates the cumulative distribution function (CDF) of the computation time for both algorithms at the same SNR values which reveals the computational efficiency of the proposed g-GPA algorithm and its modified versions of both Mu-GPA and Md-GPA.

5.8 Conclusion

Power allocation to achieve maximum data throughput under constraints on the transmit power and the maximum QAM level has been discussed. The optimum solution is provided by the greedy power allocation algorithm (GPA), which operates across all subchannels but is computationally very expensive. Therefore, in this Chapter sub-optimal low-complexity alternatives have been explored. The common theme amongst the proposed algorithms is to restrict the GPA algorithm to subsets of subchannels, which are grouped according to the QAM level assigned to them in the uniform power allocation stage. In order to exploit excess (unused) power in each subset, two algorithms were created which carry left-over (LO) power forward into the next subset that is optimised by a local greedy algorithm. Two different schemes have been suggested, of which one moves the LO power upwards from the lowest to the highest subgroup, where in the high SNR case a limitation by the maximum defined QAM level can restrict the performance. A second scheme moves the power from the highest towards lower subgroups, whereby at low SNR the channel quality in the lowest subgroups may not be such that it can be lifted across the lowest QAM level, and hence no bits may be loaded with the excess power. However, in general both algorithms perform very close to the GPA in their respective domains of preferred operation,

Table 5.3: Simulation results for the parametric analysis of the GPA and g-GPA algorithms given in Table 5.2 for a 1024-subcarrier system and different SNR values.

SNR	15 dB		25 dB		35 dB	
GPA						
L_1	112.5		600.6		621.2	
number of operations$\times 10^3$	**235.4**		**1,238.3**		**1,280.6**	
g-GPA						
QAM-groups:	N_k	L_2^k	N_k	L_2^k	N_k	L_2^k
G_0	1,024	103.2	946.8	425.1	234.7	140.6
G_1	0	0	71.5	23.1	178.2	89.6
G_2	0	0	5.7	0.89	293.0	140.2
G_3	0	0	0	0	229.5	96.7
G_4	0	0	0	0	80.9	27.0
G_5	0	0	0	0	7.7	1.55
$L_2 = \sum_{k=0}^{K-1} L_2^k$	-	103.2	-	449.1	-	495.7
number of operations$\times 10^3$ (no order)	**213.8**		**812.2**		**232.8**	
number of operations$\times 10^3$ (order)	**108.3**		**408.5**		**118.9**	

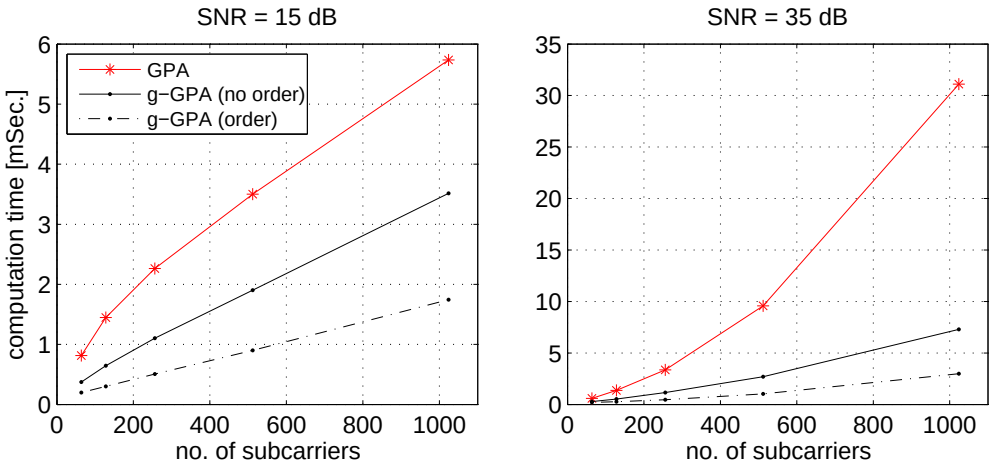

Figure 5.11: Average computation time comparison between g-GPA and GPA algorithms for $\mathcal{P}_{\mathrm{b}}^{\mathrm{target}} = 10^{-3}$ and varying N-subcarrier system at different SNR applications for (left) 15 dB SNR and (right) 35 dB SNR.

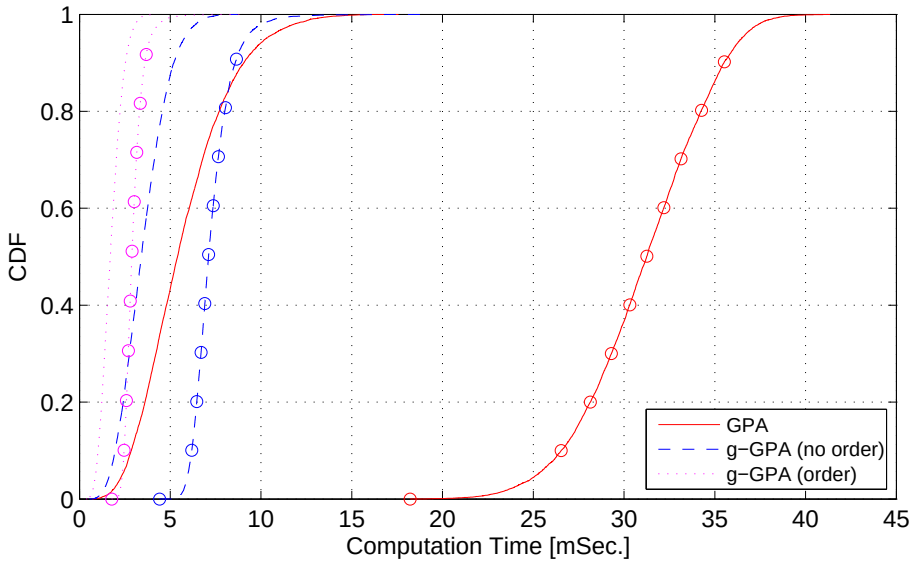

Figure 5.12: Cumulative distribution function of the computation time for a 1024-subcarrier system and $\mathcal{P}_{\mathrm{b}}^{\mathrm{target}} = 10^{-3}$ at SNR values of 15 dB (without circles) and 35 dB (with circles).

thus permitting power allocation close to the performance of the GPA at a much reduced complexity.

Chapter 6

Conclusions and Future Work

This chapter first summarises the research reported in this thesis in Section 6.1, while Section 6.2 provides ideas for potential future directions.

6.1 Thesis Summary

This thesis has been concerned with transceiver components for broadband MIMO communications. In combination with a decoupling of the broadband MIMO system by means of a BSVD, non-linear precoding and equalisation methods have been investigated. Further, a number of bit and power allocation algorithms have been surveyed in order to exploit the subchannels in a multichannel transmission scenario such as the one arising from a combined BSVD and precoding/equalisation approach.

In Chapter 2, linear precoding and equalisation methods for narrowband and broadband MIMO communications channels have been reviewed. We have also introduced the BSVD approach suggested by McWhirter *et al.* [19] to decouple a broadband MIMO system into a series of spectrally majorised SISO subchannels, which can avoid the spectral inefficiencies of block-based transceivers.

In Chapter 3, we have first proposed a suboptimum spatial THP precoding ordering scheme to deal with flat-fading MIMO channels. The performance of this scheme can achieve an SNR gain of $\approx 3\,\text{dB}$ and only $0.5\,\text{dB}$ loss in SNR at BER $= 10^{-2}$ compared, respectively, to a THP system without ordering and the optimised ordering provided by the V-BLAST algorithm. The advantage of this scheme lies in the significant reduction in computational complexity achieved over the algorithm of V-BLAST ordering.

Secondly in Chapter 3, dealing with the broadband MIMO channels, a novel non-linear precoding and equalisation system has been proposed. This approach is

accomplished in two steps: firstly, the recently developed BSVD algorithm [19] is applied to decouple the broadband MIMO channel into a number of independent frequency selective and spectrally majorised (i.e with ordered gains) SISO subchannels, thus cancelling CCI. However, the SISO subchannels are dispersive and therefore incur ISI which we mitigate non-linearly using either DFE or THP systems in the second step. The advantage of the THP system over the DFE one is the absence of propagation errors. Moreover, in order to efficiently utilise the spectral majorisation of the resulting SISO subchannels, a heuristic bit loading has been applied to match the subchannels qualities and achieve better data throughputs. Benchmarked against a state-of-the-art MIMO broadband THP scheme, our proposed method has been shown that better BER performance can be achieved, specially for higher data throughput targets, under the constraints of identical data throughput and transmit power.

The decoupling achieved by the BSVD is not ideal due to the iterative nature of the algorithm and needs to be approximated by a fixed number of iterations (NoI). The impact of this NoI on the overall performance is twofold. Firstly, some of the energy is lost in the off-diagonal entries of the MIMO channel, secondly these non-zero entries increase the level of CCI and produce more detection errors as a result. In order to rely on the BSVD algorithm with a reasonable complexity, the NoI has been investigated in the remainder of Chapter 3 leading to a significantly simplified BSVD version that can achieve performance very close to the idealised BSVD.

Further research in bit and power loading to optimise the achievable data throughput for systems with different subchannel/subcarrier gains, such as our proposed BSVD-THP model presented in Chapter 3, has been considered in Chapter 4. There, the design is constrained by a transmit power budget, a target BER, and a fixed number of permissible modulation orders. The optimum power allocation for discrete bit loading of such systems can be achieved using the greedy approach. Two greedy schemes are considered that can be described as greedy power allocation (GPA) and greedy bit allocation (GBA) algorithms. Both of these aim to maximise the sum-rate of a multichannel system, whereby either power or bit is allocated under the greedy algorithm for the same set of constrained parameters. A fair comparison between the two algorithms is provided and underpinned by simulation results which show the superiority of the GPA over the GBA and both of them achieve higher data throughput than the non-adaptive uniform power allocation (UPA) algorithm.

Since both GPA and UPA algorithms cannot completely use the power bud-

get due to the fixed modulation orders, this excess power has been allocated in a second optimisation step to improve the actual mean BER as opposed to the value specified by the target BER. Two power redistribution algorithms are proposed with different design aspects, namely uniform power redistribution (UPR) and fairness-BER power redistribution (FPR). Analyses for both algorithms have been derived and numerically supported by simulations, which interestingly demonstrate reciprocal behaviour across both schemes when coupled with UPA and GPA algorithms.

The GPA scheme proposed in Chapter 4 is optimum in terms of the achieved data throughput and power conservation senses. However, this power allocation has been shown to be computationally very complex as in every single bit allocation iteration all subchannels/subcarriers have to be considered. For multicarrier systems with a very high number of subcarrier, this results in an unrealistic complexity.

In order to achieve a near-optimum data throughput but at a significantly reduced complexity, reduced-complexity GPA schemes have been proposed in Chapter 5. These schemes have been based on a subcarrier grouping concept, whereby all subcarriers are divided into subgroups bounded by the minimum QAM modulation SNR levels that are required to achieve the target BER. Therefore starting with the UPA algorithm, all subcarriers can be categorised into these QAM groups according to their SNRs. Thereafter, the GPA is independently applied for each local subgroup aiming to maximise the achieved data throughput of that group which results in a left-over (LO) power for each subgroup.

These LO powers are further redistributed with two different scenarios, whereby LO powers are utilised by permitting power moving up or down w.r.t. QAM groups, leading to two different versions of the grouped GPA algorithm denoted, respectively, by Mu-GPA and Md-GPA algorithms. Interestingly, the two algorithms perform very close to the standard GPA algorithm, however, in two distinct SNR regions — for the Mu-GPA at low SNR and for the Md-GPA at high SNR. Computational complexity of the proposed grouped GPA scheme has been analytically evaluated and compared to that required by the GPA algorithm. Numerical results have shown that a significant reduction in gain of an order of magnitude can be reached for large number of subcarriers and at high SNR level with minimal degradation in achieved data throughput provided that the correct algorithmic version (Mu-GPA or Md-GPA) is chosen according to the SNR situation.

6.2 Future Work

A number of research topics appear promising for future work, but are beyond the scope of this thesis. A number of these ideas are briefly elaborated below.

BSVD-THP with adaptive bit and/or power loading.
The proposed BSVD-THP scheme in Chapter 3 assumes a heuristic bit loading to utilise the inherent spectral majorisation property of the BSVD algorithm. However, we believe that if this scheme is combined with an adaptive bit and/or power loading such as given in Chapter 4, further performance improvements can be achieved. Moreover, the optimality advantages of the GPA and GBA algorithms in data throughput maximisation for a specified target BER can also be directed towards minimising the mean BER for a fixed target data rate for the proposed BSVD-THP scheme.

Joint bit and power loading approach.
Referring to both GPA and GBA algorithms addressed in Chapter 4, it is noted that either bit or power is selected as the greedy parameter to be controlled. The results of GPA and GBA do always completely achieve the desired target BER or expending the power budget. Therefore a power redistribution algorithm appears useful, as proposed in Chapter 4. A more flexible design could be created, if these parameters are jointly optimised such that switching between both bit and power allocation schemes can be accomplished to solve the designated optimisation problem.

Reduced GPA scheme with a proper algorithmic selection.
It has been shown in Chapter 5 that both algorithmic versions of the g-GPA algorithm with power refinement step perform closely to the full GPA algorithm, but exhibit this characteristic in two separate SNR regions. For a real-world implementation, it is helpful to resort to only one algorithm leaving the selection between the two algorithmic versions blind to the operator or overall system. Therefore, a suitable threshold should be identified based on current propagation scenarios for MIMO communication channel to assist in the algorithm selection. This can be achieved by considering the parameters of the transmit power budget, the CSI, and the target BER along with the permissible modulation orders.

List of Figures

List of Tables

References

[1] H. Boche, A. Bourdoux, J. R. Fonollosa, T. Kaiser, A. Molisch, and W. Utschick, "Smart Antennas: State of the Art," *IEEE Vehicular Technology Magazine*, vol. 1, no. 1, pp. 8–17, Mar. 2006.

[2] M. Haardt and Q. Spencer, "Smart Antennas for Wireless Communications beyond the Third Generation," *Computer Communications*, vol. 26, no. 1, pp. 41–45, Jan. 2003.

[3] A. Alexiou and M. Haardt, "Smart Antenna Technologies for Future Wireless Systems: Trends and Challenges," *IEEE Communications Magazine*, vol. 42, no. 9, pp. 90–97, Sep. 2004.

[4] G. Foschini and M. Gans, "On Limits of Wireless Communications in a Fading Environment when Using Multiple Antennas," *Wireless Personal Communications*, vol. 6, no. 3, pp. 311–335, Mar. 1998.

[5] I. E. Telatar, "Capacity of Multi-antenna Gaussian Channels," *European Transactions on Telecommunications*, vol. 10, no. 6, pp. 585–595, Dec. 1999.

[6] G. J. Foschini, G. D. Golden, R. A. Valenzuela, and P. W. Wolniansky, "Simplified Processing for High Spectral Efficiency Wireless Communication Employing Multi-Element Arrays," *IEEE Journal on Selected Areas in Communications*, vol. 17, no. 11, pp. 1841–1852, Nov. 1999.

[7] G. Golden, C. Foschini, R. Valenzuela, and P. Wolniansky, "Detection Algorithm and Initial Laboratory Results Using V-Blast Space-Time Communication Architecture," *IEEE Electronics Letters*, vol. 35, no. 1, pp. 14–16, Jan. 1999.

[8] G. B. Giannakis, Z. Liu, X. Ma, and S. Zhou, *Space-Time Coding for Broadband Wireless Communications*. John Wiley & Sons, Inc., 2007.

[9] N. Eltayeb, "Space-time coding for broadband point-to-point and collabrative wireless communications," Ph.D. dissertation, Lougborough University, 2009.

[10] A. Scaglione, S. Barbarossa, and G. B. Giannakis, "Filterbank Transceivers Optimizing Information Rate in Block Transmissions over Dispersive Channels," *IEEE Transactions on Information Theory*, vol. 45, no. 3, pp. 1019–1032, Apr. 1999.

[11] A. Scaglione, P. Stoica, S. Barbarossa, G. B. Giannakis, and H. Sampath, "Optimal Designs for Space-Time Linear Precoders and Decoders," *IEEE Transactions on Signal Processing*, vol. 50, no. 5, pp. 1051–1064, May 2002.

[12] C.-C. J. Kuo, S.-H. Tsai, L. Tadjpour, and Y.-H. Chang, *Precoding Techniques for Digital Communication Systems*. Springer, 2008.

[13] R. F. Fischer and J. B. Huber, "Equalization Strategies for Transmission over Space and Time," *Electronik und Informationstechnik*, vol. 6, pp. 187–195, 2005.

[14] A. Lozano and C. Papadias, "Layered Space-Time Receivers for Frequency-Selective Wireless Channels," *IEEE Transactions on Communications*, vol. 50, no. 1, pp. 65–73, Jan. 2002.

[15] L.-U. Choi and R. D. Murch, "A Pre-BLAST-DFE Technique for the Downlink of Frequency-Selective Fading MIMO Channels," *IEEE Transactions on Communications*, vol. 52, no. 5, pp. 737–743, May 2004.

[16] R. F. H. Fischer, C. Windpassinger, A. Lampe, and J. B. Huber, "Tomlinson-Harashima Precoding in Space-Time Transmission for Low-Rate Backward Channel," in *International Zurich Seminar on Broadband Communications*, 2002, pp. 7.1–7.6.

[17] M. Joham, D. A. Schmidt, J. Brehmer, and W. Utschick, "Finite-Length MMSE Tomlinson-Harashima Precoding for Frequency Selective Vector Channels," *IEEE Transactions on Signal Processing*, vol. 55, no. 6, pp. 3073–3088, Jun. 2007.

[18] M. Vu and A. Paulraj, "MIMO Wireless Linear Precoding," *IEEE Signal Processing Magazine*, vol. 24, no. 5, pp. 86–105, Sep. 2007.

[19] J. G. McWhirter, P. D. Baxter, T. Cooper, S. Redif, and J. Foster, "An EVD Algorithm for Para-Hermitian Polynomial Matrices," *IEEE Transactions on Signal Processing*, vol. 55, no. 5, pp. 2158–2169, May 2007.

[20] C. H. Ta and S. Weiss, "A design of precoding and equalisation for broadband MIMO systems," in *International Conf. on Digital Signal Pocessing*, 2007, pp. 571–574.

[21] C. H. Ta, "Precoding and Equalisation for Broadband MIMO Systems," Ph.D. dissertation, University of Strathclyde, 2008.

[22] M. Tomlinson, "New Automatic Equaliser Employing Modulo Arithmetic," *IEE Electronics Letters*, vol. 7, no. 5/6, pp. 138–139, Mar. 1971.

[23] H. Harashima and H. Miyakawa, "Matched-Transmission Technique for Channels with Intersymbol Interference," *IEEE Transactions on Communications*, vol. 20, pp. 774–780, Aug. 1972.

[24] W. Al-Hanafy and S. Weiss, "Efficient Tomlinson-Harashima Precoding Ordering using QR Decomposition," in *The 17th European Signal Processing Conference, EUSIPCO 2009*, Glasgow, UK, Aug. 2009, pp. 343–347.

[25] D. Wubben, R. Bohnke, J. Rinas, V. Kuhn, and K. Kanimeyer, "Efficient Algorithm for Decoding Layered Space-Time Codes," *Electronics Letters*, vol. 37, pp. 1348–1350, Oct. 2001.

[26] W. Al-Hanafy, A. P. Millar, C. H. Ta, and S. Weiss, "Broadband SVD and non-linear precoding applied to broadband MIMO channels," in *42nd Asilomar Conference on Signals, Systems and Computers, ACSSC 2008*, Pacific Grove, CA, USA, Oct. 2008, pp. 2053–2057.

[27] W. Al-Hanafy and S. Weiss, "Comparison of precoding methods for broadband MIMO systems," in *3rd IEEE International Workshop on Computational Advances in Multi-Sensor Adaptive Processing, CAMSAP 2009*, Dec. 2009, pp. 388 –391.

[28] ——, "Trade-off between Complexity and BER Performance of a Polynomial SVD-Based Broadband MIMO Transceiver," in *27th National Radio Science Conference, NRSC 2010*, Menouf, Egypt, Mar. 2010.

[29] ——, "Sum-Rate Maximisation Comparison using Incremental Approaches with Different Constraints," in *The Third Mosharaka International Conference on Communications, Computers and Applications, MIC-CCA 2009*, Amman, Jordan, Oct. 2009.

[30] W. Al-Hanafy, M. N. Hussin, and S. Weiss, "Incremental Rate Maximisation Power Loading with BER Improvements," in *18th European Signal Processing Conference, EUSIPCO 2010*, Aalborg, Denmark, Aug. 2010, pp. 382–386.

[31] W. Al-Hanafy and S. Weiss, "A New Low-Cost Discrete Bit Loading using Greedy Power Allocation," in *The Third Mosharaka International Conference on Communications, Computers and Applications, MIC-CCA 2009*, Amman, Jordan, Oct. 2009.

[32] ——, "Greedy Power Allocation for Multicarrier Systems with Reduced Complexity," in *27th National Radio Science Conference, NRSC 2010*, Menouf, Egypt, Mar. 2010.

[33] ——, "Reduced Complexity Schemes to Greedy Power Allocation for Multicarrier Systems," in *18th International Conference on Microwave, Radar and Wireless Communications, MIKON 2010*, Vilnius, Lithuania, Jun. 2010.

[34] U. Reimers, "DVB-The Family of International Standards for Digital Video Broadcasting," *Proceedings of the IEEE*, vol. 94, no. 1, pp. 173 –182, Jan. 2006.

[35] U. Ladebusch and C. Liss, "Terrestrial DVB (DVB-T): A Broadcast Technology for Stationary Portable and Mobile Use," *Proceedings of the IEEE*, vol. 94, no. 1, pp. 183 –193, Jan. 2006.

[36] G. Faria, J. Henriksson, E. Stare, and P. Talmola, "DVB-H: Digital Broadcast Services to Handheld Devices," *Proceedings of the IEEE*, vol. 94, no. 1, pp. 194 –209, Jan. 2006.

[37] C.-W. Yu and H.-P. Ma, "A Low Complexity Scalable MIMO Detector," in *IWCMC 06*, Vancouver, British Columbia, Canada, Jul. 2006, pp. 605–610.

[38] M. Noda, M. Muraguchi, T. G. Khanh, K. Sakaguchi, and K. Araki, "Eigenmode Tomlinson-Harashima Precoding for Multi-Antenna Multi-User

MIMO Broadcast Channel," in *6th International Conference on Information, Communications & Signal Processing*, Dec. 2007, pp. 1–5.

[39] K. Kusume, M. Joham, W. Utschick, and G. Bauch, "Efficient Tomlinson-Harashima Precoding for Spatial Multiplexing on Flat MIMO Channel," in *IEEE International Conference on Communications*, vol. 3, May 2005, pp. 2021–2025.

[40] M. Huang, X. Zhang, S. Zhou, and J. Wang, "Tomlinson-Harashima Precoding in Multiuser MIMO Systems with Imperfect Channel State Information," in *IEEE Global Telecommunications Conference, GLOBECOM 07*, Washington, DC,, Nov. 2007, pp. 2806–2810.

[41] R. Bohnke, D. Wubben, V. Kuhn, and K.-D. Kammeyer, "Reduced Complexity MMSE Detection for BLAST Architectures," in *IEEE Global Telecommunications Conference, GLOBECOM '03*, vol. 4, Dec. 2003, pp. 2258–2262.

[42] A. Benjebbour, H. Murata, and S. Yoshida, "Comparison of Ordered Successive Receivers for Space-Time Transmission," in *IEEE VTS 54th Vehicular Technology Conference, VTC 2001 Fall*, vol. 4, Atlantic City, NJ, USA, 2001, pp. 2053–2057.

[43] C. Stierstorfer and R. F. H. Fischer, "Lattice-Reduction-Aided Tomlinson-Harashima Precoding for Point-to-Multipoint Transmission," *International Journal of Electronics and Communications, AEU*, vol. 60, no. 4, pp. 328–330, Apr. 2006.

[44] J. Benesty, Y. A. Huang, and J. Chen, "A Fast Recursive Algorithm for Optimum Sequential Signal Detection in a BLAST System," *IEEE Transactions on Signal Processing*, vol. 51, no. 7, pp. 1722–1730, Jul. 2003.

[45] R. Fischer, "MMSE DFE for high-rate MIMO transmission over channels with ISI," in *Fifth IEE International Conference on 3G Mobile Communication Technologies*, 2004.

[46] J. Liu and W. A. Kizymien, "Improved Tomlinson-Harashima Precoding for the Downlink of Multi-User MIMO Systems," *Canadian Journal of Electrical and Computer Engineering*, vol. 32, no. 3, pp. 133–144, 2007.

[47] C. Peel, Q. Spencer, A. L. Swindlehurst, and B. Hochwald, "Downlink Transmit Beamforming in Multi-User MIMO Systems," in *IEEE Workshop on Sensor Array and Multichannel Signal Processing*, 2004, pp. 43–51.

[48] M. Joham, W. Utschick, and J. A. Nossek, "Linear Transmit Processing in MIMO Communications Systems," *IEEE Transactions on Signal Processing*, vol. 53, no. 8, pp. 2700–2712, Aug. 2005.

[49] S. Lin, W. W. L. Ho, and Y.-C. Liang, "Block-Diagonal Geometric Mean Decomposition (BD-GMD) for Multiuser MIMO Broadcast Channels," in *The 17th Annual IEEE International Symposium on Personal, Indoor and Mobile Radio Communications (PIMRC 06)*, Sep. 2006, pp. 1–5.

[50] R. Fischer, C. Windpassinger, A. Lampe, and J. Huber, "Space-Time Transmission using Tomlinson-Harashima Precoding," in *4th International ITG Conference on Source and Channel Coding, Berlin*, Jan. 2002.

[51] K. Kusume, M. Joham, W. Utschick, and G. Bauch, "Cholesky Factorization With Symmetric Permutation Applied to Detecting and Precoding Spatially Multiplexed Data Streams," *IEEE Transactions on Signal Processing*, vol. 55, no. 6, pp. 3089–3103, Jun. 2007.

[52] C.-B. Chae, D. Mazzarese, and R. W. H. Jr., "Coordinated Beamforming for Multiuser MIMO Systems with Limited Feedforward," in *Fortieth Asilomar Conference on Signals, Systems and Computers, ACSSC 06*, 2006, pp. 1511–1515.

[53] M. Joham, J. Brehmer, A. Voulgarelis, and W. Utschick, "Multiuser Spatio-Temporal Tomlinson-Harashima Precoding for Frequency Selective Vector Channels," in *8th ITG Workshop on Smart Antennas, WSA 2004*, Munich, Germany, Mar. 2004, pp. 208–215.

[54] M. Joham, J. Brehmer, and W. Utschick, "MMSE Approaches to Multiuser Spatio-Temporal Tomlinson-Harashima Precoding," in *Proc. ITG SCC 04*, Jan. 2004, pp. 387–394.

[55] A. Scaglione, G. B. Giannakis, and S. Barbarossa, "Redundant Filterbank Precoders and Equalizers Part I: Unification and Optimal Designs," *IEEE Transactions on Signal Processing*, vol. 47, no. 7, pp. 1988–2005, Jul. 1999.

[56] G. Stuber, J. Barry, S. McLaughlin, Y. Li, M. Ingram, and T. Pratt, "Broadband MIMO-OFDM wireless communications," *Proceedings of the IEEE*, vol. 92, no. 2, pp. 271–294, Feb. 2004.

[57] A. van Zelst and T. Schenk, "Implementation of a MIMO OFDM-based wireless LAN system," *Signal Processing, IEEE Transactions on*, vol. 52, no. 2, pp. 483–494, Feb. 2004.

[58] S. D'Alessandro, A. M. Tonello, and L. Lampe, "Bit-Loading Algorithms for OFDM with Adaptive Cyclic Prefix Length in PLC Channels," in *The 13th IEEE International Symposium on Power Line Communications and its Applications (ISPLC)*, Dresden, Germany, 2009, pp. 177–181.

[59] W. Martins and P. Diniz, "Block-Based Transceivers With Minimum Redundancy," *Signal Processing, IEEE Transactions on*, vol. 58, no. 3, pp. 1321 –1333, Mar. 2010.

[60] A. A. M. Saleh and R. Valenzuela, "A Statistical Model for Indoor Multipath Propagation," *IEEE Journal on Selected Areas in Communications*, vol. 5, no. 2, pp. 128–137, 1987.

[61] J. Foster, J. McWhirter, and J. Chambers, "Limiting the order of polynomial matrices within the sbr-2 algorithm," in *IMA International Conference on Mathematics in Signal Processing*, Cirencester, 2006.

[62] C. H. Ta and S. Weiss, "Shortening the Order of Paraunitary Matrices in SBR2 Algorithm," in *6th International Conference on Information, Communications & Signal Processing*, Singapore, Dec. 2007, pp. 1–5.

[63] J. G. Proakis, *Digital Communications*, 4, Ed. New York: McGraw-Hill, 2001.

[64] G. K. Psaltopoulos, M. Joham, and W. Utschick, "Generalized MMSE Detection Techniques for Multipoint-to-Point Systems," in *IEEE Global Telecommunications Conference, GLOBECOM 06*, San Francisco, CA, USA, Nov. 2006, pp. 1–5.

[65] J. Jalden and B. Ottersten, "On the complexity of sphere decoding in digital communications," *IEEE Transactions on Signal Processing*, vol. 53, no. 4, pp. 1474–1484, Apr. 2005.

[66] K. Kusume, M. Joham, and W. Utschick, "MMSE block decision-feedback equalizer for spatial multiplexing with reduced complexity," in *Global Telecommunications Conference, 2004. GLOBECOM '04. IEEE*, vol. 4, 29 2004, pp. 2540 – 2544 Vol.4.

[67] J. M. Cioffi, G. P. Dudevoir, M. V. Eyuboglu, and J. G. David Fomey, "MMSE Decision-Feedback Equalizers and Coding–Part II: Coding Results," *IEEE Transactions on Communications*, vol. 43, no. 10, pp. 2595–2604, Oct. 1995.

[68] M. R. Gibbard and A. B. Sesay, "Asymmetric Signal Processing for Indoor Wireless LAN's," *IEEE Transactions on Vehicular Technology*, vol. 48, no. 6, pp. 2053–2064, Nov. 1999.

[69] R. F. H. Fischer and C. Siegl, "Inflated Lattice Precoding, Bias Compensation, and the Uplink/Downlink Duality: The Connection," *IEEE Communications Letters*, vol. 11, no. 2, pp. 185–187, Feb. 2007.

[70] J.-K. Zhang, A. Kavcic, and K. M. Wong, "Equal-Diagonal QR Decomposition and its Application to Precoder Design for Successive-Cancellation Detection," *IEEE Transactions on Information Theory*, vol. 51, no. 1, pp. 154–172, Jan. 2005.

[71] O. Simeone, Y. Bar-Ness, and U. Spagnolini, "Linear and Nonlinear Preequalization/Equalization for MIMO Systems with Long-Term Channel State Information at the Transmitter," *IEEE Transactions on Wireless Communications*, vol. 3, no. 2, pp. 373–378, Mar. 2004.

[72] N. Al-Dhahir, A. F. Naguib, and A. R. Calderbank, "Finite-Length MIMO Decision Feedback Equalization for Space-Time Block-Coded Signals over Multipath-Fading Channels," *IEEE Transactions on Vehicular Technology*, vol. 50, no. 4, pp. 1176–1182, Jul. 2001.

[73] G. J. Foschini, "Layered Space-Time Architecture for Wireless Communication in a Fading Environment When Using Multi-Element Antennas," *Bell Labs Technical Journal*, vol. Autumn, pp. 41–59, 1996.

[74] P. W. Wolniansky, G. J. Foschini, G. D. Golden, and R. A. Valenzuela, "V-BLAST: An Architecture for Realizing Very High Data Rates Over the Rich-Scattering Wireless Channel," in *International Symposium on Signals, Systems, and Electronics, ISSSE 98*, 1998, pp. 295–300.

[75] G. Ginis and J. M. Cioffi, "On the Relation Between V-BLAST and the GDFE," *IEEE Communications Letters*, vol. 5, no. 9, pp. 364–366, Sep. 2001.

[76] Y. Li and Z.-Q. Luo, "Parallel Detection for V-BLAST System," in *IEEE International Conference on Communications, ICC 2002*, vol. 1, NY, USA, 2002, pp. 340–344.

[77] S. Baro, G. Bauch, A. Pavlic, and A. Semmler, "Improving BLAST Performance using Space-Time Block Codes and Turbo Decoding," in *IEEE Proceedings of Globecom 2000*, San Francisco, USA, Nov. 2000, pp. 1067–1071.

[78] F. Sobhanmanesh and S. Nooshabadi, "A Robust QR-Based Detector for V-Blast and its Efficient Hardware Implementation," in *IEEE Proceedings of International Symposium on Intelligent Signal Processing and Communication Systems, ISPACS*, Nov. 2004, pp. 482– 485.

[79] B. Hassibi, "An efficient square-root algorithm for BLAST," in *IEEE International Conference on Acoustics, Speech, and Signal Processing, ICASSP'00*, vol. 2, 2000, pp. II737–II740.

[80] K. A.-M. M. O. Damen and S. Burykh, "Iterative QR Detection for BLAST," *Wireless Personal Communications*, vol. 19, no. 3, pp. 179–191, Dec. 2001.

[81] C.-Y. Chen and P. P. Vaidyanathan, "Precoded V-BLAST for ISI MIMO channels," in *IEEE International Symposium on Circuits and Systems, ISCAS 2006*, May 2006, pp. 1143–1146.

[82] C. Windpassinger, T. Vencel, and R. Fischer, "Optimising MIMO DFE for Systems with Spatial Loading," *IEEE Electronics Letters*, vol. 38, no. 24, pp. 1591–1593, Nov. 2002.

[83] M. H. M. Costa, "Writing on Dirty Paper," *IEEE Transaction Information Theory*, vol. 29, pp. 439–441, May 1983.

[84] C. B. Peel, "On "Dirty-Paper Coding"," *IEEE Signal Processing Magazine*, vol. 20, no. 3, pp. 112–113, May 2003.

[85] H. Weingarten, Y. Steinberg, and S. Shamai, "The Capacity Region of the Gaussian Multiple-Input Multiple-Output Broadcast Channel," *IEEE Transactions on Information Theory*, vol. 52, no. 9, pp. 3936–3964, Sept. 2006.

[86] R. F. H. Fischer and C. A. Windpassinger, "Improved MIMO Precoding for Decentralized Receivers Resembling Concepts from Lattice Reduction," in *IEEE Global Telecommunications Conference GLOBECOM 03*, vol. 4, Dec. 2003, pp. 1852–1856.

[87] C. Windpassinger, R. F. H. Fischer, T. Vencel, and J. B. Huber, "Precoding in Multiantenna and Multiuser Communications," *IEEE Transactions on Wireless Communications*, vol. 3, no. 4, pp. 1536–1276, Jul. 2004.

[88] R. F. H. Fischer, C. Stierstorfer, and J. B. Huber, "Precoding for Point-to-Multipoint Transmission over MIMO IS1 Channels," in *Int. Zurich Seminar on Communications, IZS*, Feb. 2004, pp. 208–211.

[89] F. Liu, L. Jiang, and C. He, "Lattice Reduction Aided MMSE Tomlinson-Harashima Precoding Based on VBLAST Algorithm for MIMO Systems," *Journal of Shanghai Jiaotong University (Science)*, vol. 13, no. 1, pp. 12–15, Feb. 2008.

[90] R. F. H. Fischer, *Precoding and Signal Shaping for Digital Transmission.* John Wiley & Sons, Inc., 2002.

[91] F. K. Lee, S. M. Emami, O. F. Oteri, and A. J. Paulraj, "Tomlinson-Harashima Precoding for MISO Frequency-Selective Broadcast Channels," in *Conference Record of the Thirty-Ninth Asilomar Conference on Signals, Systems and Computers*, 2005, pp. 1508–1513.

[92] E. Peh and Y.-C. Liang, "Power and Modulo Loss Tradeoff for Tomlinson-Harashima Precoding Applied to Geometric Mean Decomposition based MIMO Systems," in *The 18th Annual IEEE International Symposium on Personal, Indoor and Mobile Radio Communications (PIMRC 07)*, Athens, Sep. 2007, pp. 1–5.

[93] E. C. Y. Peh and Y.-C. Liang, "Power and Modulo Loss Tradeoff with Expanded Soft Demapper for LDPC Coded GMD-THP MIMO Systems," *IEEE Transactions on Wireless Communications*, vol. 8, no. 2, pp. 714–724, Feb. 2009.

[94] W. Shi and R. Wesel, "The Effect of Mismatch on Decision-Feedback Equalization and Tomlinson-Harashima Preceding," in *Conference Record of the Thirty-Second Asilomar Conference on Signals, Systems & Computers*, vol. 2, Pacific Grove, CA, USA, Nov. 1998, pp. 1743–1747.

[95] F. A. Dietrich and W. Utschick, "Robust Tomlinson-Harashima Precoding," in *IEEE 16th International Symposium on Personal, Indoor and Mobile Radio Communications, PIMRC 2005*, Sep. 2005, pp. 136–140.

[96] F. A. Dietrich, P. Breun, and W. Utschick, "Tomlinson-Harashima Precoding- A Continuous Transition From Complete to Statistical Channel Knowledge," in *IEEE Global Telecommunications Conference, GLOBECOM 05*, vol. 4, 2005, pp. 2379–2384.

[97] M. B. Shenouda and T. N. Davidson, "Tomlinson-Harashima Precoding for Broadcast Channels with Uncertainty," *IEEE Journal on Selected Areas in Communications*, vol. 25, no. 7, pp. 1380–1389, Sep. 2007.

[98] H. K. Bizaki and A. Falahati, "Tomlinson-Harashima Precoding with Imperfect Channel Side Information," in *The 9th International Conference on Advanced Communication Technology, ICACT2007*, Gangwon-Do,, Feb. 2007, pp. 987–991.

[99] R. D. Wesel and J. M. Cioffi, "Achievable Rates for Tomlinson-Harashima Precoding," in *IEEE International Symposium on Information Theory*, Whistler, BC, Canada, Sep. 1995, p. 399.

[100] ——, "Achievable Rates for Tomlinson-Harashima Precoding," *IEEE Transactions on Information Theory*, vol. 44, no. 2, pp. 824–831, Mar. 1998.

[101] M. Huang, S. Zhou, and J. Wang, "Analysis of Tomlinson-Harashima Precoding in Multiuser MIMO Systems With Imperfect Channel State Information," *IEEE Transactions on Vehicular Technology*, 2008.

[102] Z. Khan, T. Arslan, J. S. Thompson, and A. T. Erdogan, "Area & Power Efficient VLSI Architecture for Computing Pseudo Inverse of Channel Matrix in a MIMO Wireless System," in *19th International Conference on VLSI Design*, Jan. 2006.

[103] J. G. McWhirter and P. D. Baxter, "A Novel Technique for Broadband SVD," in *The 12th adaptive sensor array processing workshop, MIT Lincoln Labs*, Mar. 2004.

[104] P. A. Voois, I. Lee, and J. M. Cioffi, "The Effect of Decision Delay in Finite-Length Decision Feedback Equalization," *IEEE Transactions on Information Theory*, vol. 42, no. 2, pp. 618–621, Mar. 1996.

[105] R. F. H. Fischer, "Sorted Spectral Factorization of Matrix Polynomials in MIMO Communications," *IEEE Transactions on Communications*, vol. 53, no. 6, pp. 945–951, Jun. 2005.

[106] L. Song, R. C. de Lamare, A. Hjørungnes, M. R. Bhatnagar, and A. G. Burr, "Approximate ML Serial Detector Based on Tomlinson-Harashima Pre-Equalization," in *IEEE Vehicular Technology Conference, VTC Spring*, May 2008, pp. 1301–1305.

[107] A. Goldsmith, S. Jafar, N. Jindal, and S. Vishwanath, "Capacity limits of MIMO channels," *Selected Areas in Communications, IEEE Journal on*, vol. 21, no. 5, pp. 684–702, Jun. 2003.

[108] A. Leke and J. M. Cioffi, "A Maximum Rate Loading Algorithm for Discrete Multitone Modulation Systems," in *IEEE Global Telecommunications Conference, GLOBECOM '97*, vol. 3, Phoenix, AZ, USA, Nov. 1997, pp. 1514–1518.

[109] X. Zhang and B. Ottersten, "Power Allocation and Bit Loading for Spatial Multiplexing in MIMO Systems," in *IEEE International Conference on Acoustics, Speech, and Signal Processing, (ICASSP '03)*, vol. 5, Apr. 2003, pp. V–53–56.

[110] J. Campello, "Practical bit loading for DMT," in *IEEE International Conference on Communications, ICC '99*, vol. 2, 1999, pp. 801–805.

[111] G. Kulkarni, S. Adlakha, and M. Srivastava, "Subcarrier allocation and bit loading algorithms for OFDMA-based wireless networks," *IEEE Transactions on Mobile Computing*, vol. 4, no. 6, pp. 652–662, Nov.-Dec. 2005.

[112] D. Palomar and J. Fonollosa, "Practical Algorithms for a Family of Waterfilling Solutions," *IEEE Trans on Signal Processing*, vol. 53, no. 2, pp. 686–695, Feb. 2005.

[113] R. Fischer and J. Huber, "A New Loading Algorithm for Discrete Multitone Transmission," in *Global Telecommunications Conference, GLOBECOM '96*, vol. 1, London, Nov. 1996, pp. 724–728.

[114] H. Rohling and C. Fellenberg, "Successive bit loading scheme," *Electronics Letters*, vol. 45, no. 4, pp. 214–216, Feb. 2009.

[115] L. Zeng, S. McGrath, and E. Cano, "Rate Maximization for Multiband OFDM Ultra Wideband Systems Using Adaptive Power and Bit Loading Algorithm," in *IEEE Fifth Advanced International Conference Telecommunications, AICT '09*, Venice/Mestre, Italy, May 2009, pp. 369–374.

[116] A. M. Wyglinski, F. Labeau, and P. Kabal, "Bit Loading with BER-Constraint for Multicarrier Systems," *IEEE Transactions on Wireless Communications*, vol. 4, no. 4, pp. 1383–1387, Jul. 2005.

[117] E. Baccarelli, A. Fasano, and M. Biagi, "Novel Efficient Bit-Loading Algorithms for Peak-Energy-Limited ADSL-Type Multicarrier Systems," *IEEE Transactions on Signal Processing*, vol. 50, no. 5, pp. 1237–1247, May 2002.

[118] N. Papandreou and T. Antonakopoulos, "Bit and Power Allocation in Constrained Multicarrier Systems: The Single-User Case," *EURASIP Journal on Advances in Signal Processing*, vol. 2008, pp. 1–14, 2008.

[119] J. M. Cioffi, "A Multicarrier Primer," ANSI Contribution T1E1.4/91-157, Clearfield, Fla, USA, Tech. Rep., 1991.

[120] A. Garcia-Armada, "SNR Gap Approximation for M-PSK-Based Bit Loading," *IEEE Transactions on Wireless Communications*, vol. 5, no. 1, pp. 57–60, Jan. 2006.

[121] T. Starr, J. M. Cioffi, and P. J. Silverman, *Understanding Digital Subscriber Line Technology*. Prentice Hall, 1999.

[122] A. Goldsmith, *Wireless Communications*. Cambridge University Press, 2005.

[123] B. Krongold, K. Ramchandran, and D. Jones, "Computationally efficient optimal power allocation algorithms for multicarrier communication systems," *IEEE Transactions on Communications*, vol. 48, no. 1, pp. 23–27, Jan. 2000.

[124] M. Jankiraman, *Space-Time Codes and MIMO Systems*. Artech House, 2004.

[125] A. Fasano, G. Di Blasio, E. Baccarelli, and M. Biagi, "Optimal discrete bit loading for DMT based constrained multicarrier systems," in *IEEE International Symposium on Information Theory*, 2002, pp. 243–.

[126] G. L. Nemhauser and L. A. Wolsey, *Integer and Combinatorial Optimization*. New York, NY, USA: JohnWiley & Sons, 1988.

[127] R. Sonalkar and R. Shively, "An efficient bit-loading algorithm for DMT applications," *IEEE Communications Letters*, vol. 4, no. 3, pp. 80–82, Mar. 2000.

[128] C. Assimakopoulos and F.-N. Pavlidou, "New bit loading algorithms for DMT systems based on the greedy approach," *Wireless Communications and Mobile Computing*, vol. 6, no. 8, pp. 1047–1056, 2006.

Appendix A

Some Thesis Derivations

A.1 MMSE Equaliser Solution

Starting with (2.7), the mean square error φ is given for equaliser $\mathbf{W}^{\mathrm{H}}$ by

$$\begin{aligned} \varphi &= tr\left(\mathbb{E}\left[\left(\mathbf{s}-\mathbf{W}^{\mathrm{H}}\mathbf{y}\right)\left(\mathbf{s}-\mathbf{W}^{\mathrm{H}}\mathbf{y}\right)^{\mathrm{H}}\right]\right), \\ &= tr\left(\mathbb{E}\left[\mathbf{s}\mathbf{s}^{\mathrm{H}}+\mathbf{W}^{\mathrm{H}}\mathbf{y}\mathbf{y}^{\mathrm{H}}\mathbf{W}-\mathbf{s}\mathbf{y}^{\mathrm{H}}\mathbf{W}-\mathbf{W}^{\mathrm{H}}\mathbf{y}\mathbf{s}^{\mathrm{H}}\right]\right), \\ &= tr\left(\mathbf{R}_{ss}+\mathbf{W}^{\mathrm{H}}\mathbf{R}_{yy}\mathbf{W}-\mathbf{R}_{sy}\mathbf{W}-\mathbf{W}^{\mathrm{H}}\mathbf{R}_{ys}\right). \end{aligned} \tag{A.1}$$

Where $\mathbf{R}_{ss}=\mathbb{E}\left[\mathbf{s}\mathbf{s}^{\mathrm{H}}\right]$ and $\mathbf{R}_{yy}=\mathbb{E}\left[\mathbf{y}\mathbf{y}^{\mathrm{H}}\right]$ are, respectively, the channel's input and output signal covariance matrices whereas $\mathbf{R}_{sy}=\mathbb{E}\left[\mathbf{s}\mathbf{y}^{\mathrm{H}}\right]$ is the cross-covariance matrix between vectors $\mathbf{s}$ and $\mathbf{y}$. Note that the last two terms of the r.h.s of (A.1) are the hermitian of each other, i.e $\mathbf{R}_{sy}\mathbf{W}=\left(\mathbf{W}^{\mathrm{H}}\mathbf{R}_{ys}\right)^{\mathrm{H}}$as $\mathbf{R}_{ys}^{\mathrm{H}}=\mathbf{R}_{sy}$. Differentiating (A.1) w.r.t $\mathbf{W}^{\mathrm{H}}$ and equating to 0, the MMSE filter $\mathbf{W}_{\mathrm{MMSE}}^{\mathrm{H}}$ can be deduced as follows

$$\begin{aligned} \frac{\partial\varphi}{\partial\mathbf{W}^{\mathrm{H}}}=tr\left(\mathbf{R}_{yy}\mathbf{W}_{\mathrm{MMSE}}-\mathbf{R}_{ys}\right) &= 0 \\ \longrightarrow \mathbf{W}_{\mathrm{MMSE}}^{\mathrm{H}}\mathbf{R}_{yy} &= \mathbf{R}_{sy} \end{aligned} \tag{A.2}$$

Note that since $\mathbf{R}_{yy}$ is a positive semi-definite matrix, it equals its hermitian $\mathbf{R}_{yy}=\mathbf{R}_{yy}^{\mathrm{H}}$ as substituted in (A.2). Also (A.2) is identical to the Wiener-Hopf equation that appeared in (2.8). From (2.3), both $\mathbf{R}_{yy}$ and $\mathbf{R}_{sy}$ are obtained as follows.

$$\begin{aligned}\mathbf{R}_{yy} &= \mathbb{E}\left[\mathbf{y}\mathbf{y}^{\mathrm{H}}\right], \\ &= \mathbb{E}\left[(\mathbf{H}\mathbf{s}+\mathbf{v})(\mathbf{H}\mathbf{s}+\mathbf{v})^{\mathrm{H}}\right], \\ &= \mathbb{E}\left[\mathbf{H}\mathbf{s}\mathbf{s}^{\mathrm{H}}\mathbf{H}^{\mathrm{H}}+\mathbf{H}\mathbf{s}\mathbf{v}^{\mathrm{H}}+\mathbf{v}\mathbf{s}^{\mathrm{H}}\mathbf{H}^{\mathrm{H}}+\mathbf{v}\mathbf{v}^{\mathrm{H}}\right], \\ &= \mathbf{H}\mathbb{E}\left[\mathbf{s}\mathbf{s}^{\mathrm{H}}\right]\mathbf{H}^{\mathrm{H}}+\mathbf{H}\mathbb{E}\left[\mathbf{s}\mathbf{v}^{\mathrm{H}}\right]+\mathbb{E}\left[\mathbf{v}\mathbf{s}^{\mathrm{H}}\right]\mathbf{H}^{\mathrm{H}}+\mathbb{E}\left[\mathbf{v}\mathbf{v}^{\mathrm{H}}\right]. \qquad \text{(A.3)}\end{aligned}$$

Assuming independent and identically distributed (i.i.d) substreams of $\mathbf{s}$ and $\mathbf{v}$ and uncorrelation between them, we can substitute the expectation terms in (A.3) as; $\mathbb{E}\left[\mathbf{s}\mathbf{s}^{\mathrm{H}}\right]=\sigma_s^2\mathbf{I}_{N_t}$, $\mathbb{E}\left[\mathbf{v}\mathbf{v}^{\mathrm{H}}\right]=\sigma_v^2\mathbf{I}_{N_r}$, and $\mathbb{E}\left[\mathbf{s}\mathbf{v}^{\mathrm{H}}\right]=\mathbb{E}\left[\mathbf{v}\mathbf{s}^{\mathrm{H}}\right]=\mathbf{0}$ resulting in

$$\mathbf{R}_{yy}=\sigma_s^2\mathbf{H}\mathbf{H}^{\mathrm{H}}+\sigma_v^2\mathbf{I}_{N_r}, \qquad \text{(A.4)}$$

similarly

$$\mathbf{R}_{sy}=\sigma_s^2\mathbf{H}^{\mathrm{H}}. \qquad \text{(A.5)}$$

Substituting from (A.4) and (A.5) into (A.2) yields the MMSE Linear filter for flat-fading MIMO system as

$$\begin{aligned}\mathbf{W}_{\mathrm{MMSE}}^{\mathrm{H}} &= \mathbf{H}^{\mathrm{H}}\left(\mathbf{H}\mathbf{H}^{\mathrm{H}}+\tfrac{\sigma_v^2}{\sigma_s^2}\mathbf{I}_{N_r}\right)^{-1}, \\ &= \left(\mathbf{H}^{\mathrm{H}}\mathbf{H}+\tfrac{\sigma_v^2}{\sigma_s^2}\mathbf{I}_{N_t}\right)^{-1}\mathbf{H}^{\mathrm{H}}.\end{aligned}$$

A.2 MMSE Solution for SISO-DFE

Since the MSE for the SISO-DFE system presented in Sec. 3.5.2.1 is quadratic in both $\mathbf{f}$ and $\mathbf{b}$, we can find the optimum solution using a standard gradient approach. In order to achieve joint optimality, we combine the feedforward and feedback coefficients into a single vector

$$\mathbf{w}=\begin{bmatrix}\mathbf{f}\\ -\mathbf{b}\end{bmatrix}\in\mathbb{C}^{L_f+L_b},$$

which leads to the following notation for the MSE:

$$\xi_{\mathrm{DFE}}=\left(\mathbf{w}^{\mathrm{H}}\begin{bmatrix}\boldsymbol{\mathcal{H}}\\ \mathbf{D}\end{bmatrix}-\mathbf{d}^{\mathrm{T}}\right)\mathbf{R}_{xx}\left(\begin{bmatrix}\boldsymbol{\mathcal{H}}\\ \mathbf{D}\end{bmatrix}^{\mathrm{H}}\mathbf{w}-\mathbf{d}\right)+\mathbf{w}^{\mathrm{H}}\begin{bmatrix}\mathbf{R}_{vv} & \mathbf{0}_{L_f\times L_b}\\ \mathbf{0}_{L_b\times L_f} & \mathbf{0}_{L_b\times L_b}\end{bmatrix}\mathbf{w}.$$

The gradient can be obtained by differentiating with respect to the filter coefficients (note that $\mathbf{f}$ and $\mathbf{b}$ for convenience contain the complex conjugated

coefficients, hence the differentiation has to be performed with respect to the unconjugated variables in $\mathbf{w}^*$):

$$\frac{\partial}{\partial \mathbf{w}^*}\xi_{\mathrm{DFE}} = \begin{bmatrix} \boldsymbol{\mathcal{H}} \\ \mathbf{D} \end{bmatrix} \mathbf{R}_{xx} \left(\begin{bmatrix} \boldsymbol{\mathcal{H}} \\ \mathbf{D} \end{bmatrix}^{\mathrm{H}} \mathbf{w} - \mathbf{d} \right) + \begin{bmatrix} \mathbf{R}_{vv} & \mathbf{0}_{L_f \times L_b} \\ \mathbf{0}_{L_b \times L_f} & \mathbf{0}_{L_b \times L_b} \end{bmatrix} \mathbf{w} \,.$$

Equating the gradient to zero yields the optimum solution:

$$\mathbf{w}_{\mathrm{opt}} = \left(\underbrace{\begin{bmatrix} \boldsymbol{\mathcal{H}} \\ \mathbf{D} \end{bmatrix} \mathbf{R}_{xx} \begin{bmatrix} \boldsymbol{\mathcal{H}} \\ \mathbf{D} \end{bmatrix}^{\mathrm{H}} + \begin{bmatrix} \mathbf{R}_{vv} & \mathbf{0}_{L_f \times L_b} \\ \mathbf{0}_{L_b \times L_f} & \mathbf{0}_{L_b \times L_b} \end{bmatrix}}_{\mathcal{R}} \right)^{-1} \begin{bmatrix} \boldsymbol{\mathcal{H}} \\ \mathbf{D} \end{bmatrix} \mathbf{R}_{xx} \mathbf{d} \,.$$

If the MSE-optimal set of coefficients are selected, the MMSE is given by

$$\min \xi_{\mathrm{DFE}} = \mathbf{w}_{\mathrm{opt}}^{\mathrm{H}} \mathcal{R} \mathbf{w}_{\mathrm{opt}} \; - \; 2\Re \left(\mathbf{w}_{\mathrm{opt}}^{\mathrm{H}} \begin{bmatrix} \boldsymbol{\mathcal{H}} \\ \mathbf{D} \end{bmatrix} \mathbf{R}_{xx} \mathbf{d} \right) \; + \; \mathbf{d}^{\mathrm{T}} \mathbf{R}_{xx} \mathbf{d} \,.$$

A.3 Water-Filling Solution Proof

The proof of the water filling solution given in (4.14) for the optimisation problem given in (4.1a)-(4.1e) can be obtained following the Lagrange multiplier method as follows.

Formulating the Lagrange function as

$$\mathcal{L}(P_i, \lambda) = \sum_{i=1}^{K} \log_2 (1 + P_i \cdot \theta_i) - \lambda (\sum_{i=1}^{K} P_i - P_{\mathrm{budget}}) \,. \tag{A.6}$$

Then set the partial derivative of $\mathcal{L}$ w.r.t. both P_i and λ to zero yields

$$\frac{\partial \mathcal{L}}{\partial P_i} = \frac{1}{\ln 2} \cdot \frac{\theta_i}{1 + P_i \theta_i} - \lambda = 0, \tag{A.7}$$

and

$$\frac{\partial \mathcal{L}}{\partial \lambda} = \sum_{i=1}^{K} P_i - P_{\mathrm{budget}} = 0 \,. \tag{A.8}$$

Note that $\frac{\partial \mathcal{L}}{\partial \lambda}$ in (A.8) results in the original problem constraint, which is common using the Lagrange multiplier method. Now from (A.7) we can obtain $P_i = \frac{1}{\lambda \ln 2} - \frac{1}{\theta_i} = \alpha - \theta_i^{-1}$, where $\alpha = \frac{1}{\lambda \ln 2}$ is the water-level constant selected to fulfil the constraint of the total power budget in (4.1b).